Molecular Simulations of Structure and Dynamics of Neat and Hydrated Imidazolium Ionic Liquids

A

thesis submitted

in partial fulfillment of the requirements for the degree of

DOCTOR OF PHILOSOPHY

by

Praveen Kumar

Roll No.: 20123201

Indian Institute of Science Education and Research, Pune

2018

Certificate

Certified that the work incorporated in the thesis entitled "*Molecular Simulations of Structure and Dynamics of Neat and Hydrated Imidazolium Ionic Liquids*", submitted by **Praveen Kumar** was carried out by the candidate, under my supervision. The work presented here or any part of it has not been included in any other thesis submitted previously for the award of any degree or diploma from any other University or institution.

Date:

Dr. Arun Venkatnathan

(Supervisor)

Declaration

I declare that this written submission represents my ideas in my own words and where others' ideas have been included, I have adequately cited and referenced the original sources. I also declare that I have adhered to all principles of academic honesty and integrity and have not misrepresented or fabricated or falsified any idea/data/fact/source in my submission. I understand that violation of the above will be cause for disciplinary action by the Institute and can also evoke penal action from the sources which have thus not been properly cited or from whom proper permission has not been taken when needed.

Date: **Praveen Kumar**

Dedicated to my parents and wife

Acknowledgement

I would like to express my gratitude to my research supervisor Dr. Arun Venkatnathan for advising me during the course of this thesis work. I also thank him for his continuous support and motivation during my Ph.D. study and research. His guidance and suggestions helped me a lot throughout my research work and writing of this thesis. I value his contributions to my professional development during this long, arduous journey at Indian Institute of Science Education and Research (IISER) Pune.

I would like to thank my RAC members - Dr. Srabanti Chaudhury, Dr. Guruswamy Kumaraswamy and Dr. Neelanjana Sengupta for their insightful comments and encouragement, and also for the critical review which helped me a lot in my research work from various perspectives. I acknowledge IISER Pune for the graduate fellowship. I thank the Chemistry department for providing the necessary facility.

I thank my labmates, K. R Ramya and Minal for all scientific and non-scientific discussions and for all the fun we have had in the last few years. I especially thank my labmates Rakesh and Prabhat for discussion and providing useful suggestions during my projects. Also, I thank my friends Meghna, Rohit, Jitender, Sachin, Mohit, Bappa, and Rishabh for their support and scientific discussions.

I would like to thank my family: my parents, my wife Varsha, my son Pravansh for supporting me spiritually throughout my research work. I would like to thank every individual whom I met during my Ph.D. life at IISER Pune for their help and support.

I would like to thank American Chemical Society, American Institute of Physics, and Royal Society of Chemistry (Great Britain) for permissions to include figures from copyrighted articles.

IISER, PUNE **Praveen Kumar**

List of Publications

1. K. R. Ramya, **Praveen Kumar**, Ashish Kumar and Arun Venkatnathan,
   Interplay of Phase Separation, Tail Aggregation, and Micelle Formation in the Nanostructured Organization of Hydrated Imidazolium Ionic Liquid,
   J. Phys. Chem. B **118**, 8839 (2014).

2. K. R. Ramya[†], **Praveen Kumar**[†] and Arun Venkatnathan,
   Molecular Simulations of Anion and Temperature Dependence on Structure and Dynamics of 1-Hexyl-3-methylimidazolium Ionic Liquids,
   J. Phys. Chem. B **119**, 14800 (2015).

3. **Praveen Kumar**[†], Prabhat Prakash[†], K. R. Ramya and Arun Venkatnathan,
   Probing translational and rotational dynamics in hydrophilic/hydrophobic anion based imidazolium ionic liquid - water mixtures,
   Soft Matter **14**, 6109 (2018).

[†] Equal contribution

Contents

List of Figures

List of Tables

Abbreviations

IL	:	Ionic Liquid
MD	:	Molecular Dynamics
Bmim	:	1-butyl-3-methylimidazolium
Hmim	:	1-hexyl-3-methylimidazolium
$C_n$mim/Xmim	:	1-alkyl-3-methyimidazolium, X = alkyl
BF_4	:	Tetrafluoroborate
PF_6	:	Hexafluorophosphate
OTf	:	Trifluoromethanesulfonate
NTf_2	:	Bis(trifluoromethylsulfonyl)imide
SPC/E	:	Extended Simple Point Charge
PME	:	Particle-Mesh Ewald
λ	:	Water Concentration
MSD	:	Mean Square Displacement
NPT	:	Isobaric Isothermal
NVT	:	Isochoric Isothermal
RDF	:	Radial Distribution Function
IE	:	Interaction Energy
SDF	:	Spatial Distribution Function
IP	:	Ion-pair
RACF	:	Rotational Autocorrelation Function
τ_{rot}	:	Rotational Correlation Time

Abstract

Ionic Liquids (ILs) are highly ionic compounds where its physical and chemical properties can be appropriately tuned by varying the choice of cations and anions. The complex interactions of ILs with water or other solvents can also influence the structure and dynamics of these mixtures and can determine its suitability in applications to gas absorption, metal ion extraction, liquid extraction, electrochemistry, catalysis etc. Molecular Dynamics simulations (using all atom forcefields) can provide enormous physical insights into the structure and dynamics of ILs in neat and hydrated environments. For example, a molecular understanding on the effect of anion on structural and dynamical properties in neat imidazolium ILs shows the following trends: ILs with smaller anions like Cl^-, Br^-, BF_4^- have relatively higher cation-anion interactions, unlike larger anions like PF_6^- , OTf^- , NTf_2^-. The cationic and anionic diffusion (ionic conductivity) are lowest in ILs with Cl^- and Br^- anions, and highest with BF_4^-, OTf^- and NTf_2^- anions. While the magnitude of diffusion coefficients is primarily dependent on anionic size and shape, ion-pair lifetimes will decisively provide a direct qualitative trend with diffusion coefficients (conductivity) of ILs. The addition of water to a hydrophobic IL ([Hmim][NTf_2]) shows the following structural features: (a) At low water concentration, small regions of water molecules are surrounded by several cation-anion pairs. (b) At medium water concentration, cation tail aggregation starts, and phase separation between the IL and water is observed. (c) At high water concentration, increasing cationic tail aggregation leads to micelle formation. Further aggregates of cations and anions are solvated by large water channels. The Radial Distribution Functions show that cation-anion, cation-cation, and anion-anion interactions decrease and water-water interaction increases with water concentration. The translational and rotational dynamics in hydrated [Hmim][Cl] ILs and [Hmim][NTf_2] ILs is also investigated. At low, intermediate, and high water concentration, dynamical properties (diffusion coefficient) of hydrophobic/hydrophilic ILs shows the following trends: Cl^- > $Hmim^+$; Cl^- > NTf_2^- ; $Hmim^+$ ([Hmim][Cl]) > $Hmim^+$ ([Hmim] [NTf_2]). At ultra-low water concentration, hydrophilic ([Hmim][Cl]) IL shows several bridges like

configurations between water molecules and Cl^- anions which is supported by a complex distribution of water clusters and positive value of water-water interaction energy. The rotational relaxation time of $Hmim^+$ cations is larger in neat [Hmim][Cl] compared to neat [Hmim][NTf_2] IL with an opposite trend seen with hydration.

Chapter 1

Introduction

1.1 Ionic Liquids

Ionic Liquids (ILs) are materials which exist as cations and anions with melting points below 100 ^{0}C [1]. ILs are highly ionic species where at least one of the ions have larger

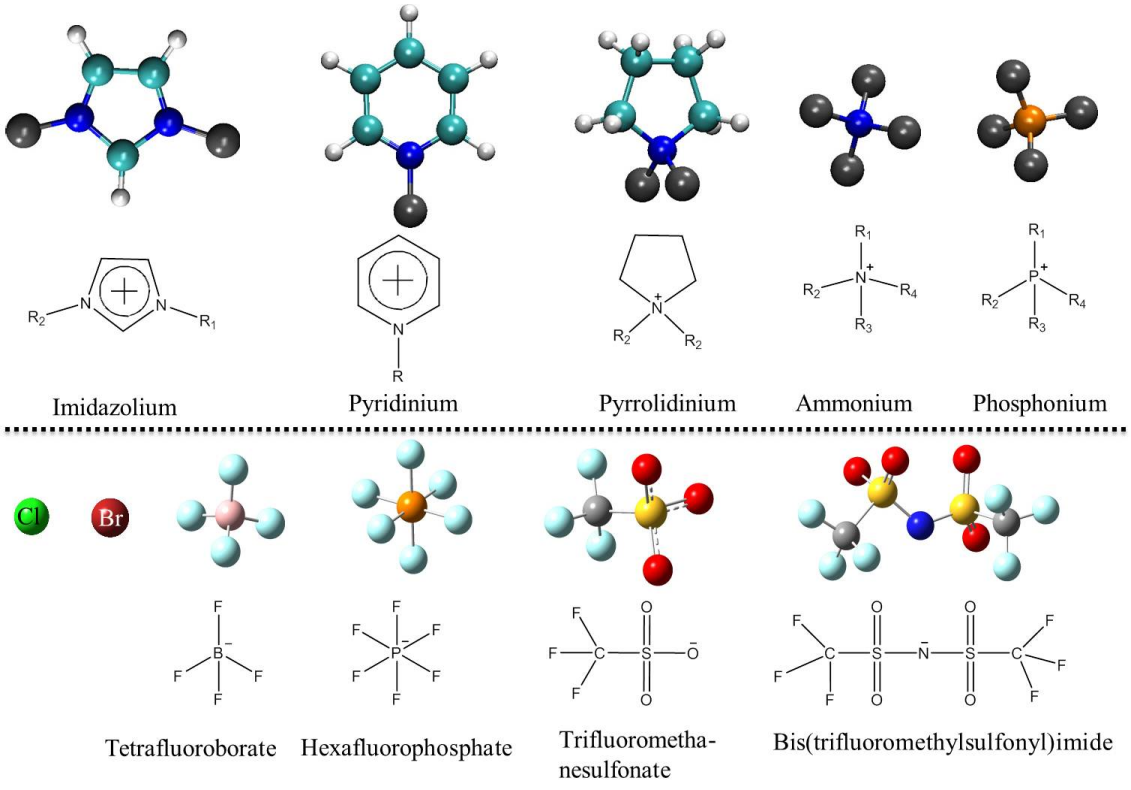

Figure 1.1: Representative cations and anions of ILs.

size and are asymmetric which leads to reduced melting points [2]. Several ILs exist as liquid at room temperature and hence are called as Room Temperature ILs [3]. The interionic interaction in ILs can be classified as π - π [4], electrostatic and H-bonding [5,6]. These interactions in ILs leads to unique properties such as low vapor pressure [7], low flammability [8], high thermal, chemical, and electrochemical stability [1]. A large body of experimental work [1, 9, 10] has been devoted to the synthesis and characterization of ILs. The chemical structure of commonly investigated ILs with representative cations and anions are shown in Figure **1.1**. By varying the choice of cation and anion, a large number of ILs can be synthesized and hence, they are called as 'designer solvents' [11] in the scientific community. Among several families of ILs, the imidazolium class of ILs has been extensively investigated from experiments and computer simulations [9, 12–20].

1.1.1 Imidazolium Ionic Liquids

One of the earliest reported imidazolium IL was the dialkylimidazolium chloroaluminate IL [21]. This IL was investigated for its applications to electrochemistry, synthesis and spectroscopy. Subsequently, several imidazolium ILs (with varying alkyl chain length on the imidazolium cations and different anions) have been synthesized and characterized for industrial and laboratory applications as solvent for organic synthesis [22–26], nanostructured materials [27–29], bio-selective catalysis [30, 31]. Few examples of such ILs are outlined below. Gonzalez-Miquel et al. [32] explored the CO_2 absorption capacity in [C_4mim[PF_6], [C_4mim[FAP] and [C_4mim[NTf_2] ILs using a Gravimetric High Pressure Sorption Analyzer. Wang et al. [33] investigated [$C_{10}C_{10}$IM][BF_4] IL as a solvent for synthetic applications. Xu et al. [34] the cellulose dissolution in [$C_n$mim][CH_3COO] (n = 2, 4, 6, 8) ILs. The effect of alkyl chain length on the imidazolium cations, choice of anions and co-solvents (e.g., water) are the key factors which can influence the physical, structural and dynamical properties of imidazolium ILs. A background of several experimental and theoretical investigations on the properties of various imidazolium ILs are described in the subsequent subsections.

1.2 Physical Properties

Rogers and co-workers [35] investigated the melting point (m.p.) of [$C_n$mim][X] (n = 1-4, X = $AlCl_4^-$, BF_4^-, PF_6^-, NO_2^-, TfO^-, NTf_2^-) ILs by Differential Scanning Calorimetry (DSC). The authors observed (see Figure 1.2a) that m.p. of ILs lowers with increasing

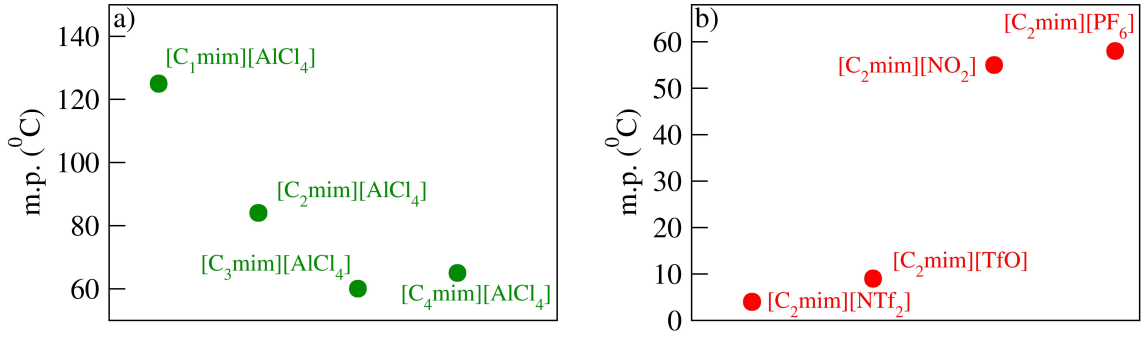

Figure 1.2: Melting point of imidazolium IL with the effect of a) alkyl chain length on the cations, b) anions.

alkyl chain length on the imidazolium cation. The authors observed (see Figure 1.2b) that ILs containing bulkier anions (TfO^- and NTf_2^-) have a lower melting point compared to ILs containing symmetric and smaller size anions (NO_3^- and PF_6^-).

The authors investigated the density of [$C_n$mim][X] (n = 4, 6, 8, X = Cl^-, BF_4^-, PF_6^- and NTf_2^-) ILs using gravimetric analysis. The authors observed (see Figure 1.3a) that the density of ILs decrease with increasing alkyl chain length. The authors observed (see

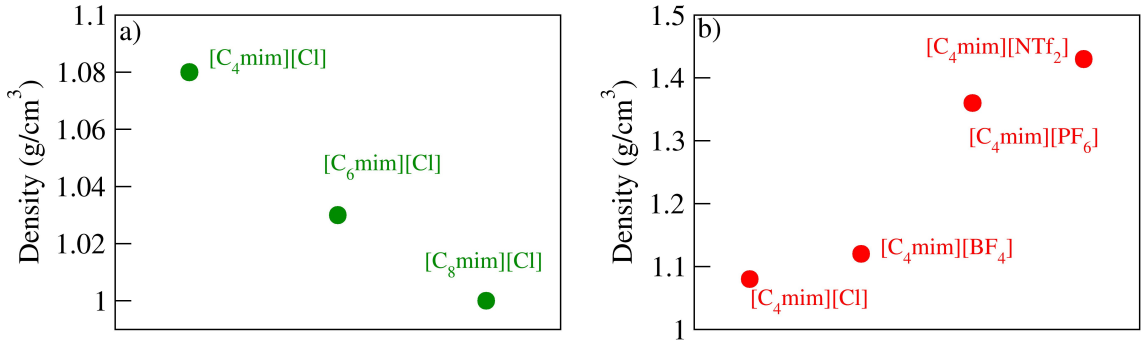

Figure 1.3: Density of imidazolium IL with the effect of a) alkyl chain length on the cations, b) anions.

Figure 1.3b) the increase in density of these ILs with increase in anionic size (Cl^- < BF_4^-

< PF_6^- < NTf_2^-). The authors examined the viscosity of [$C_n$mim][X] (n = 4, 6, 8, X = I^-, BF_4^-, PF_6^- and NTf_2^-) ILs by a viscometer. The authors observed (see Figure **1.4**a) that the viscosity increases with increasing alkyl chain on the imidazolium cation. The authors also observed (see Figure **1.4**b) that viscosity decreases with lower symmetry of the anion. The authors characterized the thermal stability of [$C_n$mim][X] (n = 2, 4, 6, 8, X = Cl^-,

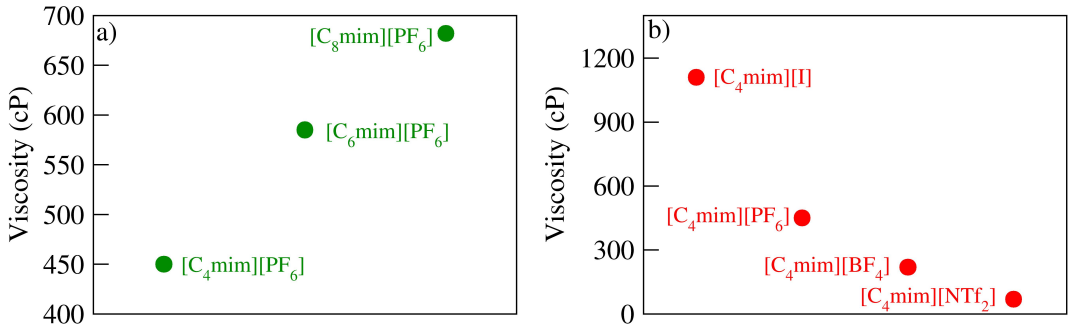

Figure 1.4: Viscosity of imidazolium IL with the effect of a) alkyl chain length on the cations, b) anions.

I^-, BF_4^-, and NTf_2^-) ILs by thermogravimetric analysis (TGA). The authors observed (see Figure **1.5**a) that the decomposition temperature of ILs did not show any correlation with the alkyl chain length of the imidazolium cation. The authors reported (see Figure **1.5**b) that ILs containing hydrophilic anions (Cl^-, I^-) have lower decomposition temperature, compared to ILs containing less hydrophilic (more hydrophobic) anions (BF_4^-, NTf_2^-).

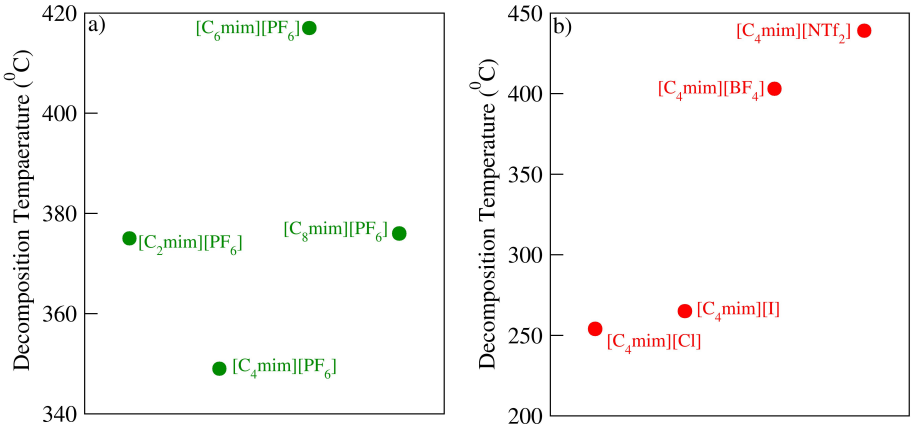

Figure 1.5: Decomposition temperature of imidazolium IL with the effect of a) alkyl chain length on the cations, b) anions.

1.3 Structure

1.3.1 Neat Imidazolium ILs

The structural properties of materials can be characterized by several spectroscopic techniques such as Raman-induced Kerr effect, Small Angle Neutron Scattering (SANS), Small Angle X-ray Scattering (SAXS), Small Wide Angle X-ray Scattering (SWAXS), TEM and cryo-TEM, and X-ray, etc. Triolo et al. [36] employed X-ray on neat and supercooled $[C_n\text{mim}][BF_4]$ (n = 2, 4, and 6) and $[C_n\text{mim}][\text{Cl}]$ (n = 3, 4, 6, 8, and 10) ILs and observed a nano segregated structure of ILs formed by the alkyl chain of imidazolium cations. The authors reported that the size of the structural heterogeneities (formation of polar and nonpolar domains) was directly proportional to the alkyl chain length of imidazolium cations. Russina et al. [37] employed SWAXS and Raman-induced Kerr effect spectroscopy to characterize the structure of $[C_n\text{mim}][NTf_2]$ (n = 1 - 10) ILs. The authors observed the presence of chain aggregates where the alkyl chain length on the imidazolium cation was found to be ≥ 3. Xiao et. al. [38] observed similar structural properties between $[C_n\text{mim}][NTf_2]$ and $[(C_n)_2\text{im}][NTf_2]$ (n = 2-5) ILs using SWAXS. The authors also observed that symmetric cations $[(C_n)_2\text{im}]^+$ were more compactly packed as compared to asymmetric cations $[C_n\text{mim}]^+$. Hardacre et al. [39] studied the structure of ILs composed of $[C_n\text{mim}]^+$ cations (n = 12-20) with Cl^-, Br^-, OTf^-, NTf_2^- and tetrachloropalladate(II) anions using SAXS. The authors observed that ILs containing a long alkyl chain on the imidazolium cation showed a liquid crystalline phase (also known as smectic A [40]). The smectic A shows an interlayer spacing to be dependent on the choice of anions and the alkyl chain length of the imidazolium cation. Xiao et al. [41] employed the Raman-induced Kerr and optical Kerr effect spectroscopy to study structural organization in $[C_5\text{mim}][\text{Br}]$, $[C_5\text{mim}][PF_6]$ and $[C_5\text{mim}][NTf_2]$ ILs. The authors reported that solid-like domains exist in $[C_5\text{mim}][\text{Br}]$ IL and liquid like domains were seen in $[C_5\text{mim}][NTf_2]$ IL, which illustrates the role of an anion. In solid domains, two similar charged anions which are geometrically close to each other results in a van der

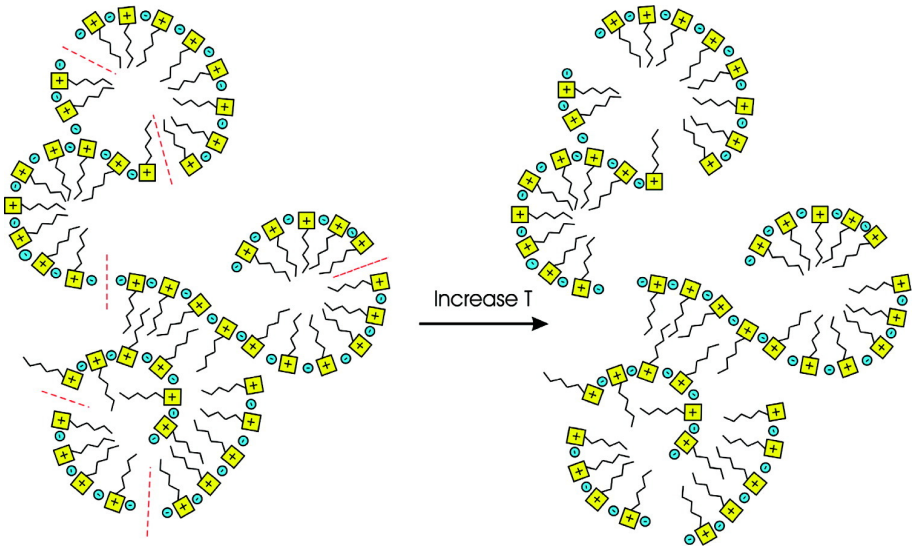

Figure 1.6: Schematic illustration of nanostructural organization in an ionic liquid showing how thermal expansion can occur without affecting the local structure of the domains in the ionic networks. Reprinted with permission from [41]. Copyright (2007) American Chemical Society.

Waals repulsion creating a gap called as a defect. The authors showed (see Figure **1.6**) that [C_5mim][Br] IL form ionic networks separated by defects. Further, the authors reported that temperature does not affect the local structure due to the persistent presence of these defects.

Lopes and Padua [42] employed MD simulations to investigate the structural organization of [$C_n$mim][PF_6] and [$C_n$mim][NTf_2] (n = 2 to 12) ILs. The authors observed polar domains (imidazolium ring) and non-polar domains (alkyl chain of imidazolium cation). The authors also observed the tri-dimensional arrangement of ionic channels in the polar domains. However, non-polar domains form a dispersed microphase in ILs containing a smaller cation ([emim]) and a continuous microphase in ILs containing a longer alkyl chain (e.g., hexyl, octyl, or dodecyl). On the imidazolium cation, with increasing alkyl chain length, the evolution of polar (red) and non-polar domains (green) occurs (see Figure **1.7**). Ji et al. [43] studied the structural properties of [$C_n$mim][NO_3] (n = 6, 8, ...22) ILs using coarse-grained MD simulations. The authors observed that with increasing alkyl chain length, van der Waals forces between the alkyl chains increase, leading to transformation

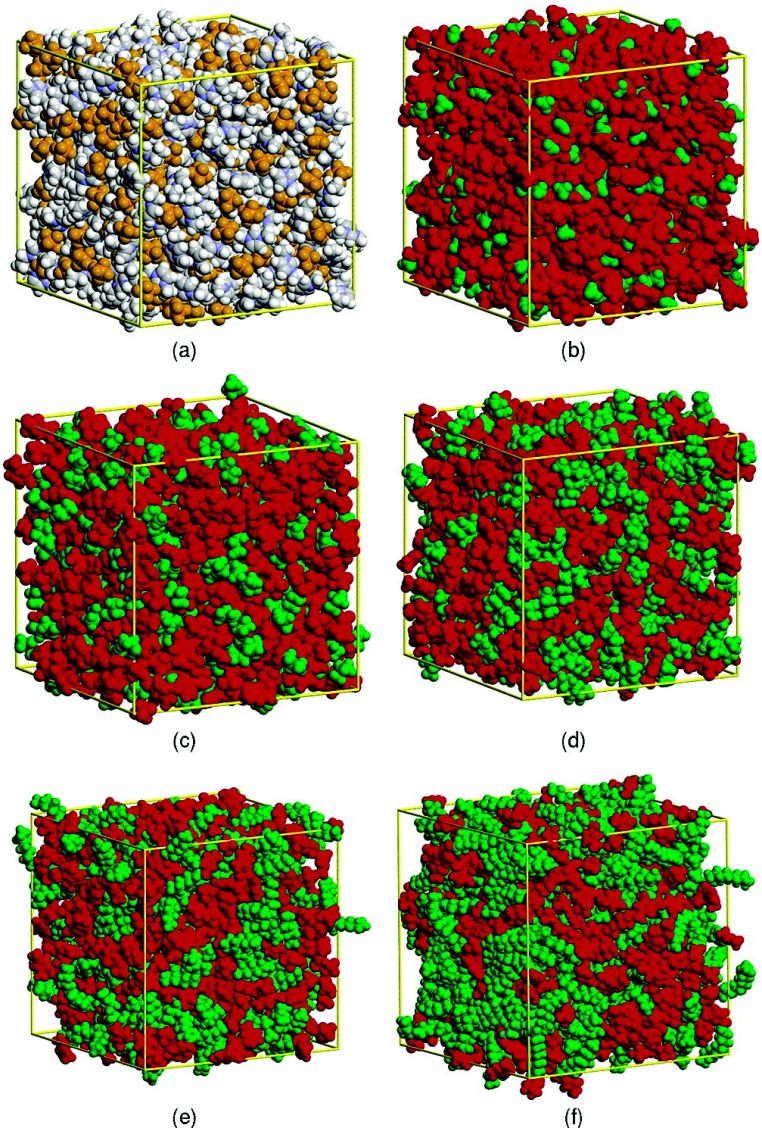

Figure 1.7: Snapshots of simulation boxes containing 700 ions of $[C_n mim][PF_6]$. The application of a coloring code enables clear identification of the charged and nonpolar domains that form in ionic liquids. The lengths of the box sides are given: (a) $[C_2 mim][PF_6]$ CPK coloring; (b) $[C_2 mim][PF_6]$ same configuration as in a with red/green (charged/nonpolar) coloring; (c) $[C_4 mim][PF_6]$ l = 49.8 Å; (d) $[C_6 mim][PF_6]$ l = 52.8 Å; (e) $[C_8 mim][PF_6]$ l = 54.8 Å; (f) $[C_{12} mim][PF_6]$ l = 59.1 Å. Reprinted with permission from [42]. Copyright (2006) American Chemical Society.

of heterogeneous structure of ILs to an IL crystal structure. Kapoor and Shah [44] studied the effect of alkyl chain length on structural properties of $[C_n mim][C_8 SO_4]$ (n = 2, 4, 6, 8, 10, and 12) ILs using MD simulations. The authors observed that ILs with smaller

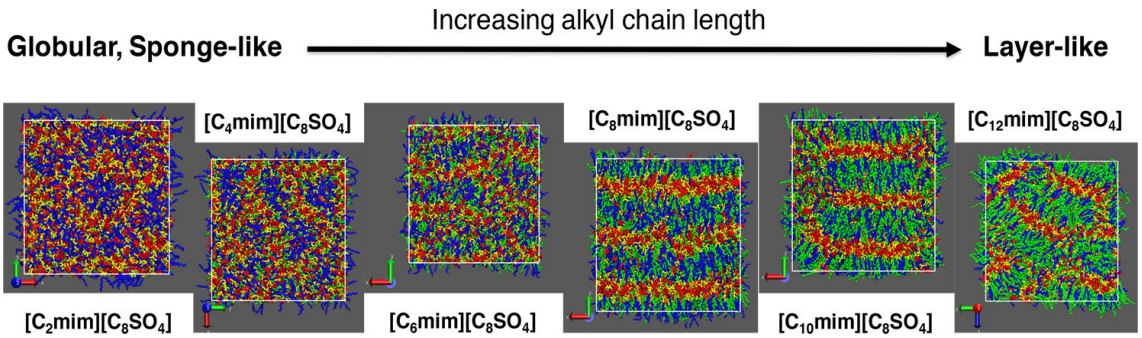

Figure 1.8: Instantaneous snapshot of the equilibrated system for $[C_n\text{mim}][C_8SO_4]$ IL homologous series. The snapshots are color-coded to reflect the polar and nonpolar components on both cation and anion. (Cation-polar: red, Anion-polar: yellow, Cation-nonpolar: green, and Anion-nonpolar: blue). Reprinted with permission from [44]. Copyright (2018) American Chemical Society.

alkyl chain length (n = 2, and 4) forms a "globular" and "sponge" like arrangement. Upon further increase in alkyl chain length (n = 8, 10, and 12), ILs form a "layer" type arrangement (see Figure **1.8**). Raabe and Köhler [45] employed MD simulations on 1-alkyl-3-methylimidazolium chloride ILs and 1-alkyl-3-methylimidazolium teterfluoroborate ILs and observed that the probability of finding the Cl^- and BF_4^- anions were higher in the following spatial regions: near the acidic hydrogen atom, between the non-acidic hydrogen of imidazolium ring and near the alkyl chains (see Figure **1.9**). However, the spatial distribution density of Cl^- and BF_4^- anions in these regions remain different. For example, the authors found a lower probability of Cl^- anions above and below the plane of the imidazolium ring, but higher in front of the acidic hydrogen atom (see Figure **1.9**a, b). However, the probability of finding BF_4^- anions was higher above and below the plane of the imidazolium ring. (see Figure **1.9**c, d).

1.3.2 Hydrated Imidazolium ILs

Blesic et al. [46] studied the structural properties in hydrated $[C_n\text{mim}][Cl]$ (n = 2-14), $[C_n\text{mim}][PF_6]$(n = 4 or 10), and $[C_{10}\text{mim}][NTf_2]$ ILs. The authors concluded that imidazolium cations with Cl^- anions form aggregates for n ≥ 8. The authors could not observe any micelles in ILs containing the $[C_{10}\text{mim}]^+$ cations with NTf_2^-, or PF_6^- anions.

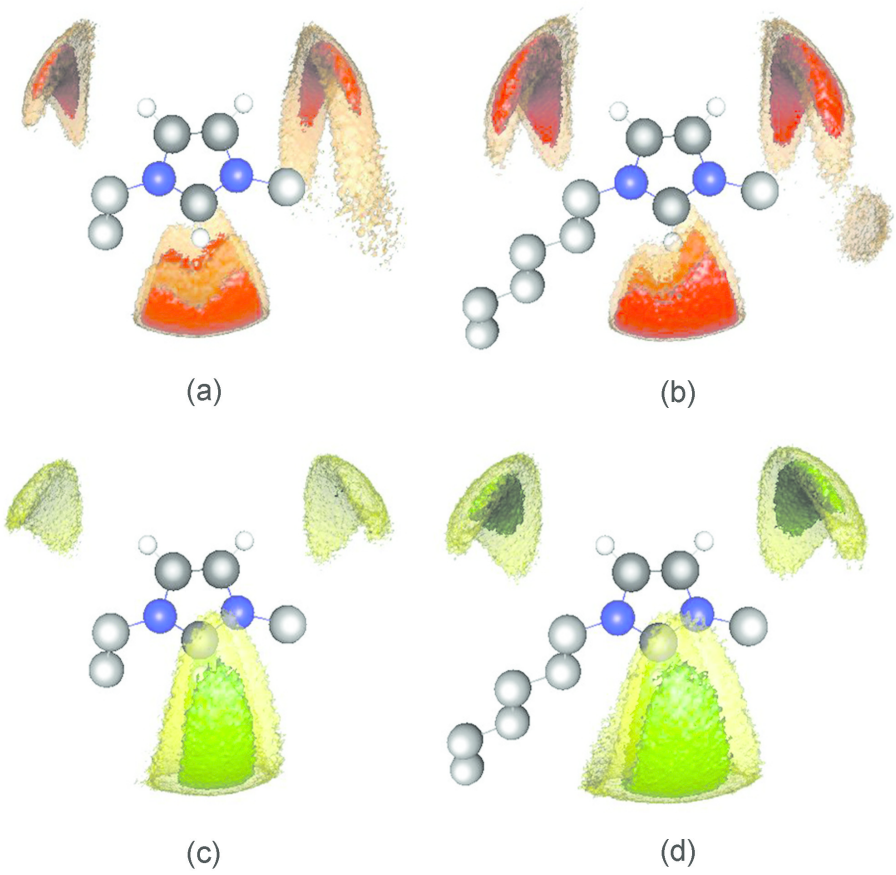

Figure 1.9: Spatial distribution functions (SDFs) of the anion around the cation at 363.15K as a function of the anion type and the size of the cation from molecular simulations in this work: (a) [emim][Cl], (b) [hmim][Cl], (c) [emim][BF_4], and (d) [hmim][BF_4]. The surfaces are drawn at 14 (green, red) and eight (yellow, orange) times of the average density, respectively. Reprinted from [45], with the permission of AIP Publishing.

Wang et al. [47] employed the negative stain TEM and cryo-TEM techniques and observed that depending on the water concentration, aggregates of [C_{12}mim][Br] ILs exist either as spherical micelles, rod-like micelles, and vesicles (see Figure **1.10**). Gao and Wagner [48] examined the structural properties of hydrated [C_4mim][BF_4] IL by SANS. The authors concluded that IL can dissolve water up to a ~2:1 water/IL concentration. At higher water concentration (mole fraction of water ~0.80), water percolate occurs. Further addition of water (mole fraction of water = 0.925-0.985) to ILs leads to phase inversion with the formation of IL aggregates. The mole fraction of water = 0.985 was reported as the Critical

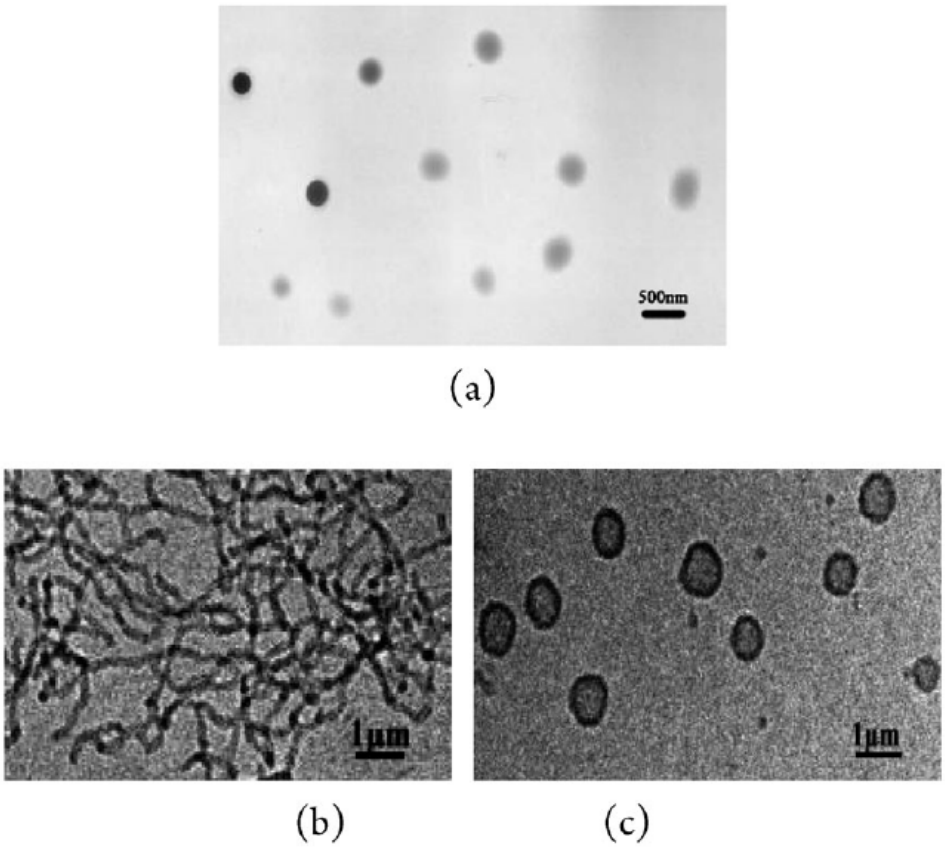

Figure 1.10: TEM images of the aggregates of $[C_{12}mim]Br$ in aqueous solution at different concentrations of IL: (a) 0.06; (b) 0.56; and (c) 0.93 mol L^{-1}; (a) negative stain TEM; (b) and (c) Cryo-TEM. Reproduced from Ref. [47] with permission from the Royal Society of Chemistry

Micelle Concentration (CMC) (see Figure **1.11**). Tran et al. [49] studied the effect of water on structural properties of imidazolium ILs with a common cation $[Bmim]^+$ with different (BF_4^-, PF_6^-, and NTf_2^-) anions by Near-Infrared (NIR) spectroscopy. The authors observed that the strength of the anion-water interaction shows the following trends: $BF_4^-...H_2O$ > $NTf_2^-...H_2O$ > $PF_6^-...H_2O$, suggesting that $[Bmim][BF_4]$ IL can absorb more water compared to $[Bmim][PF_6]$ IL.

Palchowdhury and Bhargava [50] examined the structural properties of hydrated $[C_nC_{10}im][Br]$ (n = 1, 4, 7 and 10) ILs by MD simulations. The authors observed the quasi-spherical aggregates of $[C_1C_{10}im][Br]$ IL and spherical aggregates of comparatively larger size for long chain $[C_{10}C_{10}im][Br]$ IL (see Figure **1.12**). Vicent-Luna et al. [51] studied

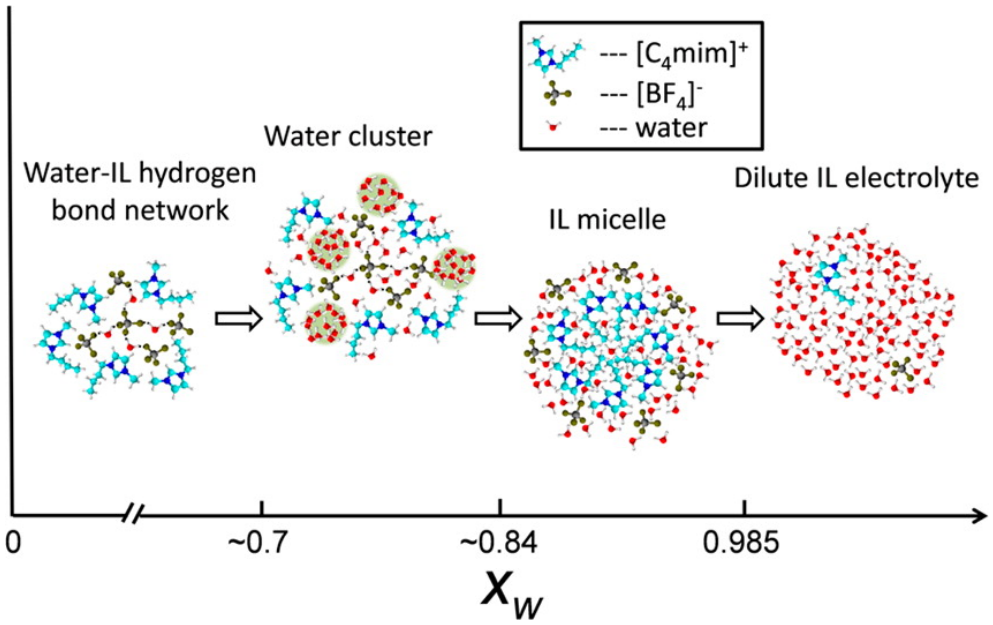

Figure 1.11: Schematic illustration of structures in mixtures of $[C_4mim][BF_4]$ and D_2O. Reprinted with permission from [48]. Copyright (2016) American Chemical Society.

the structural properties of hydrated $[C_n mim][Cl]$ (n = 4, 6, 8, 10 and 12) ILs and calculated the CMC value for $[C_8mim][Cl]$, $[C_{10}mim][Cl]$ and $[C_{12}mim][Cl]$ ILs. The authors also observed the formation of micelles at a particular water concentration. Nickerson et al. [52] studied the structural properties of hydrated [Bmim][I] IL using experiments and MD simulations. The authors observed that at lower water concentration, each water molecule interacts with at least one I^- anion. With increase in water concentration, the I^- anions preferentially interact with water molecules compared to the imidazolium cations leading to a disordered IL structure.

1.4 Dynamics

1.4.1 Neat Imidazolium ILs

Xu et al. [53] experimentally measured the conductivities of [Bmim][RCOO] ILs with varying alkyl chain length on the carboxylate anion. The authors concluded that the number of ionic aggregates increase with alkyl chain length on the carboxylate anion. This was

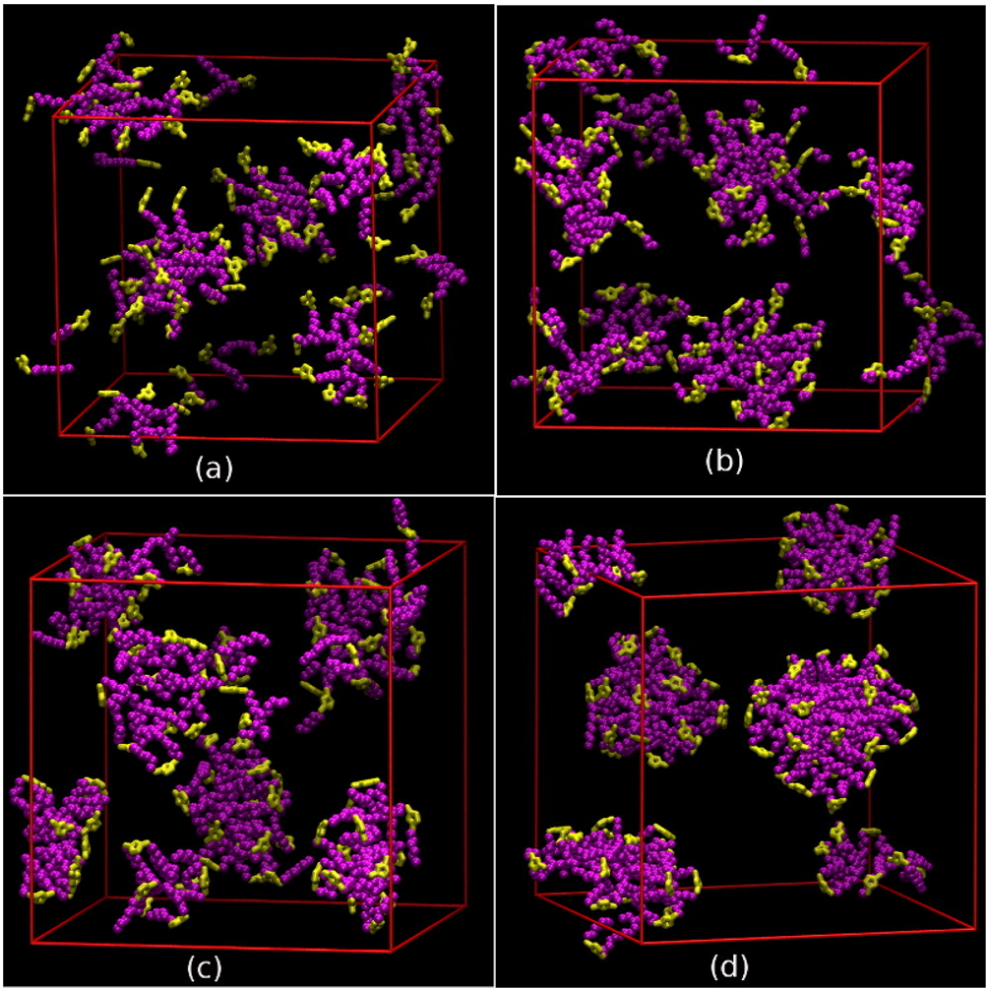

Figure 1.12: Snapshot of the aqueous solution after a 25 ns simulation. (a)[C_1C_{10}Im][Br], (b) [C_4C_{10}Im][Br], (c) [C_7C_{10}Im][Br], and (d) [$C_{10}C_{10}$Im][Br]. The hydrophilic region of the head group is shown in yellow, whereas atoms belonging to hydrophobic alkyl chains are shown in magenta. Anions, water molecules, and H-atoms on the cations are not shown for the ease of visualization. Reprinted with permission from [50]. Copyright (2014) American Chemical Society.

attributed to an increase in the van der Waals forces between the alkyl chains, which leads to an increase in the bulk viscosity and hence a decrease in electrical conductivity. Sippel et al. [54] recorded the dielectric response of thirteen imidazolium ILs and observed that ILs with low glass temperature and high fragility show the highest electrical conductivity. Vila et al. [55] calculated the electrical conductivity of [$C_n$mim][X] IL (n = 2, 4, 6, 8 and X = Cl^-, Br^-, BF_4^-, PF_6^-, ethyl sulfate (ES^-) and tosylate (TY^-)) using a conductivimeter.

The authors observed that the electrical conductivity of ILs decrease with an increase in alkyl chain length of imidazolium cation. The order of electrical conductivity with increasing anion size shows as follows: $Cl^- < Br^- < BF_4^- > PF_6^- > ES^- > TY^-$.

Kowsari and Fakhraee [56] studied the effect of alkyl chain and functional group on the dynamical properties of imidazolium ILs with ([bmmim]$^+$, 1-butyl-2,3-dimethylimidazolium; [bmim]$^+$; [apmim]$^+$, 1-(3-aminopropyl)-3-methylimidazolium; [mim]$^+$, 1-methylimidazolium) cation and NTf_2^- anion by MD simulations. The authors observed that the motion of terminal carbon was higher than the motion of nitrogen and carbon atoms of the imidazolium ring. The authors also observed the order of MSD of cations as: [bmim]$^+$ $\geq$ [apmim]$^+$ $\geq$ [bmmim]$^+$ $\geq$ [mim]$^+$. The authors also reported the MSD of NTf_2^- anions follow the order: [bmim][NTf_2] $\geq$ [apmim][NTf_2] $\geq$ [bmmim][NTf_2] $\geq$ [mim][NTf_2]. Rey-Castro and Vega [57] employed MD simulations to study the transport properties in [Emim][Cl] IL. The authors observed that the diffusion of cation was higher than the anion, though the size and mass of the [Emim]$^+$ cation were larger than the Cl^- anion. Mondal and Balasubramanian [58] studied the dynamical properties of [bmim][X] (X = PF_6^-, BF_4^-, $CF_3SO_3^-$, NTf_2^-, and NO_3^-) ILs by MD simulations. The authors observed the following trends in electrical conductivity: [Bmim][PF_6] > [Bmim][BF_4] > [Bmim][NO_3] > [Bmim][NTf_2] > [Bmim][CF_3SO_3]. Kowsari and co-workers [59] studied the structural and dynamical properties of [Hmim][PF_6] IL by MD simulations. The authors observed that diffusion of [Hmim]$^+$ cations was faster than [PF_6]$^-$ anions.

1.4.2 Hydrated Imidazolium ILs

Kaneko et al. [60] studied the effect of alkyl chain length on the diffusion coefficients of hydrated [$C_n$mim][BF_4] (n = 2, 4, 6, 8) ILs using NMR spectroscopy. The authors concluded that the relative diffusion coefficient of water molecules increased with the alkyl chain length of the imidazolium cations of the [$C_n$mim][BF_4] IL. Menjoge et al. [61] studied the diffusion in hydrated [Emim][ES] IL and [Emim][OTf] IL using Pulsed Field Gradient NMR spectroscopy. The authors concluded that in both ILs (with increasing

water concentration) the diffusion coefficients of cation and anion increase, and the difference in the magnitude of diffusion coefficients between the cation and anion decreases.

Hegde et al. [62] investigated structural and dynamical properties of hydrated ([$C_n$mim][OAc], n = 2, 4, and 8) ILs with increasing alkyl chain length. The authors observed that (at all IL concentration), the diffusion of cations, anions and water molecules decreases exponentially. At IL concentration between 25% and 75%, diffusion of ions and water molecules decreases very fast. Between 75% to 100% , the diffusion of ions and water molecules decreases gradually. Méndez-Morales et al. [63] employed MD simulations on hydrated [$C_n$mim] (n = 2, 4, 6, and 8) ILs with hydrophilic anions (Cl^- and Br^-) and hydrophobic anions (PF_6^-). The authors observed that the diffusion of hydrophobic ILs ([$C_n$mim][PF_6]) was higher than the diffusion of hydrophilic ILs ([$C_n$mim][Cl]). Zhong et al. [64] studied the local structure and transport properties of hydrated [C_4mim][BF_4] IL. The authors observed that at low water concentration (mole fraction of water < 0.2), the diffusion coefficient of cations and anions was similar to that seen in neat ILs. With increasing water concentration (mole fraction of water > 0.4), the diffusion coefficient of anions was faster than the diffusion coefficient of cations.

1.5 Scope and outline of the thesis

The scope of the thesis is to systematically investigate the effect of anions and water concentration on the structure and dynamics of 1-hexyl-3-methylimidazolium ILs from MD simulations. A concise description of forcefield and properties elucidated from MD simulations are discussed in the subsequent sections. The methodology and MD simulation protocol for the construction of IL and IL-water mixtures precede the results from MD simulation in subsequent chapters. The results from MD simulations are outlined in the following chapters: **Chapter 2** describes an MD simulation study on the effect of anions on the structure and dynamics of neat ILs. **Chapter 3** describes the structure in hydrated [Hmim][NTf_2] IL. **Chapter 4** describes the translational and rotational dynamics in hydrated [Hmim][Cl] and [Hmim][NTf_2] ILs. **Chapter 5** summarizes the key findings of

this thesis with a brief description of future directions in this research area.

1.6 Force Field

A force field is defined as a mathematical form of potential energy which depends on the coordinates of its atoms/molecules of a chemical system. The potential energy [65] of a chemical system is the sum of all bonded and non-bonded interactions, where

$$U_{\text{total}} = U_{\text{bonded}} + U_{\text{non-bonded}} \tag{1.1}$$

$$U_{\text{bonded}} = \sum_{bonds} k_b(r - r_0)^2 + \sum_{angles} k_\theta(\theta - \theta_0)^2 + \sum_{torsions}^{n=0-5} C_n(cos(\psi))^n \tag{1.2}$$

where k_b and k_θ are the force constants corresponding to the bonds and angles, C_n are the torsional coefficient. $\psi = \phi$-180^0, where ϕ is the dihedral angle. The non-bonded potential energy is defined as:

$$U_{\text{non-bonded}} = \sum_{ij} 4\epsilon_{ij}\left[\left(\frac{\sigma_{ij}}{r_{ij}}\right)^{12} - \left(\frac{\sigma_{ij}}{r_{ij}}\right)^{6}\right] + \frac{1}{4\pi\epsilon_0}\frac{q_i q_j}{\epsilon_r r_{ij}} \tag{1.3}$$

where, σ_{ij} is the well depth of potential energy, r_{ij} is the distance between the atoms i and j, σ_{ij} is the distance between the atom i and j. q_i and q_j are the atomic charges of the atoms, ϵ_0 is the permittivity of vacuum and ϵ_r is the dielectric constant. The harmonic terms in the bonded interactions represent the classical nature of the force field. The commonly used and most popular classical force fields are CHARMM [66], AMBER [67], OPLS-AA [68], COMPASS [69], GROMOS [70], etc. Among them, the OPLS-AA force field has been extremely popular and extensively used [71–77] to model interactions and examine structure and dynamics in ILs in neat and hydrated environments. This has motivated the use of OPLS-AA forcefield for MD simulations of IL and IL-water mixtures in this thesis. A comprehensive description of force fields and MD simulations can be seen in references [65, 78].

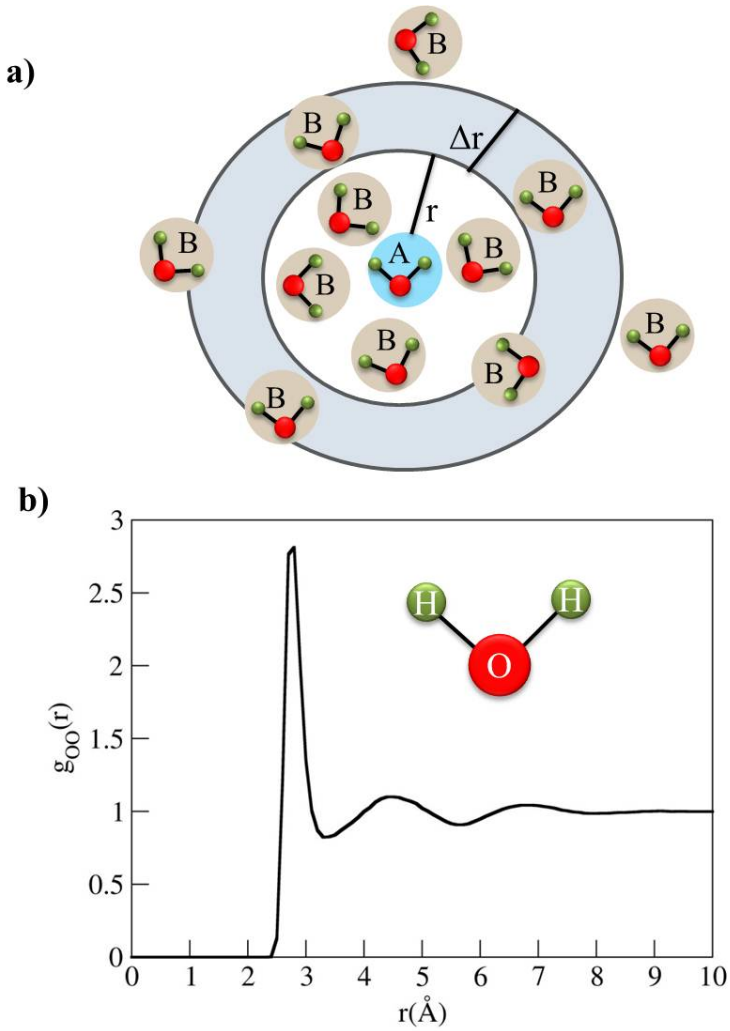

Figure 1.13: a) Schematic representation of Radial Distribution Function, b) Oxygen-Oxygen RDF (g_{OO}(r)).

1.6.1 Radial Distribution Function

The structure of a material can be calculated as a Radial Distribution Function (RDF) and is written as [78]:

$$g_{AB}(r) = \frac{1}{< \rho_B >_{local} N_A} \sum_{i\epsilon A}^{A} \sum_{i\epsilon B}^{B} \frac{\partial(r_{ij} - r)}{4\pi r^2} \tag{1.4}$$

where, $< \rho_B >_{local}$ is the particle density of particle B averaged over all spheres around a reference particle A. A schematic representation of RDFs in liquid water and the calculated RDF (between oxygen atom of water molecules) is shown in Figure **1.13**). The

Coordination Number of molecules can be calculated up to any particular distance r (e.g., first minima of solvation shell) and can be written as:

$$\text{Coordination Number} = 4\pi\rho \int_0^r g(r).r^2 dr \tag{1.5}$$

where, ρ is the number density.

1.6.2 Mean Square Displacement and Diffusion Coefficient

The Mean Square Displacement (MSD) can be written as [78]:

$$\lim_{t\to\infty} \underbrace{\langle \|r_i(t) - r_i(0)\|^2 \rangle_{i\epsilon A}}_{\text{MSD}} = 6D_A t \tag{1.6}$$

where r_i are the positions (coordinates) of molecular systems extracted from the trajectories of MD simulation runs. In general, the various possibilities of diffusion in any chemical system can be seen in Figure **1.14**. Using the Einstein relationship [78], the diffusion coefficient (D_A) of any molecule "A" can be calculated from the linear regime of

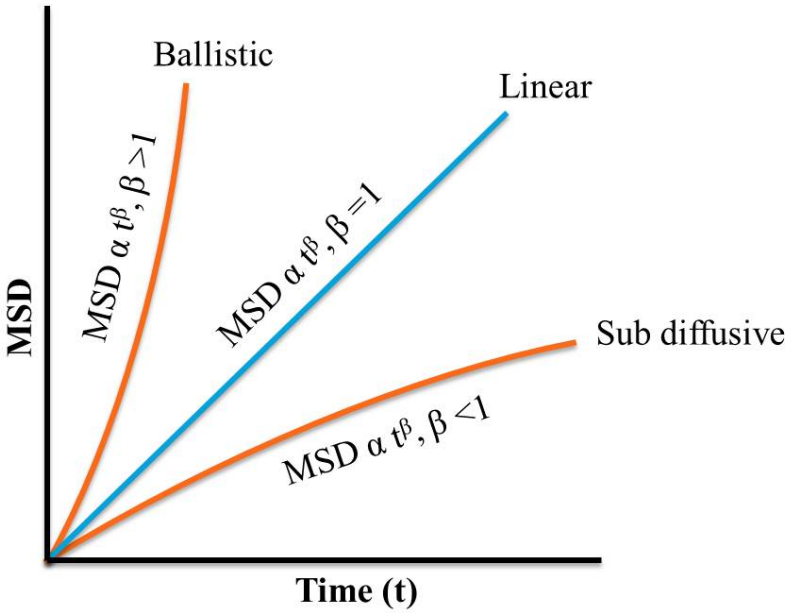

Figure 1.14: Schematic representation of diffusion.

the corresponding MSD. The linear regime is determined using a parameter, β(t), defined as:

$$\beta(t) = \frac{dlog(MSD)}{dlog(t)} \tag{1.7}$$

1.6.3 Ionic Conductivity

The ionic conductivity (λ_{IL}) can be calculated using the Nernst-Einstein relationship [78] and can be written as:

$$\lambda_{IL} = \frac{N_A e^2}{V_{mol}\ k_B T}(D_+ + D_-) \tag{1.8}$$

where, N_A is Avogadro number, $V_{mol} = \frac{mol.wt}{Density}$, D_+ and D_- are the diffusion coefficients of the cations and anions, N is the number of ion pairs, T is the temperature, e is the charge of an electron and k_B is the Boltzmann constant.

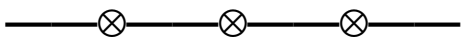

Chapter 2

Anion and temperature dependence on structure and dynamics of 1-hexyl-3-methylimidazolium ionic liquids

2.1 Introduction

Room temperature ILs have low vapor pressure, large electrochemical window, and high chemical and thermal stability and hence are suited for a variety of technological applications [7, 8, 79, 80]. However, various physical and chemical properties of these ILs can be tailored [81–83] by choosing combinations of cations (and its derivatives) and anions. Grätzel and co-workers [84] investigated ILs containing the 1,3-dialkylimidazolium cations with various hydrophobic anions. The authors concluded that ILs with smaller cations and anions have high conductivity. Huddleston et al. [35] characterized the effect of anions on physical properties and thermal stability of several hydrophilic and hydrophobic imidazolium ILs. The authors observed that the thermal stability of ILs decrease with the following anions: $PF_6^- > NTf_2^- \sim BF_4^- > Cl^- \sim I^-$. Ngo et al. [85] observed an exothermic thermal decomposition of ILs with organic anions, unlike ILs containing

inorganic anions. Fredlake et al. [86] and Muhammad et al. [87] concluded that thermal stability of ILs increases with anionic size. Katsyuba et al. [88] employed single crystal X-Ray Diffraction (XRD) and infrared and Raman spectroscopy and found that hydrogen bonding strength between the 1-(2′-hydroxylethyl)-3-methylimidazolium cation and anions were: $[PF_6] < [BF_4] < [NTf_2] << [OTf] << [TFA]$.

MD simulations have also been employed to characterize the effect of anions on nano scale properties of ILs. Urahata and Ribeiro [89] used MD simulations and found that at 400 K, the [Bmim][Cl] IL show higher mobility compared to $[Bmim][PF_6]$ IL. Lee et al. [90] observed that ionic conductivity of [Bmim] ILs increase with the following anions: $[C_4F_9SO_3^-] < [C_3F_7COO^-] < [PF_6^-] < [CF_3COO^-] < [CF_3SO_3^-]$. Deetlefs et al. [91] examined hydrogen bonding interactions (from XRD and MD simulations) between the 1,3-dimethylimidazolium cation and Cl^-, PF_6^- and NTf_2^- anions. The authors concluded that strength of hydrogen bonds between the cation and anion was dependent on charge density of the anion and its size and increases as $[NTf_2^-] < [PF_6^-] < [Cl^-]$. Kowsari et al. [92] concluded that diffusion coefficients are in the order of $NO_3^- > PF_6^- > Cl^-$ anions in ILs with 1-alkyl-3-methylimidazolium (alkyl = methyl, ethyl, propyl and butyl) cations. The authors argued that while anionic size of Cl^- is smallest and the PF_6^- anion is the largest, the higher value of diffusion coefficients of NO_3^- anion was due to its shape.

Existing MD simulations have focused on the comparison of diffusion coefficients (conductivity) of ILs with different anions. Tsuzuki et al. [76] reported that the magnitude of diffusion coefficient of cations and anions depend on the size and shape of ions (cations and anions) and the interaction strength between cations and anions. The authors also examined interionic interactions and attempted to show a relationship between dynamics of ILs with IE (calculated using quantum chemistry calculations). The conclusions from their work have motivated further investigations to explore an in-depth understanding on the effect of anions (using a common cation) and temperature on various interionic interactions, diffusion coefficients, and ionic conductivities. In order to observe these effects, the 1-hexyl-3-methylimidazolium cation ($Hmim^+$) have been chosen with hydrophilic anions (Cl^-, Br^-, BF_4^-) and hydrophobic anions (PF_6^-, OTf^-, NTf_2^-) in this study. The choice

of the imidazolium cation and various anions stems from its wide variety of scientific and technological applications such as dissolution of cellulose by [Hmim][Cl] [93] IL, as solvent and catalysts in organic synthesis by [Hmim][Br] [94] IL, liquid separation by [Hmim][BF_4] [95] and [Hmim][OTf] [96] ILs, and CO_2 absorption by [Hmim][PF_6] [97] and [Hmim][NTf_2] [98] ILs. The influence of temperature is examined by MD simulations performed at T = 300, 353, 403 and 435 K.

2.2 Computational details

All simulations were performed using the GROMACS 4.5.4 [99] program. The force-field parameters of cations and anions were taken from the work of Tsuzuki et al. [76]. The long-range electrostatic interactions were calculated using the particle mesh Ewald (PME) [100, 101] method. The nonbonded interactions were calculated within a cutoff of 12 Å. The equations of motion were integrated by a leapfrog algorithm [78] using a 1 fs time step. The chemical structure of the 1-hexyl-3-methylimidazolium cation and anions (Cl^-, Br^-, BF_4^-, PF_6^-, OTf^-, NTf_2^-) are shown in Figure **2.1**. The input configurations of

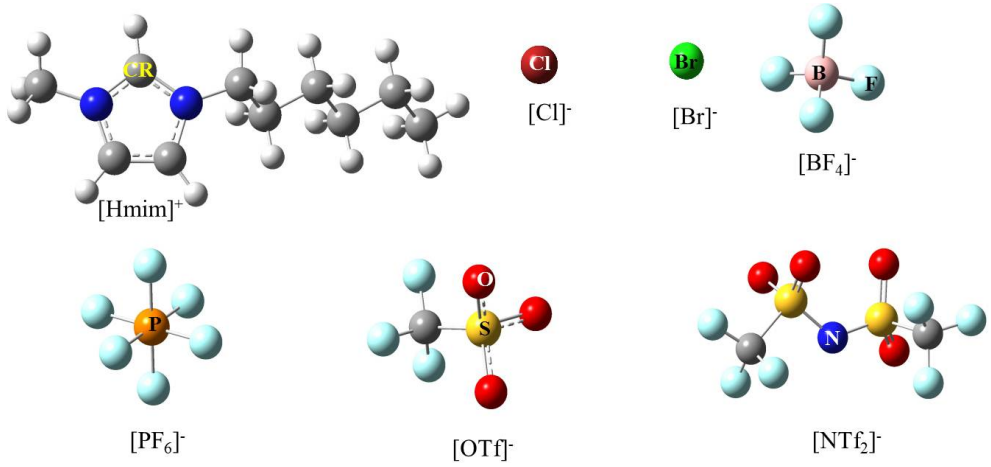

Figure 2.1: Chemical structure of 1-hexyl-3-methylimidazolium ($Hmim^+$), Chloride (Cl^-), Bromide (Br^-), Tetrafluoroborate (BF_4^-), Hexafluorophosphate (PF_6^-), Trifluoromethanesulfonate (OTf^-) and bis(trifluoromethylsulfonyl)imide (NTf_2^-).

each IL (which have a common cation) are created as follows: A single IP was optimized

using MP2/6-311G** basis set and replicated in a cubic box of 512 IPs. The replicated IPs were energy-minimized using the steepest descent algorithm [102]. To randomly mix these IPs, a simulated annealing (NPT ensemble) was performed as follows: The replicated 512 IP system was warmed from 453 K to 703 K (steps of 50 K every 250 ps) and equilibrated further for 500 ps at 703 K. The final configuration at 703 K was used and cooled to 453 K (steps of 50 K every 250 ps) followed by an equilibration for 500 ps at 453 K. The simulated annealing procedure was repeated twice with a total annealing simulation time of 7.25 ns. The final configurations from annealing were chosen as input for a 5 ns equilibration runs at 453 K (NPT ensemble). The final configuration from equilibration at 453 K were used as inputs for independent 5 ns equilibration NPT simulation runs performed at 300, 353 and 403 K. The v-rescale thermostat [103] and Berendsen barostat [104] with a coupling constant of 0.1 and 1.0 ps, respectively, were used during the equilibration. The average density (obtained from equilibration) shows good agreement with experimental density (see Figure **B2-1** of appendix B). A heterogeneous mixing of cations and anions of various ILs is shown in Figure **2.2**. Each equilibration run is followed by NVT production runs for 200 ns (T = 300 K) and 50 ns (T = 353, 403 and 453 K). The Nosé-Hoover [105, 106] thermostat was used to keep temperature constant during the production run with a coupling constant of 0.2 ps. The recorded trajectories from the production run were used for calculation of structural (radial and spatial distribution functions) and dynamical properties (diffusion coefficients, ionic conductivity, IP lifetimes) as discussed in the next section.

2.3 Results and discussion

2.3.1 Structure

The size of the anion [107] which increases as $Cl^- < Br^- < BF_4^- < PF_6^- < OTf^- < NTf_2^-$ is used as comparative measure for structural and dynamical properties. The structural properties, which characterize various interionic interactions in these ILs, are examined

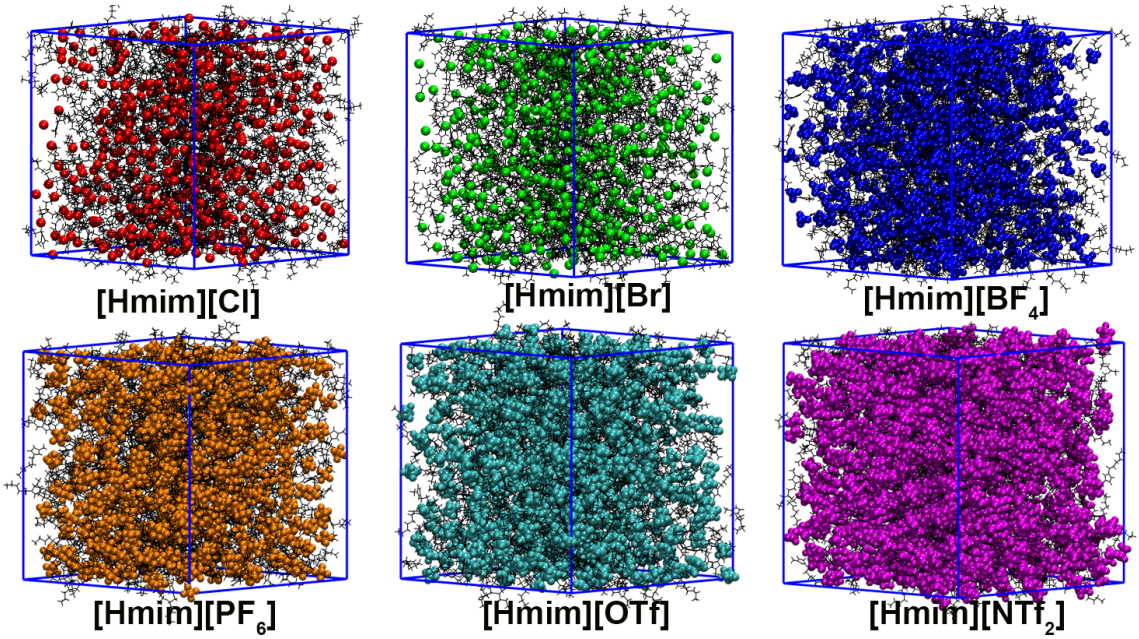

Figure 2.2: Final snapshot from 5 ns equilibration at T = 303 K. Color scheme is as follows: Black: Hmim+ cation; Red: Cl^-, Green: Br^-, Blue: BF_4^-, Orange: PF_6^-, Cyan: OTf^-, Purple: NTf_2^-.

by RDFs (see section 1.6.1) and SDF [108]. The interionic interactions like cation-cation and cation-anion RDFs are calculated using atomic sites on each ion. The cationic site is represented by the carbon atom (denoted as atom type CR shown in Figure **2.1**), which is bonded to the acidic hydrogen atom of the imidazolium ring of the cation. The anionic sites are represented by the most negatively charged atoms. The cation-cation RDFs (see Figure **2.3**) show the presence of two distinct peaks in [Hmim][Cl] IL, compared to the [Hmim][Br] IL, thereby suggesting more ordered cation-cation interactions. The cation-cation interactions in [Hmim][BF_4] and [Hmim][PF_6] ILs show similar RDFs with a more broad secondary peak from the [Hmim][PF_6] IL, again suggesting the role of anionic size and shape in cation-cation interactions. In [Hmim][OTf] and [Hmim][NTf_2] ILs, a broader first hump is observed suggesting that large size anions lead to a much bigger solvation shell to accommodate the cations. Almost similar intensities from all cation-cation RDFs, suggests that the extent of cation-cation interaction is independent of the choice of anion, as larger anions lead to bigger solvation shells. The larger solvation

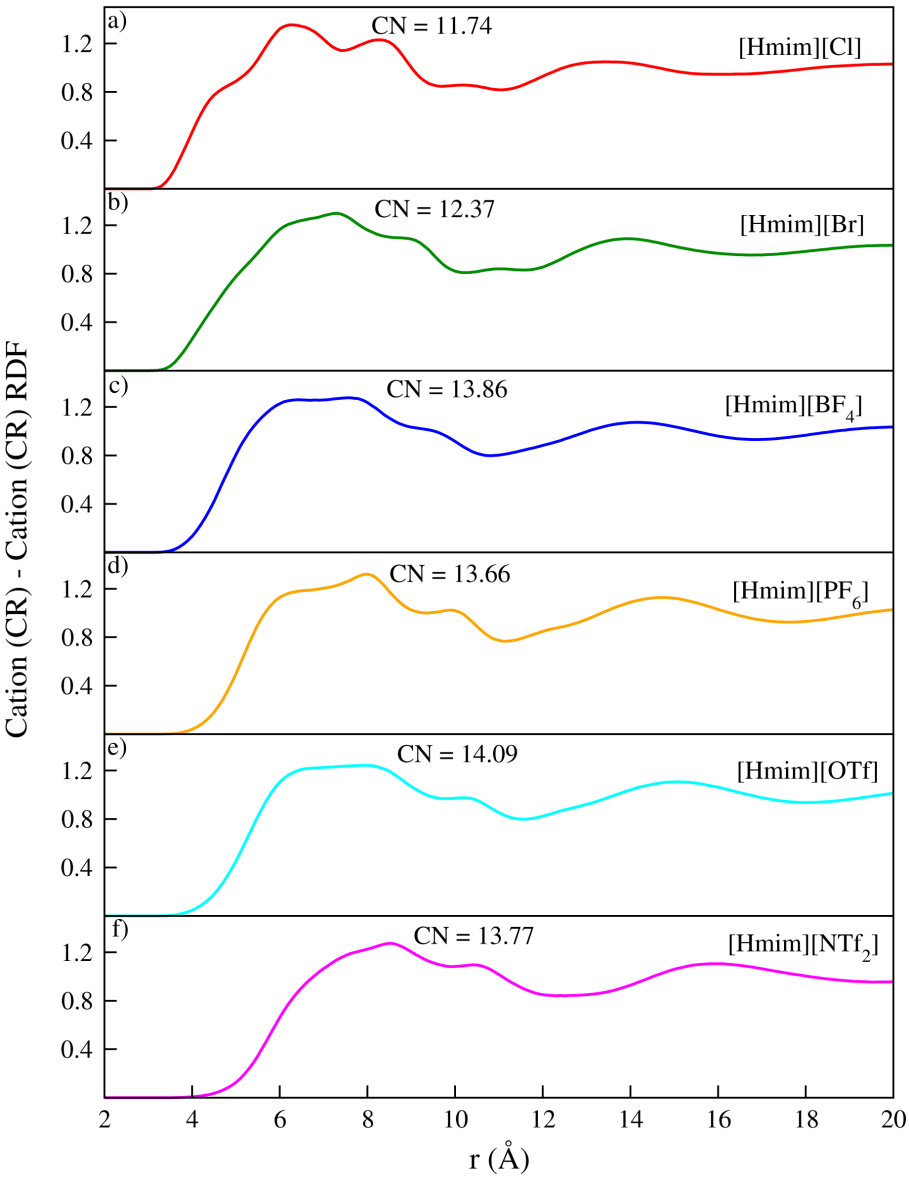

Figure 2.3: RDFs (T = 300 K) from Cation-Cation Interactions. The CR atom of the imidazolium ring of the cation is used for Cation-Cation Interactions.

shell (with increase in anion size) seen from the first minima of the cation-cation RDFs is 6.2 Å in [Hmim][Cl] IL and 8.8 Å in [Hmim][NTf_2] IL. The number of interacting cations is seen by the coordination numbers calculated at the first minima cutoff of each IL (see Table **A2-1** of Appendix A). An examination of the coordination numbers show 11-14 interacting cationic sites within the first solvation shell.

The cation-anion RDFs (see Figure **2.4**) show a sharp first peak between 3.2 and 3.8 Å

and first minima between 4.3 and 4.6 Å, where the exact peak position and minima depend

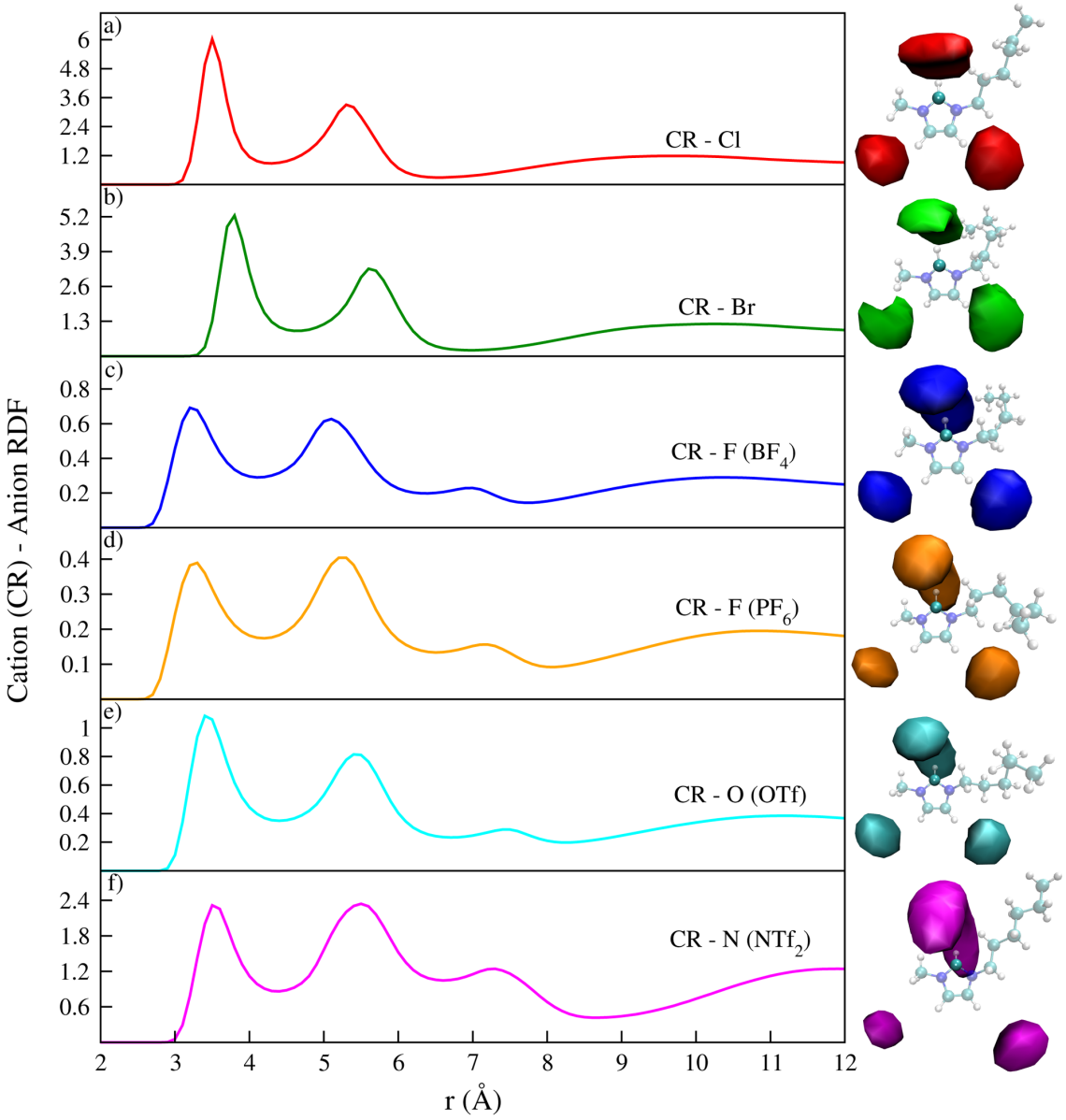

Figure 2.4: RDFs (T = 300 K) and SDFs from Cation-Anion Interactions. The CR atom of the imidazolium ring of the cation is used for Cation-Anion Interactions. Colour scheme for SDFs: Red: Cl^-, Green: Br^-, Blue: BF_4^-, Orange: PF_6^-, Cyan: OTf^-, Purple: NTf_2^-. Isovalue of SDFs (units of number of atoms per nm^3) are: 8.15 [Cl], 6.60 [Br], 5.88 [BF_4], 5.39 [PF_6], 5.28 [OTf] and 4.40 [NTf_2].

on the choice of the anion. For example, a first peak at 3.5 Å with a corresponding minimum at 4.3 Å is observed for [Hmim][Cl] IL (see Figure 2.4a). Due to the larger size of

the Br^- anion, the first peak and minima appears at 3.8 and 4.6 Å, respectively (see Figure 2.4b), which shows a shift towards larger distances, compared to the Cl^- anion. The RDF intensities show reduced cation-Br interaction compared to cation-Cl interactions, thus alluding that larger anions in ILs lead to reduced cation-anion interactions. The cation-anion RDFs of [Hmim][BF_4] and [Hmim][PF_6] IL show strikingly similar characteristics. For the sake of comparison, the fluorine atoms in BF_4^- and PF_6^- anions are chosen as interaction sites, where the RDFs are normalized by the number of fluorine atoms of the anions. The first peak and minima in CR-F(BF_4) RDFs (see Figure 2.4c) appear at 3.2 and 4.1 Å, respectively. Due to the slightly larger size of the PF_6^- anion, the first peak and minima of this CR-F(PF_6) RDF (see Figure 2.4d) appear at 3.3 and 4.2 Å, respectively. The cation-anion RDFs of [Hmim][OTf] and [Hmim][NTf_2] ILs also resemble each other. The oxygen atom of the OTf^- anions and nitrogen atom of the NTf_2^- anions are chosen as interaction sites for calculation of cation-anion RDFs in these ILs. In the case of OTf^- anion, the RDF is normalized by the number of oxygen atoms. The first peak and minima from the CR-O(OTf) RDF (see Figure 2.4e) appear at 3.4 and 4.4 Å, respectively. The first peak and minima of CR-N(NTf_2) RDF (see Figure 2.4f) appear at 3.5 and 4.5 Å, respectively. As expected, the enhanced intensity of the CR-N(NTf_2) RDF compared to the CR-O(OTf) RDF is due to higher negative charge on the nitrogen atom of the NTf_2^- anion, leading to stronger cation-anion interaction. The cation-anion RDFs also show a secondary solvation shell between 4.1 and 7.0 Å, where anions can interact with cations (though with lower intensity). The interaction between cations and anions in this solvation shell follows the same trends seen from the primary solvation shell. The effect of temperature shows no significant change in the cation-cation and cation-anion RDFs (see Figure B2-2 and Figure B2-3 of Appendix B).

The local distribution of each anion around the reference imidazolium cation is characterized by SDFs (see Figure 2.4) obtained from the TRAVIS [108] program. In order to visualize the SDFs, appropriate isosurfaces are chosen such that the local densities of anion around the reference cation are 2.2 - 2.7 times higher than the average bulk density. A visual inspection of all SDFs shows three distinct spatial distributions of anionic density:

one cloud close to the acidic hydrogen atom (hydrogen atom attached to the carbon atom, CR, of the imidazolium cation), which is relatively more bulkier and closer than the other two clouds near the non-acidic hydrogen atoms. Specifically, the SDFs show that Cl^-, Br^- and BF_4^- anions occupy a larger space along the CR-H bond vector. However, the density of PF_6^-, OTf^- and NTf_2^- anions is less near the CR-H bond vector and preferentially seen above and below the plane of imidazolium ring of the cation. In all SDFs, the presence of secondary clouds of anions (at the vicinity of the two nonacidic hydrogen atoms) confirms the dual peaks observed from cation-anion RDFs.

2.3.2 Dynamics

The mobility of ILs is seen from the MSD (see section 1.6.2) (see Figure **B2-4** of Appendix B). A preliminary examination of MSD of cations and anions shows that at each temperature, the lowest mobility arises in [Hmim][Cl] with the highest mobility from [Hmim][NTf_2] ILs. However, a quantitative measurement of mobility is derived by calculation of diffusion coefficients from the linear diffusive regime (β(t) = 1) of the MSD (see section 1.6.2). The value of β(t) for cations and anions at each IL and temperature is shown in Figure **B2-5** (Appendix B). At T = 300 and 353 K, the β(t) of cations and anions is < 1, which suggests somewhat less diffusive behavior. This could be due to higher viscosity [107] of these ILs. However, at T = 403 and 453 K, all ILs show more diffusive behavior (β(t) $\approx$ 1). By use of the Einstein relationship [78], the diffusion coefficients (see Figure **2.5**a,b) are calculated from the time interval, where β(t) fluctuates between 0.9 and 1.06. At T = 300 K, the diffusion coefficients of cations and anions are similar for all ILs. At T = 353, 403, and 453 K, the diffusion coefficients of $Hmim^+$ cations and anions show the following trends: [Hmim][Cl] < [Hmim][Br], which suggests that larger anions lead to faster diffusion. Simliar trends are seen in diffusion of cations and hydrophobic anions where [Hmim][PF_6] < [Hmim][OTf] ~ [Hmim][NTf_2]. While in general larger anions lead to higher diffusion, the intermediate size of the BF_4^- anion does not follow this trend. For example, the diffusion of cations and anions in [Hmim][BF_4] IL resemble more

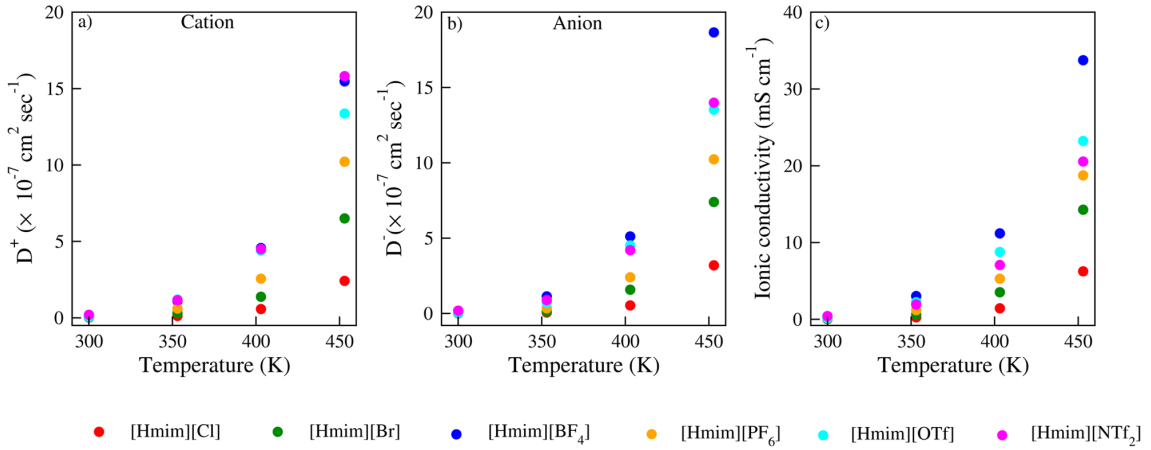

Figure 2.5: Effect of temperature on: diffusion coefficients of a) Cations and b) Anions, c) Ionic conductivity.

closely that in [Hmim][NTf_2] IL. This could also be due to the shape of the BF_4^- anion which plays a role in diffusion. A significant effect of temperature on the magnitude of diffusion coefficients of cations and anions is seen between T = 353 K and 453 K. For example, diffusion coefficients of $Hmim^+$ cations are 10 - 30 times larger and anions are 15-55 times larger at 453 K compared to 353 K. The increase in diffusion coefficients of cations and anions at 453 K is more significant in [Hmim][Cl] and [Hmim][Br] ILs, which shows that mobility of smaller anions increases significantly at higher temperatures.

Tsuzuki et al. [76] reported the following trends in diffusion coefficients: NTf_2^- > OTf^- > BF_4^- ~ PF_6^- at 353 K. Our calculated diffusion coefficients shows that BF_4^- > NTf_2^- ~ OTf^- > PF_6^- > Br^- > Cl^-. The differences in trends in diffusion coefficients between the two investigations can be due to the choice of cation, system size, and simulation time scale used for calculation of dynamical properties. For example, the magnitude of diffusion coefficients from our work using 512 IPs is ~ 1.5 times higher than that reported by Tsuzuki et al. [76] using 125 IPs. The effect of system size and simulation time scales to compute accurate diffusion coefficients have been discussed previously by Bhargava and Balasubramanian [109], Chaban et al. [110] and Gabl et al. [111]. For example, Gabl et al. [111] studied the effect of size and simulation times on the structural and dynamical properties on 1-ethyl-3-methylimidazolium triflate IL. The authors also concluded that

increasing system size shows different values of diffusion coefficients. The authors concluded that at least a system containing 500 IPs and simulation time scales of 20-30 ns were required for accurate prediction of dynamical properties. Due to high viscosity of these ILs [107], especially at room temperature, our results show that at least 200 nanoseconds of simulation time at 300 K, and 50 ns of simulation time at higher temperatures are necessary to observe a linear diffusive regime.

By use of the diffusion coefficients, the ionic conductivity is calculated (see section 1.6.3). The calculated ionic conductivities are shown in Figure **2.5**c. Similar to diffusion coefficients, ionic conductivities are lower in [Hmim][Cl] and [Hmim][Br] ILs and higher in [Hmim][NTf_2] and [Hmim][BF_4] ILs, where ionic conductivities of all ILs at 453 K are 10-25 times higher compared to 353 K. Tokuda et al. [112] employed NMR spectroscopy at 300 and 353 K and reported that ionic conductivities increases: [Bmim][PF_6] < [Bmim][OTf] < [Bmim][NTf_2] < [Bmim][BF_4], which shows that trends from our calculated ionic conductivities support their experimental observations.

Tokuda et al. [113] reported that the magnitude of IE calculated between a 1-ethyl-3-methylimidazolium cation with anions exhibit the following trends: BF_4^- > OTf^- > NTf_2^- ~ PF_6^-. The authors have compared the IE with diffusion coefficients of anions at 353 K. Subsequently, Bernard et al. [114] calculated IP binding energy of cations with few anions to elucidate its relationship with transport properties. The authors concluded that dispersion interactions are linearly related to viscosity (conductivity) for the three anions used in their work. Matthews et al. [115] calculated dimer IP energies between the 1,3-dimethylimidazolium cation with various anions. The authors choose several conformers for each IP and attempted to examine the relationship between the IE and anionic size. The authors concluded that interaction of cation with BF_4^- anion leads to the lowest IE, though larger and smaller size anions have higher IE. However, theoretical attempts to discern a relationship between the magnitude of diffusion coefficients (or IE) with anionic size have remained inconclusive. Also, IP binding energies (from quantum chemistry methods) and nonbonded potential energies (from MD simulations) have been calculated though there have been no systematic trends with diffusion coefficients nor could they explain the high-

est diffusion (conductivity) seen in [Hmim][BF_4] IL. Similarly, a comparison of hydrogen bond lifetimes (calculated between the cation and various sites of anions from MD simulations) could not correlate the magnitude of diffusion coefficients with anionic size.

To address this issue, IP lifetimes are characterized which is proposed by Zhang and Maginn [116]. The algorithm used for calculation of IP lifetimes is discussed in the work of Brehm and Kirchner [108]. The distance criteria chosen for calculation of IP lifetimes are shown in Table **A2-2** (Appendix A). Since these ILs exhibit slow dynamics at T = 300

Table 2.1: IP Lifetimes.

IL	Lifetime (ps)		
	T = 353 K	T = 403 K	T = 453 K
[Hmim][Cl]	6185.35	3114.48	777.95
[Hmim][Br]	4760.90	1286.74	386.32
[Hmim][BF_4]	1600.41	514.12	198.87
[Hmim][PF_6]	2908.32	944.30	314.56
[Hmim][OTf]	2220.71	693.71	272.54
[Hmim][NTf_2]	2364.78	778.31	308.71

K (apparent from the very small diffusion coefficients), IP lifetimes are compared only at T = 353, 403, and 453 K. In order to obtain accurate IP lifetimes, trajectories corresponding to 20-50 ns of the production run have been chosen. The IP lifetimes are shown in Table **2.1**. At each temperature, the [Hmim][Cl] IL shows the highest IP lifetime corresponding to the slowest diffusion due to the high association of the $Hmim^+$ cation with the Cl^- anion. The highest diffusion (conductivity) of BF_4^- anion is due to the lowest IP lifetime in [Hmim][BF_4] IL. The lower IP lifetime suggests that the $Hmim^+$ cation and BF_4^- anions are in a more dissociated state compared to other ILs. A comparison of IP lifetimes in all ILs shows consistent behavior with their respective diffusion coefficients and conductivities.

Chapter 3

Interplay of phase separation, tail aggregation, and micelle formation in the nanostructured organization of hydrated imidazolium ionic liquid

3.1 Introduction

In this chapter, the effect of water concentration on structural properties of hydrophobic imidazolium IL ([Hmim][NTf_2]) is examined. The effect of water on various properties of IL has been a subject of several investigations due to their applications in electrochemistry [117], catalysis [118], CO_2 absorption [119], oil recovery [120] and biomass treatment [121]. Several studies have focused on physical properties like density [122–124], viscosity [125], surface tension [126], molar excess volume [127] and structural properties [123], which change on the addition of water to or absorption of water by ILs. An absorption of water [128, 129] by these ILs or mixtures with water leads to a change in physicochemical properties such as viscosity, ionic conductivity, and solubility [122, 130]. ILs containing a short alkyl chain (e.g., ethyl) on the imidazolium cation and small size anions (Br^- or BF_4^-) form a homogeneous solution when mixed with water and can be

used in catalysis and electrochemical applications [131]. However, ILs with a longer alkyl chain (e.g., hexyl, octyl, etc.) on the imidazolium cation with large size anions ($CF_3SO_3^-$, bis(trifluoromethylsulfonyl)imide (NTf_2^-)) show a phase separation when mixed with water and show applications as green solvents, catalysis, and metal ion extraction [132–134].

Cammarata et al. [135] characterized the influence of water on interactions with ILs with imidazolium cations and several inorganic and organic anions. The authors concluded that water absorption by these ILs is influenced by hydrogen bonding interactions between anions and water molecules. Rivera-Rubero et al. [136] investigated the influence of gas-hydrophilic and hydrophobic IL interface using surface-sensitive vibrational spectroscopy. The authors concluded that orientations of cations (the imidazole cation) of hydrophilic ILs were unaffected on interaction with water. However, the authors discovered that the cations of hydrophobic ILs show a reorientation on interaction with water molecules. Takamuku et al. [137] investigated the effect of water on structure of 1-ethyl-3-methylimidazolium tetrafluoroborate ([Emim][BF_4]) IL. The authors observed hydrogen bonding interactions between anions and water molecules occur only at low water concentration. Saha et al. [138] characterized the effect of water on the molecular structure of nitrile functionalized ILs using X-ray diffraction and infrared (IR) spectroscopy. The authors observed conformational changes of the n-butyronitrile side chain of the cation due to hydrogen bonding interactions between anions and water molecules. Freire et al. [139] investigated the miscibility of water with [$C_n$mim][NTf_2] (n = 2-8) ILs using calorimetry and UV spectroscopy. The authors observed that hydrophobicity of these ILs increases with side chain length of the alkyl group of the imidazolium cation. Fazio et al. [140] and Zhang et al. [141] employed Raman and far-IR spectroscopy to characterize structural organization of 1-ethyl-3-methylimidazolium tetrafluoroborate ([Emim][BF_4]) and 1-butyl-3-methylimidazolium tetrafluoroborate ([Bmim][BF_4]) ILs at various water concentrations. The authors observed at low water concentration hydrogen bonding interactions exist between anions and water molecules. However, with increasing water concentration, competing interactions between anion-water and water-water lead to a decrease in cohesion between cations and anions.

Hanke et al. [142] performed MD simulations to characterize interactions of water molecules with 1,3-dimethylimidazolium chloride ([Dmim][Cl]) and 1,3-dimethylimidazolium hexafluorophosphate ([Dmim][PF_6]) ILs. Similar to experimental observations, the authors observed that at low water concentration hydrogen bonding exists between anions and water molecules. However, at high water concentration, water-anion interactions weaken, leading to the formation of water channels. Sieffert et al. [143] employed MD simulations to investigate interfacial properties between water and 1-butyl-3-methylimidazolium bis(trifluoromethylsulfonyl)imide ([Bmim][NTf_2]) ILs. The authors observed that water molecules interact preferentially with the oxygen atom of the NTf_2^- anion and the imidazolium ring of the $Bmim^+$ cation. Bernardes et al. [144] also observed the presence of water clusters at low water concentration and water channels at high water concentration when mixed with 1-ethyl-3-methylimidazolium ethylsulfate ILs. Voth and co-workers [145, 146] employed MD simulations to characterize structure and dynamics of 1-octyl-3-methylimidazolium [Omim] ILs at various water concentrations. The authors observed an order micelle structure at the ”turnover” region. The authors concluded that at low water concentration water-anion interactions dominate over water-water interactions, with a reverse trend observed at high water concentrations. Similar trends were observed from the MD simulations of Niazi et al. [147] on hydrated [Emim][Cl], [Bmim][Cl], and 1,3-dimethylimidazolium dimethylphosphate ([Dmim][DMP]) ILs. Voth and co-workers [146] employed MD simulations on three hydrated imidazolium ILs to investigate the effect of alkyl side chain length (on the imidazolium cation) on structural and dynamical properties. The authors observed that cationic tail aggregation increases with the length of the alkyl side chain. Balasubramanian and co-workers [148, 149] performed MD simulations on hydrated [Bmim][PF_6] ILs and observed the formation of cationic clusters at high water concentration. Klein and co-workers [150–153] performed MD simulations to investigate the effect of alkyl side chain length in [$C_n$mim][Br] (n = 2-8) IL at various water concentrations. The authors observed less cationic tail aggregation in [Bmim][Br] IL, whereas several cationic tail aggregates was observed in 1-hexyl-3-methylimidazolium bromide ([Hmim][Br]) and 1-octyl-3-methylimidazolium bromide ([Omim][Br]) ILs. The

authors also reported a micelle-like formation of imidazolium cations in [Hmim][Br] and [Omim][Br] ILs. Maginn and co-workers [154] performed MD simulations to investigate the effect of hydrophobic and hydrophilic anions on the structural properties of hydrated imidazolium-based ILs. The authors observed the dissociation of these ILs in water shows the following trends: $[C_6mim][NTf_2] < [C_4mim][NTf_2] < [C_2mim][NTf_2] < [C_2mim][C_2H_5SO_4] < [C_2mim][Cl]$. The authors concluded that increasing alkyl chain length on the cation (for the same anion) leads to lower dissociation of the IL.

To summarize, MD simulations performed so far have examined the effect of anions, alkyl chain length of the imidazolium cation, and water concentrations on structural properties of several imidazolium ILs. These studies have examined various interactions between these ILs and water molecules and have supported observations from experiments. However, existing MD simulations have focused predominantly on ILs with hydrophilic anions. The objective of the present work is to examine the effect of various water concentrations on interactions in an IL containing hydrophobic anion. The 1-hexyl-3-methylimidazolium bis(trifluoromethylsulfonyl)imide ([Hmim][NTf_2]) IL is chosen for this investigation. The [Hmim][NTf_2] IL is known for applications in extraction of metal ions from wastewater and CO_2 absorption [155]. The present work applies MD simulations to examine the effect of water concentrations (from a dry to an extremely humidified IL environment) on the following interactions: cation-anion, cation-cation, anion-anion, cation-water, anion-water, and water-water. The phenomenon of phase separation between IL and water molecules, cationic tail aggregation, and micelle formation of IL is also examined. The IE (from the nonbonded interactions of MD simulations) between IL-IL, IL-water, and water-water is analyzed.

3.2 Computational details

MD simulations of [Hmim][NTf_2] IL and its mixtures are performed using the GROMACS 4.5.4 [99] program. The force field parameters of the [Hmim][NTf_2] IL are taken from the work of Tsuzuki et al. [76] The water molecules are modeled using a SPC/E [156]

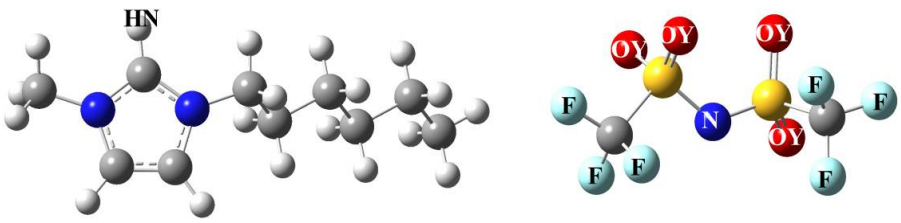

Figure 3.1: Chemical structure of 1-hexyl-3-methylimidazolium bis- (trifluoromethylsulfonyl)imide ([Hmim][NTf_2]). Color scheme:nitrogen (blue), carbon (gray), hydrogen (white), fluorine (cyan),oxygen (red), sulfur (yellow).

force field. The cutoff distance for non-bonded interactions is chosen as 12 Å. The long-range electrostatics is calculated using the particle mesh Ewald (PME) [100, 101] method. The leapfrog algorithm [78] is chosen as an integrator with a 1 fs time step. Temperature is maintained using the Nosé - Hoover [105, 106] thermostat with a coupling constant of 0.2 ps. The pressure of 1 bar is controlled using a Berendsen barostat [104] with a coupling constant of 1.0 ps.

The chemical structure of a $Hmim^+$ cation and NTf_2^- anion is shown in Figure **3.1**. The input configurations of [Hmim][NTf_2] IL-water mixtures are created as follows: Each IP is solvated to mimic a very low to extremely humidified environment. For example, $\lambda = 5$ (λ is defined as the number of water molecules per IP) is denoted as a single IP solvated by five water molecules. A similar procedure is employed to create IL-water mixtures with increasing amount of water molecules, where $\lambda = 200$ is the highest water concentration used in this study. A single IP solvated with water molecules is replicated in a cubic box, where each IL-water mixture contains 125 IPs with varying λ. Each configuration of the replicated IL-water mixtures is energy minimized using the steepest descent algorithm [102]. The energy minimized configuration is chosen as an input for a simulated annealing performed in the following manner: Each configuration is warmed from 453 to 703 K (in steps of 50 K every 250 ps) and then equilibrated for 500 ps at 703 K. The final configuration from the equilibration at 703 K is cooled to 453 K (steps of 50 K every 250 ps) and equilibrated for 500 ps at 453 K. The simulated annealing procedure performed using the NPT ensemble is repeated twice to achieve a random mixing of wa-

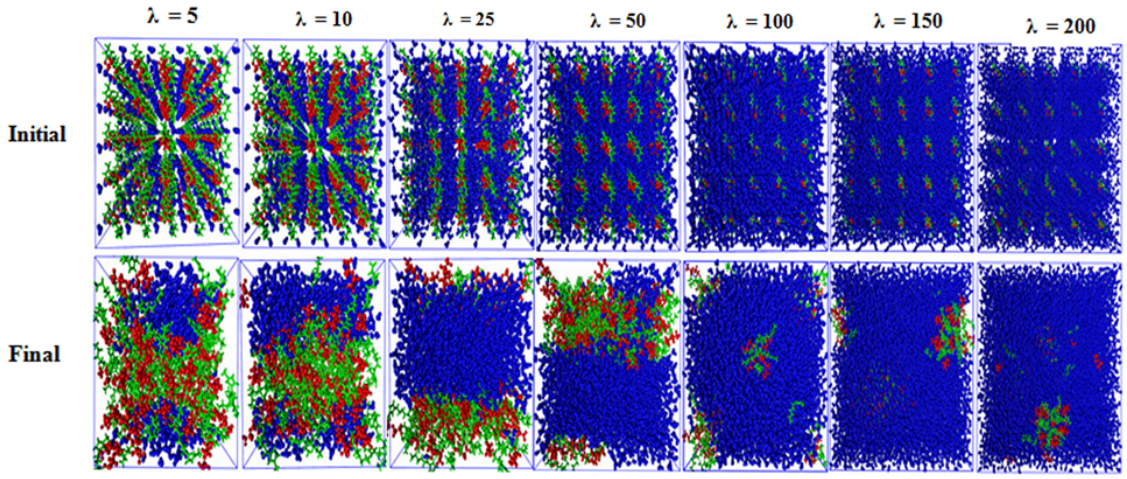

Figure 3.2: Snapshots of IL-water mixtures from annealing. Color scheme: (green) [$Hmim^+$] cation; (red) [NTf_2^-] anion, and (blue) water.

ter molecules and IL for a total simulation time of 7.25 ns. The heterogeneous mixing of water molecules with IL (for each λ) is seen by a comparison of initial and the final configuration from annealing (see Figure **3.2**). In order to ensure that configurations of these IL-water mixtures are not trapped in local minima, each IL-water mixture (input from the final configuration of annealing) was further equilibrated for a 5 ns NPT at 453 K. The final configuration from the equilibration at 453 K was chosen as an input for a subsequent 5 ns NPT equilibration at 303 K. The instantaneous density with equilibration time (see Figure **B3-1** of Appendix B) shows these IL-water mixtures to be well equilibrated. As a benchmark, the simulated density of 1.386 g cm^{-3} of neat IL is in excellent agreement with a previously reported density [76] of 1.366 g cm^{-3} . The system sizes, density, and box length of IL-water mixtures are shown in Table **3.1**. The equilibration run is followed by a 20 ns NVT production run at 303 K, where positions and velocities of IL-water mixtures are recorded every 5 ps to examine various interactions using RDFs [78].

Table 3.1: System Sizes, Density, and Box Length of [Hmim][NTf_2] IL-Water Mixtures.

no. of ion pairs	no. of water molecules	λ	water (wt %)	total no. of atoms	density (g cm^{-3})	box length (Å)
125	0	0	0	5750	1.385	38.17
125	625	5	16.74	7625	1.302	44.07
125	1250	10	28.69	9500	1.245	47.08
125	3125	25	50.14	15125	1.156	54.38
125	6250	50	66.79	24500	1.095	63.48
125	12500	100	80.01	43250	1.051	76.29
125	18750	150	85.78	62000	1.037	85.73
125	25000	200	88.94	80750	0.989	93.58

3.3 Results and discussion

The RDFs (see section 1.6.1) and coordination numbers (calculated at the first minima) from cation-anion, cation-cation, and anion-anion interactions are shown in Figure 3.3. The RDFs from cation-anion interactions (cation: center of the imidazolium ring) show increasing peak intensity with hydration. However, the cation-anion distributions of neat and hydrated ILs show similar peak characteristics with a first minima at 8.8 Å. The coordination number shows a decrease with increase in water concentration due to reduced electrostatic interactions between the cations and anions. The cation-cation RDFs show the following features: At low water concentration (λ = 5 and 10), the RDFs show two peaks at 7.9 and 10 Å and resemble the characteristic features of cation-cation interactions in neat [Hmim][NTf_2] IL. With increase in water concentration, a single peak at 9.1 Å is observed. Similar to cation-anion interactions, the coordination numbers show a decrease with water concentration, which suggests water molecules introduce several competing interactions. Similar features are observed in anion-anion RDFs and the respective coordination numbers. A visual inspection of snapshots of IL at various concentrations (see Figure 3.4) extracted from the production run shows the following features. At λ = 5,

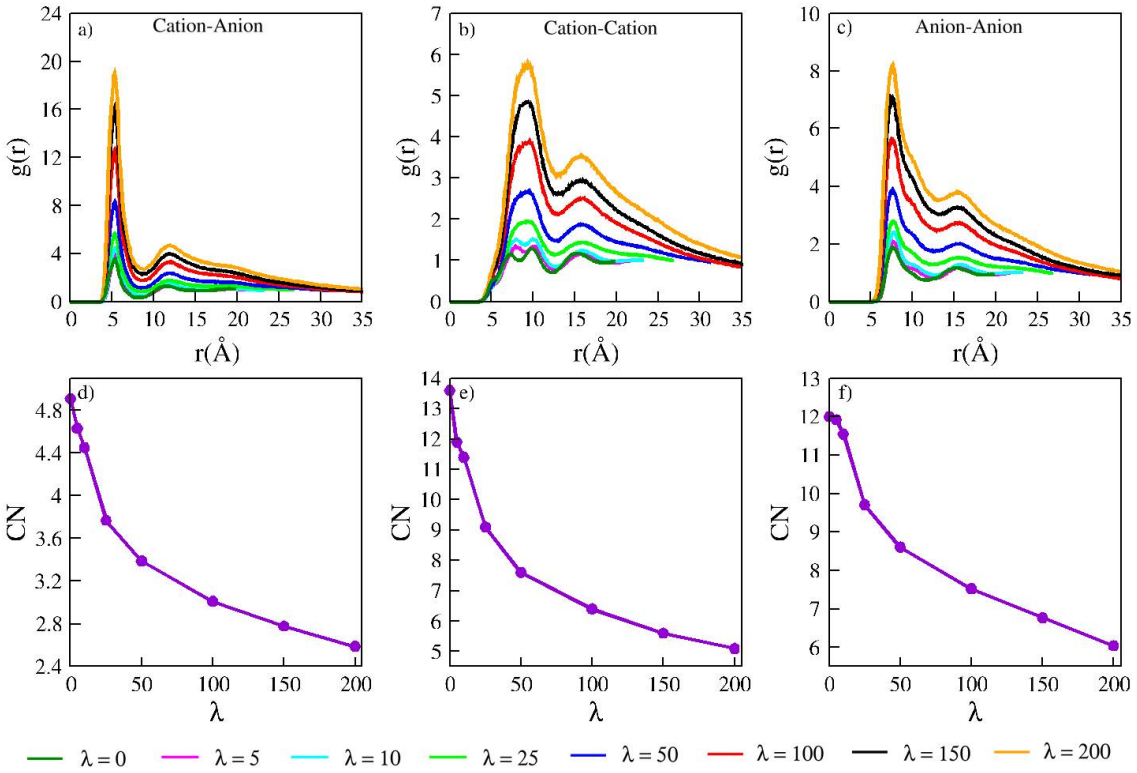

Figure 3.3: RDFs and coordination numbers of (a, d) cation-anion, (b, e) cation-cation, and (c, f) anion-anion interactions.

water molecules are surrounded by cations and anions. At λ = 10, a channel formation of water molecules is seen. At λ = 25 and 50, a distinct phase separation between water molecules and IL is observed. At λ = 100, aggregates of cation-anion pairs solvated by large number of water molecules are seen. At λ = 150 (and λ = 200), aggregates of cation-anion pairs, several free anions, and cations solvated by large number of water molecules are observed. Further examination of various possible interactions using interaction sites on cations, anions, and water molecules is seen from the RDFs discussed below.

The interaction between the acidic hydrogen (HN) of the positively charged imidazolium cation with various electronegative atoms of the anions is shown in Figure **3.5**. The RDFs are normalized by the number of similar atoms present in the anion. For each water concentration, the following features are observed: The HN-N RDFs (see Figure **3.5**a) show a strong interaction with a first sharp peak at 2.6 Å and a secondary peak at 4.7

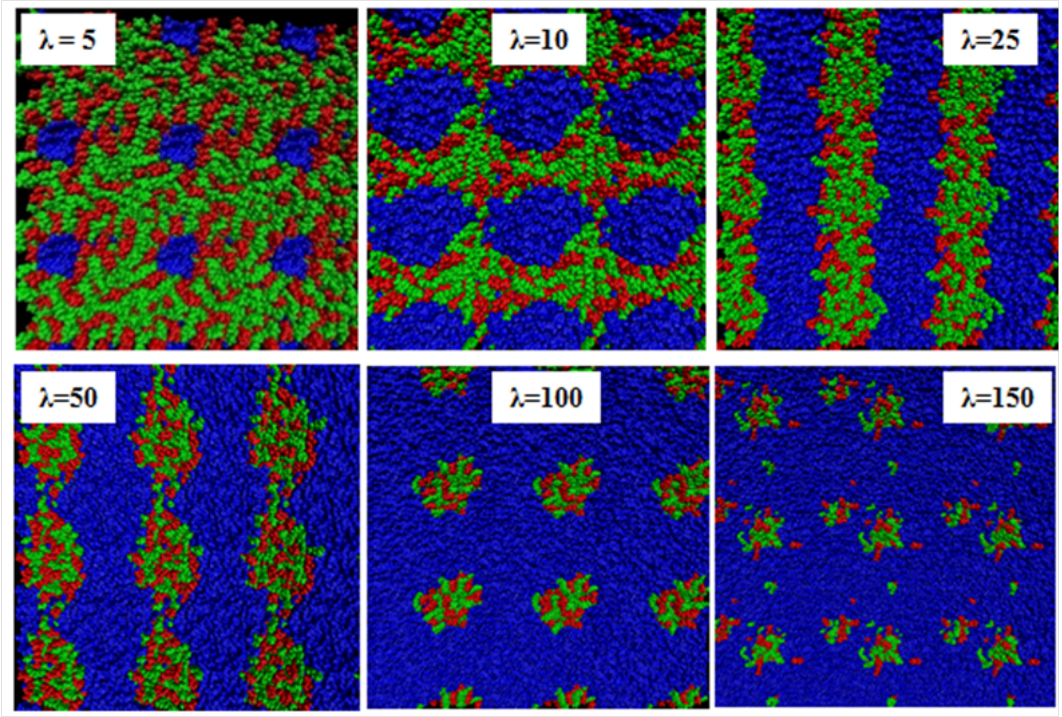

Figure 3.4: Snapshot (using periodic boundaries) from a 20 ns production run at various water concentrations. Color scheme: (green) [$Hmim^+$] cation, (red) [NTf_2^-] anion, and (blue) water.

Å. The HN-OY RDFs (see Figure **3.5**b) show a first sharp peak at 2.5 Å and a broad secondary peak at 4.8 Å. The coordination number from the HN-N RDFs (see Figure **3.5**d) shows the following trends: For neat IL, a coordination number of 0.36 is obtained. With increasing water concentration, the coordination number decreases gradually to 0.17 (λ = 200). Similar trends are seen from HN-OY (see Figure **3.5**e) and HN-F (See Figure **3.5**f) RDFs. A comparison of the intensity (y-axis of RDFs) from these RDFs shows strong hydrogen bonding with the nitrogen atom, compared to the oxygen atom for neat and hydrated ILs. This is due to the more negative charge on the nitrogen atom compared to the oxygen atom of the NTf_2^- anion. The HN-F RDFs (see Figure **3.5**c) show no peaks and suggest that fluorine atom does not participate in hydrogen bonding interactions.

Voth and co-workers [145, 146] and Klein and co-workers [150–153] observed hydrogen bonding interactions between hydrophilic anions and water molecules. In order to examine hydrogen bonding between cations/anions and water molecules, cation-water

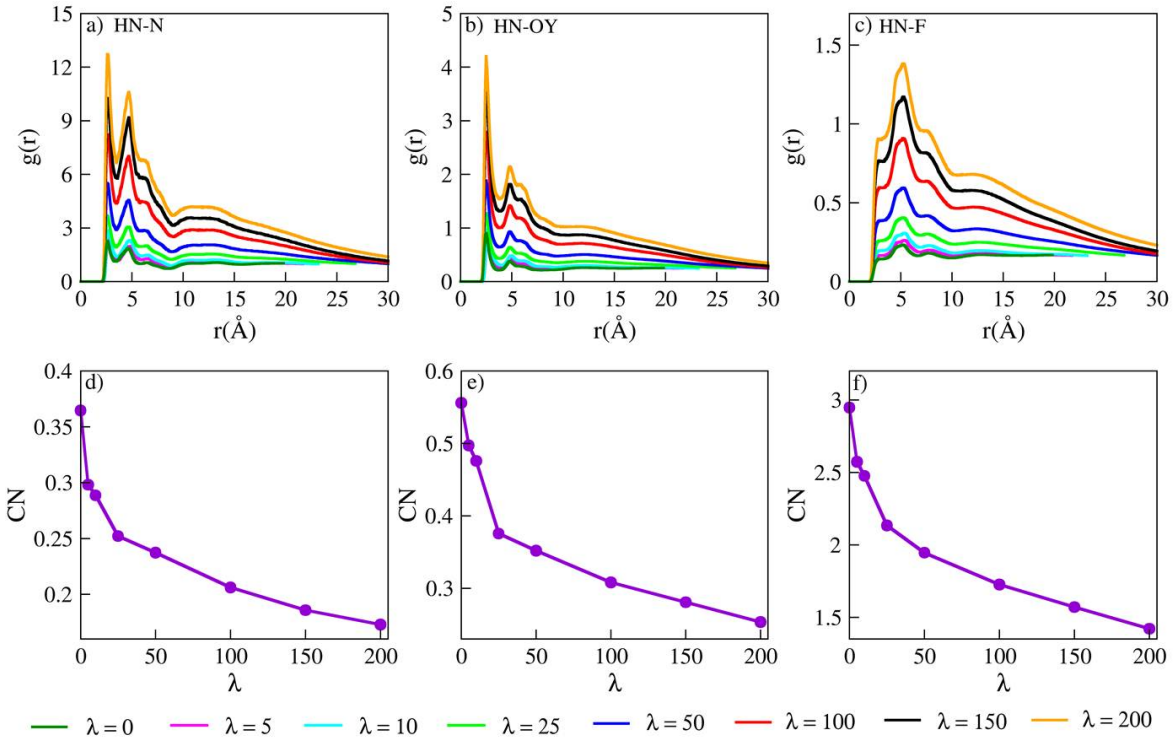

Figure 3.5: Hydrogen bonding interactions and coordination numbers (atoms on the anions with the acidic hydrogen atom (HN) of imidazolium ring of cation).

and anion-water RDFs have been calculated (see Figure **B3-2** of Appendix B). The cation-water and anion-water RDFs illustrate the hydrophobic nature of the [Hmim][NTf_2] IL. A characterization of interactions of water molecules with atoms of the cations and anions is shown in Figure **B3-3** (Appendix B). The RDFs shows that water molecules do not have hydrogen bonding with any atoms of the cations and anions due to the hydrophobic nature of this IL. The observed trends are consistent with the work of Maginn and co-workers [154] where the authors reported weak hydrogen bonding in cation-water and anion-water interactions. The water-water RDFs, coordination numbers (at the first minima), and snapshots are presented in Figure **3.6**. At λ = 5, the water-water interactions shows a definite structure with three peaks and a coordination number of 3.96. At λ = 5, the first peak occurs at 2.8 Å, which suggests the presence of nanoclusters of water molecules. At λ = 10, this peak show reduced intensity, with a coordination number of 4.23. With increasing water concentration (λ = 15 to λ = 200), the intensity of the water-

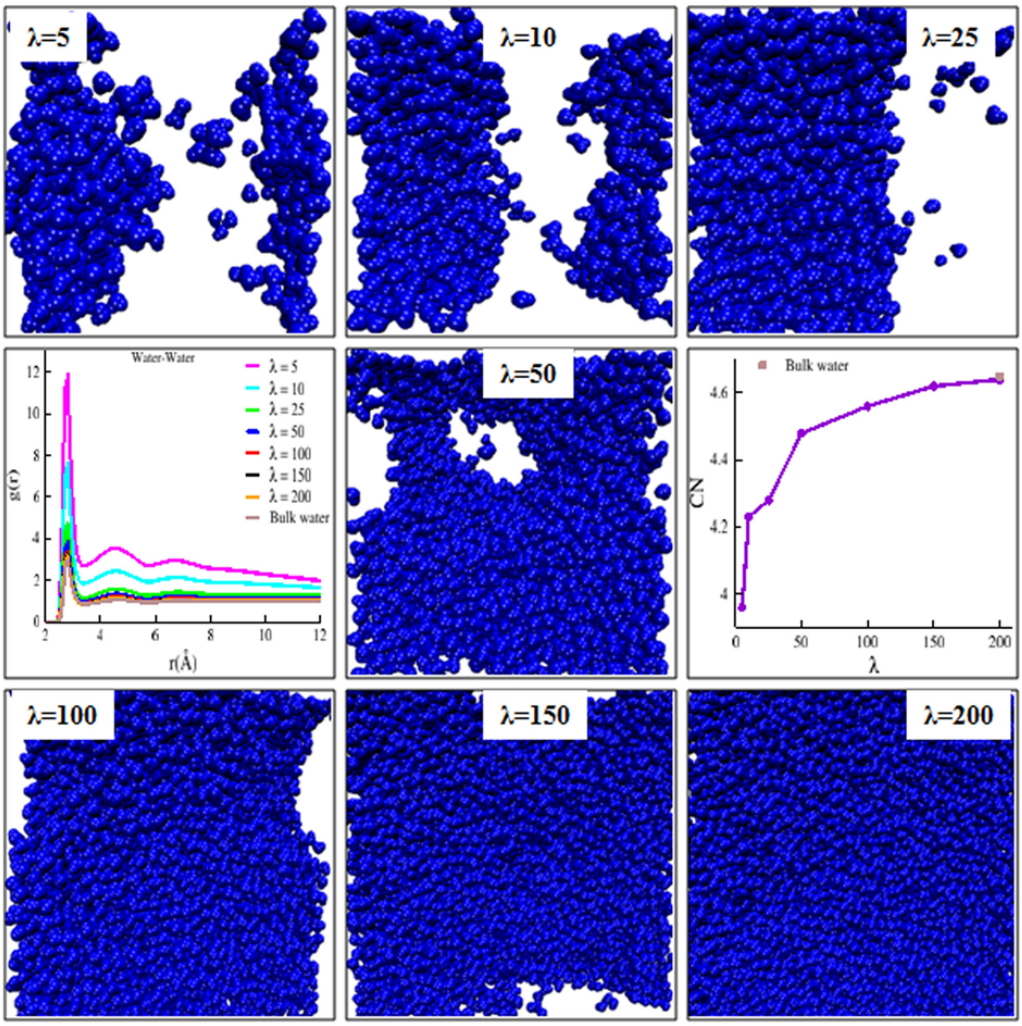

Figure 3.6: Snapshots of water aggregation from a 20 ns production run (blue color: water). RDFs and coordination numbers from water-water interactions.

water peak further diminishes, which suggests that water molecules exist as bulk water as seen from the coordination number of 4.65.

Voth and co-workers [145, 146] concluded that tail aggregation of cations occurs due to competing nonbonded interactions between the cations. The authors concluded that repulsion between the polar head (imidazolium cation) leads to alkyl tails to come closer to form cationic tail aggregates. The authors observed cationic tail aggregation in hydrophilic ILs with a longer alkyl chain (1-octyl-3-methylimidazolim) on the imidazolium cation at high water concentration. In order to understand the mechanism of cationic tail

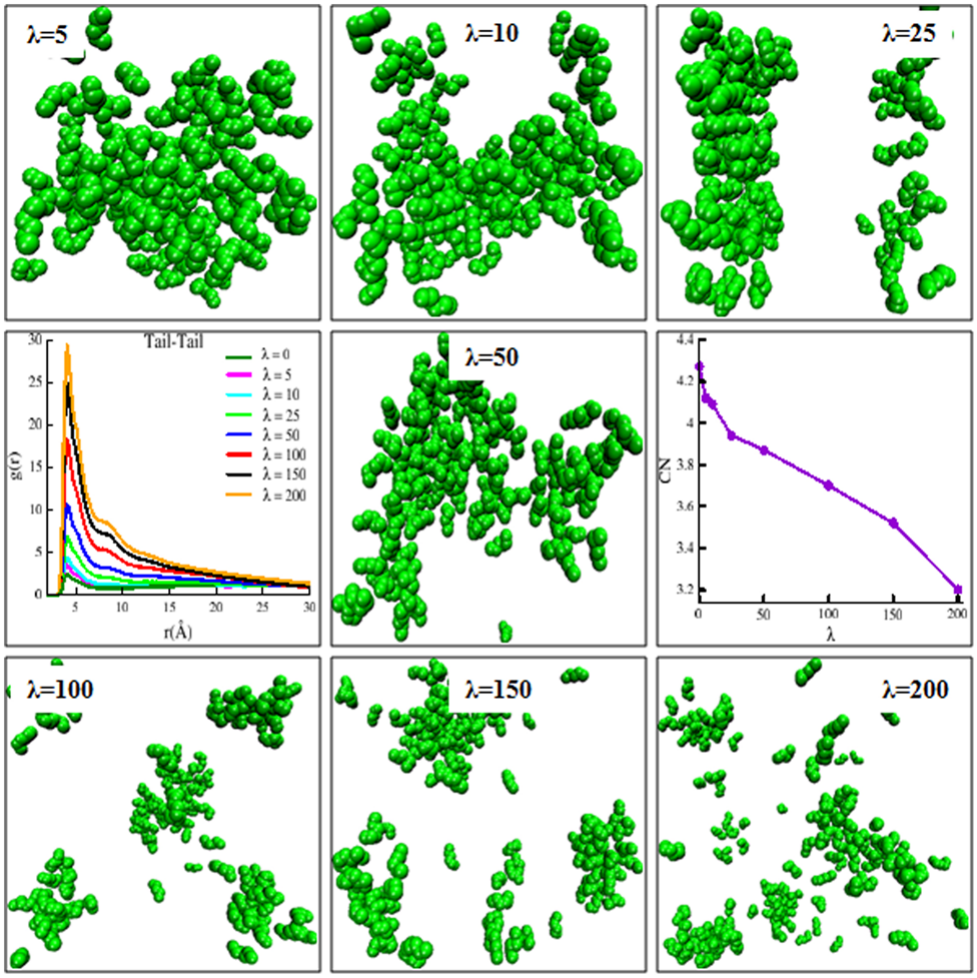

Figure 3.7: Snapshot of cationic tail aggregation at various water concentrations (green color: terminal carbon atom (hexyl tail) of the imidazolium cation). RDFs and coordination numbers from cationic tail-tail interactions.

aggregation, the cationic tail-cationic tail RDFs (tail: terminal carbon atom) are characterized with representative snapshots (see Figure 3.7). The neat IL does not show tail aggregation due to the presence of strong electrostatic interaction between IPs. However, at λ = 5, 10, and 25, few cationic tail aggregates are observed due to reduced electrostatic interactions between cations and anions (as seen from snapshots in Figure 3.7). At λ = 50, more cationic tail aggregates are observed which further increases at $\lambda \geq 100$. The observation of cationic tail aggregation is supported by a visual examination (see Figure 3.8) of micelle of ILs. The micelles are formed where the polar head faces the anions and water

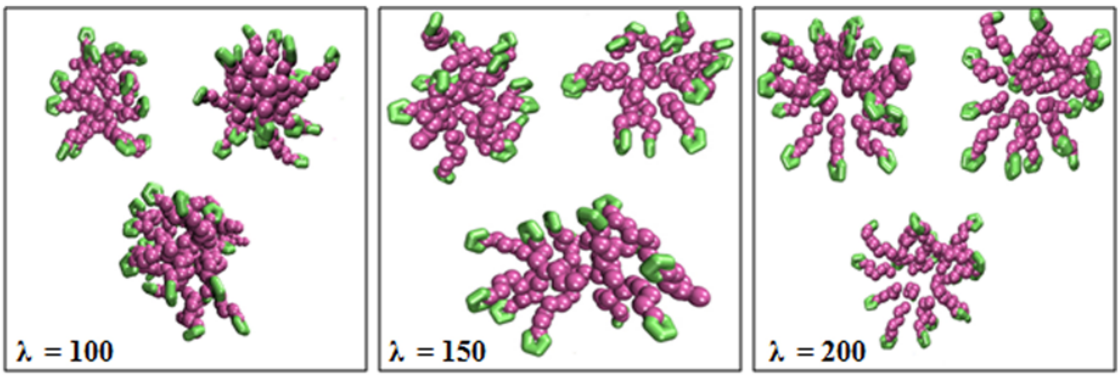

Figure 3.8: Micelle formation at λ = 100, 150, and 200 (green: imidazolium ring; purple: hexyl group attached to imidazolium ring; anions and water molecules are not displayed).

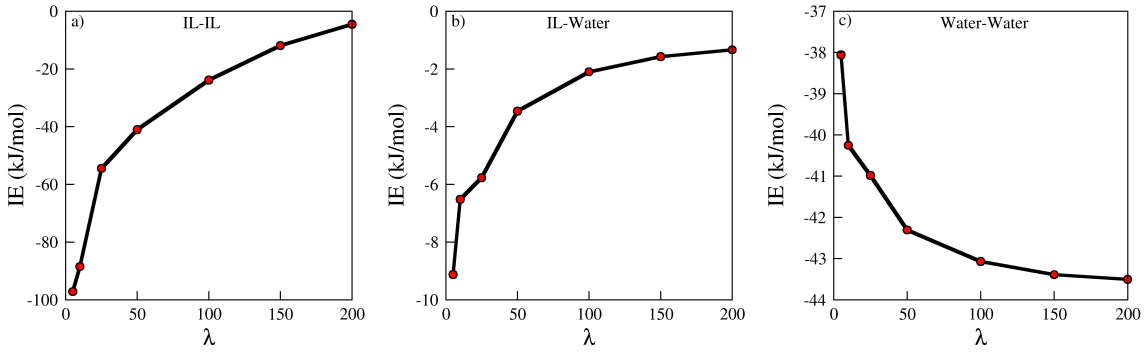

Figure 3.9: IE (calculated from nonbonded potential energies).

molecules, whereas nonpolar groups (alkyl side chain) face inward. At λ = 100, a disordered micelle structure is observed. At λ = 150 and λ = 200, ordered micelle structures are observed. However, micelles of IL were observed by Voth and co-workers [145, 146] at much higher water concentrations (90 wt %) on ILs containing hydrophilic anions and long alkyl chain length on the cations. Similarly, Klein and co-workers [150–153] also observed the formation of micelles of ILs containing hydrophilic anions at very high water concentration. The snapshots (see Figure **3.8**) that micelles can be observed even at much lower water concentration on ILs with hydrophobic anions (NTf_2^-) and cations with long alkyl chain lengths.

In order to quantify the interactions at various water concentrations, the IE between IL-IL, IL-water, and water-water interactions is calculated. The IE is derived from nonbonded potential energies (MD simulations). The calculated IE and nonbonded potential

energies are presented in the Appendix A (see Table A3-1 of Appendix A). The IE vs λ is shown in Figure **3.9**. The IE show the following trends: The IL-IL IE decreases with an increase in water concentration (see Figure **3.9**a). For example, the IL-IL IE is -97.15 kJ/mol (λ = 5) and drops significantly to -54.52 kJ/mol (λ = 25). Further increase in water concentration shows a steady decrease in IE from -41.04 kJ/mol (λ = 50) to -4.52 kJ/mol (λ = 200). Similar trends are observed in IL-water interactions (see Figure **3.9**b). For example, the IL-water IE is -9.12 kJ/mol (λ = 5). At λ = 25, the IE is -5.77 kJ/mol and asymptotically reaches to -1.34 kJ/mol (λ = 200). However, water-water IE increases with water concentration (see Figure **3.9**c). At λ = 5, the IE is -38.07 kJ/mol and increases to -42.30 kJ/mol (λ = 50). Further, increase in water concentration shows a water-water IE of -43.51 kJ/mol (λ = 200). The decrease in interactions between IL-IL and IL-water is compensated by increasing water-water interactions. A comparison of IE shows that the strength of IL-IL interactions is higher than water-water interactions and IL-water interactions.

Chapter 4

Translational and rotational dynamics in hydrophilic/hydrophobic anions based imidazolium ionic liquid-water mixtures

4.1 Introduction

In this chapter, the effect of water concentration on translational and rotational dynamics in hydrophilic/hydrophobic anions based imidazolium IL-water mixture is investigated. Haberler et al. [157] investigated the effect of water on hydrated [Emim][NTf_2] IL and observed that water molecules form a network with anions. The authors calculated the translational and rotational dynamics using a laboratory and body-fixed frame. Wong et al. [158] examined the molar conductivities (at infinite dilution) of ILs with $Emim^+$ cations and various anions (BF_4^-, $C_2H_5SO_4^-$, and $CF_3SO_3^-$). A finding from their study was that a decrease of anionic mobility occurs with an increase in its effective hydrodynamic radius [159]. Porter et al. [160] used MD simulations to characterize dynamics in hydrated [Emim][BF_4] and [Emim][NTf_2] ILs. The authors reported the presence of water clusters of different sizes where hydrogen bonds are with two anions, where the role of cation was

found to be insignificant. The authors concluded that longer simulation times were required to observe the diffusive behavior of ILs. Further, diffusion of BF_4^- and NTf_2^- anions decrease significantly up to 1% molar amount of water, with an increase observed with hydration. Spohr and Patey [161] examined interactions in model ILs and concluded that replacement of counter-anions around the cation by water molecules lead to a decrease in viscosity (increased ionic conductivity). The authors also observed the formation of anion-water chains in the size disparate model of ILs. Heintz et al. [162] observed a larger mobility of NTf_2^- anions in neat [Bmim][NTf_2] ILs compared to [Emim][NTf_2] ILs. The authors performed experiments (Taylor dispersion technique [163]) and MD simulations and concluded that at a high water concentration, there was a significant presence of solvated ions compared to few IPs. Also, the authors concluded that solvated ions have more abundance in hydrated environments compared to in methanol solvent due to the influence of polarity. Kashyap et al. [164] investigated ionic mobility in a salt solution and ILs using impedance and NMR spectroscopy. The authors concluded that the cation-anion interactions increase the conductivity in pure molten salts and RTILs, with an opposite behavior observed under hydrated conditions. Migliorati, D'Angelo and co-workers examined the structure and dynamics in hydrated [Bmim][Br] IL using EXAFS spectroscopy [165] and MD simulations [166]. The authors concluded that a complex interplay of interactions exists between cations, anions and water molecules. The authors further observed the presence of solvent-shared IPs, where water molecules mediate between cations and anions. The authors also reported self-diffusion coefficients, and rotational relaxation times of cations and water molecules. Salma et al. [167] examined the effect of water concentration on structural properties of butyl-ammonium butanoate IL using X-ray experiments and MD simulations. The authors concluded that water molecules were hydrogen bonded with cations and anions of the IL. However, preferential hydrogen bonding of the water molecules with the anions was found to reduce the hydrogen bonding network in the IL, especially with increasing water concentration. In a different IL [Bmim][PF_6], Sharma and Ghorai [168] investigated the influence of water concentration on its structure and dynamics using MD simulations. The authors concluded that water molecules

do not influence cation-anion interactions even at a high water concentration. In addition, at all water concentrations, the cations and anions were found to have a similar magnitude of diffusion coefficients. Higashi et al. [169] calculated the diffusion coefficients of [Bmim][TFSI] IL using MD simulations. The authors reported that the simulations could qualitatively reproduce experimental observations, though the magnitude of diffusion coefficients was overestimated. Khabaz et al. [170] performed MD simulations on neat methyl-imidazolium based ILs containing NTf_2^- anions and concluded that diffusion coefficients increase with temperature.

Köddermann et al. [171] reported IP lifetimes in neat [Emim][NTf_2] IL (using FTIR spectroscopy and Density Functional Theory (DFT) calculations) and observed the formation of stable IPs. Fumino et al. [172] reported from DFT calculations that the IP formed between the anion and the acidic hydrogen atom (on the head of the imidazolium cation) was more stable compared to the non-acidic hydrogen atoms. MD simulations have also been used to examine the rotational correlation times in neat ILs [173, 174]. Tsuzuki et al. [173] reported that the translational diffusion coefficient of $Emim^+$ cations and perfluoroalkyltrifluoroborate anion was strongly associated with the rotational motion of the $Emim^+$ cation. Pal and Biswas [174] examined the rotational relaxation time of neat [Bmim][PF_6] IL using MD simulations at T = 298 K and T = 450 K. The authors concluded that a slow decay of the rotational correlation function of the $Bmim^+$ cations resembles a multi-exponential function. However, due to the limited time scale of the simulation runs, the authors could only observe an incomplete decay of the rotational correlation function, and hence reported qualitative trends of the rotational relaxation time.

While existing studies so far have characterized dynamical properties on several ILs, there has been no computational investigation to examine the effect of various water concentrations and temperatures on the diffusion coefficients, IP lifetimes, ion-ion and ion-water IE, and rotational correlation time of ions/water molecules in two imidazolium ILs containing hydrophilic and hydrophobic anions respectively. To address this, the ([Hmim][Cl] and [Hmim][NTf_2]) ILs have been chosen for this study. Venkatnathan and co-workers [175] characterized structural properties of hydrated [Hmim] [NTf_2] IL and

concluded that inter-ionic interactions and ion-water interactions play an important role in ion aggregation and micelle formation. The authors also concluded that at low water concentration, water molecules are surrounded by the IL molecules, a phase separated state existed at the intermediate water concentration and solvated ions/IPs were present at a higher water concentration. In a subsequent study, Venkatnathan and co-workers [176] examined the effect of various anions on the structure and dynamics in ILs containing a common $Hmim^+$ cation. The authors concluded that diffusion coefficients of $Hmim^+$ cations and anions depend on the size and shape of the anion, where Cl^- and NTf_2^- anions along with several intermediate size anions were also investigated.

4.2 Computational details

All MD simulations were performed using the GROMACS 4.5.4 [99] program. The force-field parameters for the [Hmim][Cl] IL (except for the Cl^- anion) and [Hmim][NTf_2] IL were obtained from the work of Tsuzuki et al. [76]. The force-field parameters of Cl^- anion were obtained from the work of Lopes et al. [177]. The MD simulations on neat ILs (using the force-field parameters) reproduced the properties reported in an earlier study [176]. The cut-off distance for the calculation of non-bonded interactions was chosen to be 12 Å. The long-range electrostatic interactions were calculated using the Particle Mesh Ewald (PME) [100, 101] method. The input configurations of IL-water mixtures were generated in the following manner: A single IP corresponding to each IL (see Figure **4.1** for chemical structure) was optimized and replicated to create 125 IPs in a cubic box. The replicated IPs were suitably solvated with different concentrations of water to mimic IL-water mixtures. Water concentrations are defined as ultra-low (λ = 0.25, 0.5, 1 and 2), low (λ = 5), intermediate (λ = 10 and 25) and high (λ = 50, 100, 150 and 200). To ensure a random mixing of the water molecules with ions, each solvated configuration was annealed (for a total simulation time of 7.5 ns) as follows: (a) Heating from 453 K to 703 K under NPT ensemble over a simulation time of 1.75 ns (b) The final configuration from step "a" was chosen as an initial configuration for subsequent MD simulations and

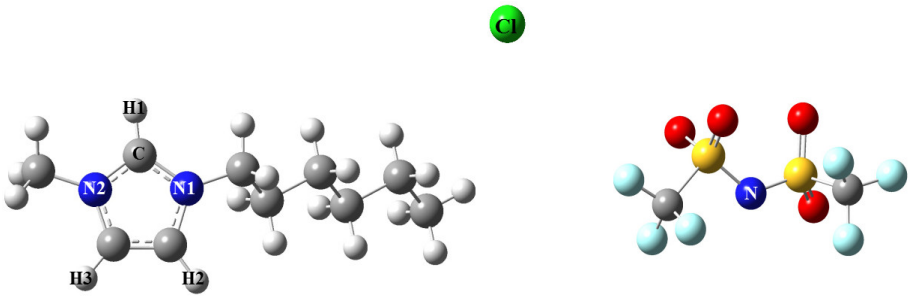

Figure 4.1: Chemical structures of 1-hexyl-3-methylimidazolium ($Hmim^+$) cation, chloride anion and bis(trifluoromethylsulfonyl)imide (NTf_2^-) anion.

cooled from 703 K to 453 K for a simulation time of 2.0 ns using the NPT ensemble. Steps "a" and "b" were repeated once and the final configuration was chosen as an input for NPT equilibration for 5 ns at T = 453 K. This was followed by MD simulations for 5 ns equilibration at T = 303 and 353 K. The temperature and pressure of the system were maintained using the v-rescale thermostat [103] and a Berendsen barostat [104], respectively, with a coupling constant of 0.1 ps and 1.0 ps. The system sizes of neat and hydrated [Hmim][Cl] and [Hmim][NTf_2] ILs with densities (from equilibration) are presented in Table **A4-1** and **A4-2** of Appendix A.

The simulated density of hydrated [Hmim][Cl] is in excellent agreement with a previously reported experimental density of Gómez et al [178]. For neat ILs and at ultra-low water concentration, 500 IPs were used in simulations to eliminate finite size effects. The dynamical properties were calculated using the trajectories recorded from a subsequent production run (NVT ensemble) at T = 303 K and 353 K. Due to slow diffusion in neat ILs and to obtain a converged rotational correlation function, production run simulations on neat [Hmim][Cl] IL were performed up to one microsecond (T = 303 K) and 200 ns (T = 353 K), respectively. Similarly, for neat [Hmim][NTf_2] IL a 50 ns production run was performed at T = 303 K. For all other water concentrations in [Hmim][Cl] and [Hmim][NTf_2] ILs at T = 303 K and T = 353 K and neat [Hmim][NTf_2] (T = 353K), a 20 ns production run was found to be very sufficient to calculate all dynamical properties. Unless explicitly specified, the discussion on dynamical properties regards simulations performed at T = 303 K. Since the trends in the dynamical properties at T = 353 K were

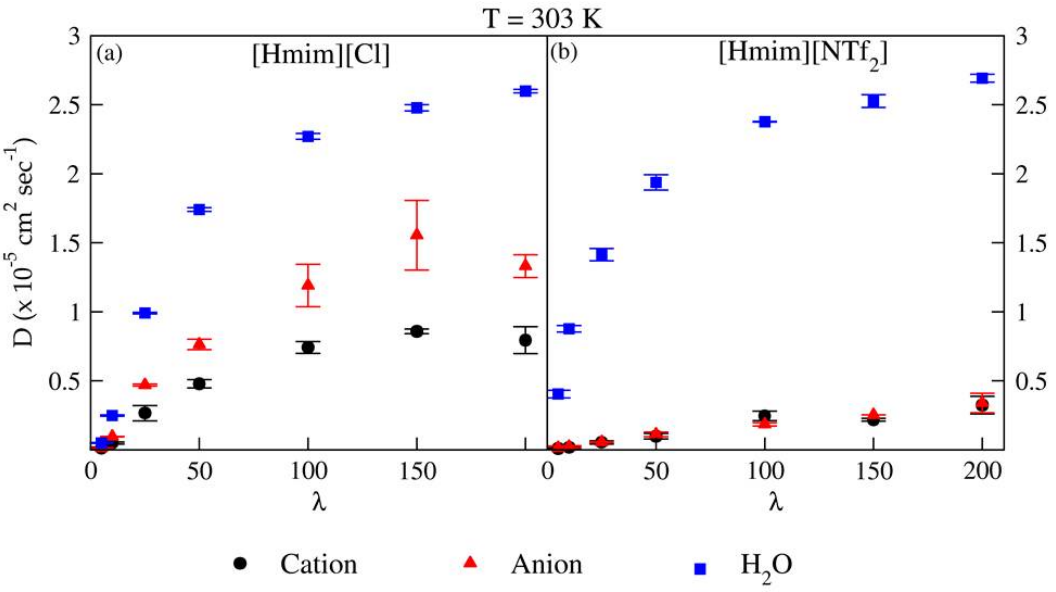

Figure 4.2: Diffusion coefficients of $Hmim^+$ cations, anions and water molecules in hydrated [Hmim][Cl] and [Hmim][NTf_2] ILs at T = 303 K.

similar to those at T = 303 K, a brief quantitative comparison between T = 353 K and T = 303 K is reported for each dynamical property.

4.3 Results and discussion

4.3.1 Mean Square Displacement

The mobility of cations, anions and water molecules is examined by the MSD (see section 1.6.2) calculated from the trajectories of the production run. The plots of log(MSD) vs. log(t) for cation, anions and water molecules are provided in Figure **B4-1** and Figure **B4-2** of Appendix B. Since linear diffusion (slope of log(MSD) vs. log(t), $\beta = 1$) is extremely difficult to observe in ILs, the diffusion coefficients (see Figure **4.2**) have been calculated from the timescale regime of MSD, where $0.9 \leq \beta \leq 1.1$.

4.3.2 Dynamics in low, intermediate and high water concentrations of [Hmim][Cl] IL

The effect of water concentration on the mobility of ions and water molecules was characterized by a comparison of the calculated diffusion coefficients. For example, at $\lambda = 5$, the diffusion coefficients of $Hmim^+$ cations and Cl^- anions are 63 and 456 times higher than the corresponding diffusion coefficients of these ions in neat [176] [Hmim][Cl] IL. The effect of water leads to an increase in the diffusion coefficients of ions as the water molecules solvate the cations and anions, disrupting the strong electrostatic cation-anion interactions. The relative mobility of the ions and water molecules can also be seen by a comparison of diffusion coefficients with an increase in water concentration. The diffusion coefficients of $Hmim^+$ cations, Cl^- anions and water molecules increase by $\sim$ 3.9, 7, and 5 times (from $\lambda = 5$ to $\lambda = 10$), $\sim$ 5.4, 4.9, and 4 times (from $\lambda = 10$ to $\lambda = 25$), and $\sim$3, 2.8, and 2.6 times (from $\lambda = 25$ to $\lambda = 200$). In neat ($\lambda = 0$) IL, the diffusion coefficient of Cl^- anions was lower than that of the $Hmim^+$ cations [176]. However, with the addition of water, an opposite trend was observed, where the diffusion coefficients of Cl^- anions are 1.1-1.8 times larger than those of $Hmim^+$ cations. The diffusion coefficients of ions and water molecules increase non-linearly up to $\lambda = 50$ and then saturate with a small increase up to $\lambda = 200$. The saturation in diffusion coefficients can be attributed to the bulk behavior of water molecules at $\lambda \geq 50$.

4.3.3 Dynamics in low, intermediate and high water concentrations of [Hmim][NTf_2] IL

The diffusion coefficients of ions and water molecules in hydrated [Hmim][NTf_2] IL show the following features: At $\lambda = 5$, the diffusion coefficients of $Hmim^+$ cations and NTf_2^- anions are 5 and 7.2 times higher compared to the corresponding ions in neat [176] [Hmim][NTf_2] IL. The diffusion coefficients of $Hmim^+$ cations, NTf_2^- anions and water molecules increase by $\sim$1.7, 1.7, and 2.2 times (from $\lambda = 5$ to $\lambda = 10$), $\sim$ 3.2, 2.5, and

1.6 times (from λ = 10 to λ = 25), and ~6, 6.1, and 1.9 times (from λ = 25 to λ = 200), respectively. In neat and hydrated [Hmim][NTf_2] IL, the mobility of $Hmim^+$ cations is almost equivalent to the mobility of NTf_2^- anions, which shows that water molecules do not influence the correlated motion of $Hmim^+$ cations and NTf_2^- anions. The similar magnitude of the diffusion coefficients of these ions is due to the equivalent molecular size and symmetry (excluding the alkyl chains on the $Hmim^+$ cation and CF_3 groups of the NTf_2^- anion) of $Hmim^+$ cations and NTf_2^- anions. The calculated diffusion coefficients of water molecules (from this work) are also in good agreement with the results of Heintz et al. [162] on [Emim][NTf_2] and [Bmim][NTf_2] ILs (λ = 200, T = 303 K). However, the diffusion coefficients of $Hmim^+$ cations and NTf_2^- anions are 3 - 4 times lower compared to the diffusion coefficients reported by Heintz et al. [162]. These differences in diffusion coefficients could arise from the force-field parameters and the choice of the cation.

4.3.4 Comparative diffusion coefficients between [Hmim][Cl] and [Hmim][NTf_2] ILs

The qualitative features of diffusion coefficients of water molecules in hydrated [Hmim][NTf_2] IL are similar to those in hydrated [Hmim][Cl] IL. The diffusion coefficients of $Hmim^+$ cations is lower [176] in neat [Hmim][Cl] IL compared to neat [Hmim][NTf_2] IL. On addition of water, the diffusion coefficient of $Hmim^+$ cations is 1.3 - 5.0 times higher in [Hmim][Cl] compared to [Hmim][NTf_2] IL, which illustrates that effect of water on the mobility of $Hmim^+$ cations is higher in the presence of Cl^- anions compared to the NTf_2^- anions. At low and intermediate water concentrations, the diffusion coefficient of water is 1.4 - 8 times lower in [Hmim][Cl] IL compared to [Hmim][NTf_2] IL, suggesting a higher interaction of water molecules with the Cl^- anions. At a high water concentration, the similarity in the magnitude of diffusion coefficients of the water molecules in [Hmim][Cl] and [Hmim][NTf_2] ILs is due to the significant presence of bulk water molecules, as can be seen from a comparison of diffusion coefficients. For example, the calculated diffusion coefficient of water molecules (at λ = 200) is 2.60×10^{-5} cm^2 sec^{-1} and 2.69×10^{-5} cm^2

sec^{-1} in [Hmim][Cl] and [Hmim][NTf_2] ILs, respectively. These diffusion coefficients are in close agreement with the diffusion coefficient in bulk water [179] (2.89×10^{-5} cm^2 sec^{-1}) calculated using the SPC/E water force field.

4.3.5 Dynamics in ultra-low water concentrations of [Hmim][Cl] and [Hmim][NTf_2] ILs

Similar to the dynamics of ions and water molecules at other water concentrations, an analysis of MSDs was performed at ultra-low concentrations of water. However, MSDs show a largely sub-diffusive behavior, which suggests the incomplete solvation of ions at such ultra-low water concentrations. A visual inspection of configurations extracted from the trajectory of a MD simulation run is shown in Figure **4.3**. At λ = 0.25 and 0.5, several bridge-like structures formed between a single water molecule and Cl^- anions can be observed. At λ = 1 and 2, several such multi-bridges formed between multiple water molecules and Cl^- anions exist. Similar bridge type structures were also discovered from various others configurations obtained from the simulation run. However, such bridge-like structures were not detected at other water concentrations ($\lambda \geq 5$), suggesting that there could be a threshold of water concentration required for the solvation of ions. The water...anion...water bridges can be quantified using a geometric criterion. For example, a water...anion...water bridge is considered to be formed when the distance between the water oxygen atom and the acceptor site of the anion (Cl^- in [Hmim][Cl] and N atom in [Hmim][NTf_2]) is $\leq$ 2.9 Å and $\angle$O-H-Cl or $\angle$O-H-N > 135^0. Using this geometric criteria, the fraction of water molecules that participate in the bridge formation was calculated for ultra-low water concentration of [Hmim][Cl] and [Hmim][NTf_2] ILs at T = 303 K and 353 K. The fraction of water bridges is shown in Table **4.1** (T = 303 K) and Table **A4-2** of Appendix A (T = 353 K). In [Hmim][Cl], at λ = 0.25, 0.5 and 1, 50-54% of water molecules form water...anion...water bridges (see Table **4.1**). However, at λ = 2, 21% of water molecules participate in the bridge formation, which implies that more water molecules are available for ion-water and water-water interactions. Such bridge-like

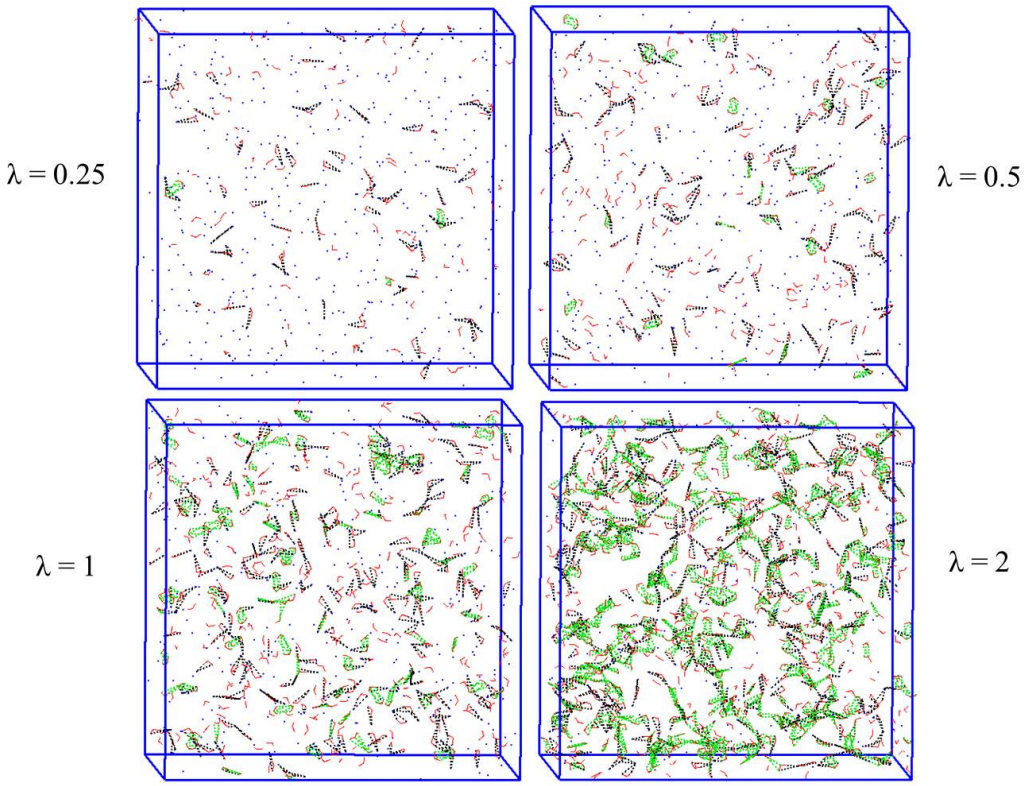

Figure 4.3: Snapshot of [Hmim][Cl] IL at ultra-low water concentrations at T = 303 K. Color scheme: blue color dots represent Cl^- anion, red color line represents water molecules, black color dotted lines represent water...anion... water/anion...water...anion bridges, and green color dotted line represents water H-bonds. $Hmim^+$ cations are not displayed.

Table 4.1: Fraction of bridging water molecules at ultra-low water concentrations of [Hmim][Cl] and [Hmim][NTf_2] ILs at T = 303 K.

λ	[Hmim][Cl]	[Hmim][NTf_2]
0.25	0.530	0.056
0.50	0.540	0.055
1.0	0.500	0.050
2.0	0.210	0.041

structures have been reported previously (from MD simulations) by Ghoshdastidar and Senapati [180] in $Emim^+$ cation-acetate, tri-fluoroacetate, and tetra-fluoroborate ILs.

At ultra-low water concentrations of [Hmim][NTf_2] IL, only a sub-diffusive behavior

of MSDs could be observed. However, bridge-like structures between water molecules and the NTf_2^- anions could barely be observed due to the hydrophobic nature and large size of the NTf_2^- anion. The participation of only ~ 5% of water molecules in the formation of bridges with NTf_2^- anion also support this contrasting behavior. Similar trends in the fraction of water molecules participating in the bridge formation are observed at T = 353 K.

In order to understand the participation of local water clusters and bulk water, the number of water clusters is characterized in ultra-low water concentration of [Hmim][Cl] and [Hmim][NTf_2] IL (see Figure **4.4**). Each water cluster is defined as the number of water molecules that appear in a cluster where the distance between the pair of water oxygen atoms ≤ 3.5 Å. The calculated water clusters were averaged over the production run time of the simulations. In [Hmim][Cl] IL, at λ = 0.25 and 0.5, a large number of water clusters contain a single water molecule (monomer) with relatively fewer water clusters containing dimers and a much lower number of water clusters with trimers. At λ = 1, there is a significant amount of water monomers and dimers, which form water clusters. However, there are some contributions to water clusters from trimers and decreasing contributions from water clusters containing higher order water molecules (tetramers etc.). At λ = 2, the number of water clusters formed from monomers and dimers decreases by an order of magnitude compared to that at λ = 1. However, the distribution of water clusters consists of contributions from trimers, tetramers, pentamers and higher order water molecular complexes.

In [Hmim][NTf_2] IL, at all ultra-low water concentrations (λ = 0.25 to λ = 2), a significant amount of water clusters is formed using monomer water. At λ = 2, the number of water monomers that form clusters is ~ 25 % lower compared to that at λ = 0.25, 0.5 and 1. The number of water clusters formed using water dimers is ~ 4 times lower compared to that of water monomers. However, the contributions from these higher order water clusters are very small compared to the water clusters formed using water monomer and dimer (e.g., λ = 2).

Similar trends in distribution of water clusters are also seen at T = 353 K (see Figure

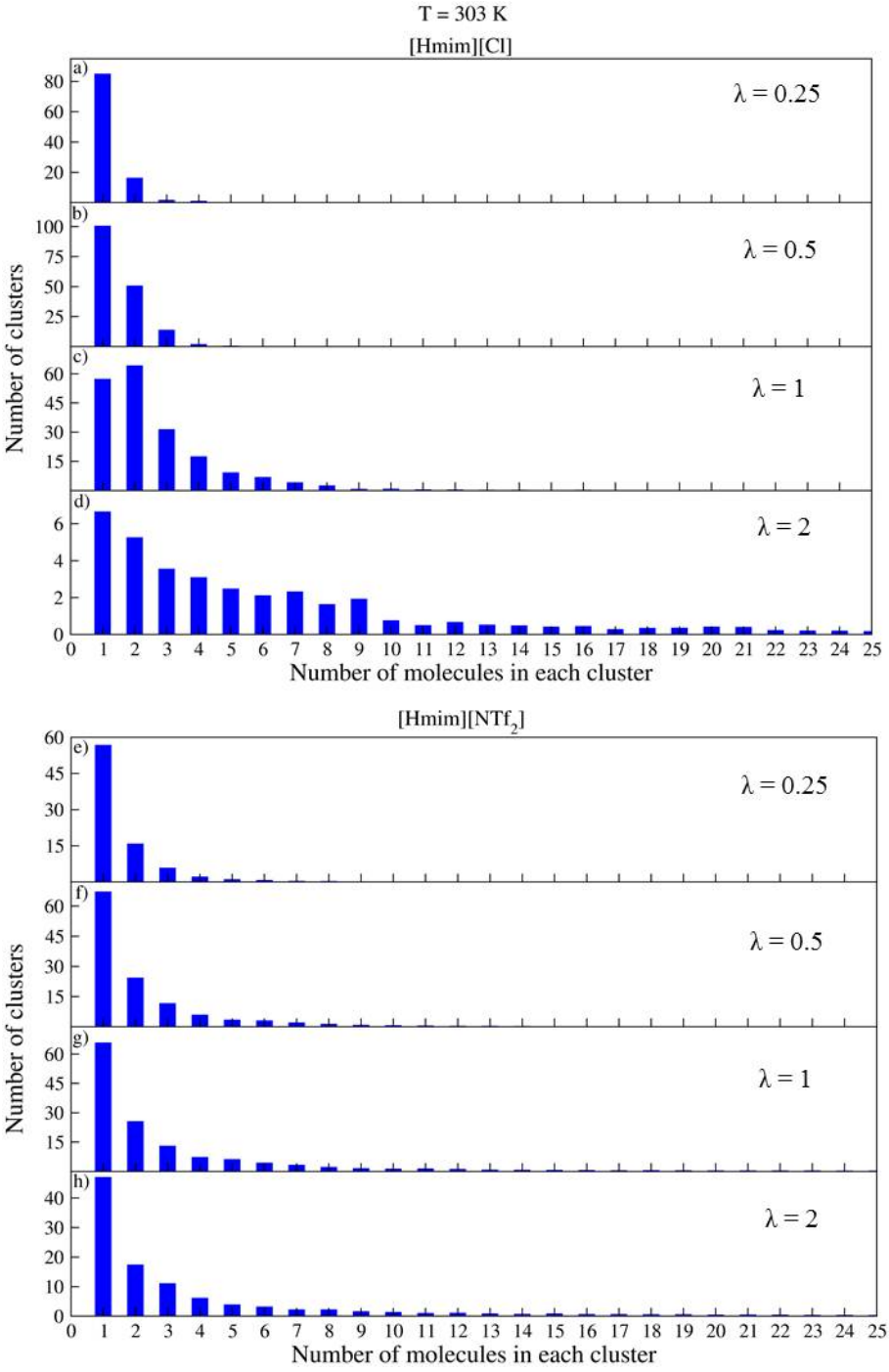

Figure 4.4: Water cluster distribution at ultra-low water concentrations in [Hmim][Cl] IL and [Hmim][NTf_2] IL at T = 303 K.

B4-3 of Appendix B).

4.3.6 Effect of temperature on diffusion coefficients

For both ILs, the qualitative trends in diffusion coefficients of cations, anions and water molecules at T = 353 K (see Figure **B4-4** of Appendix B) are similar to the trends seen at T = 303 K (see Figure **4.2**). The magnitude of diffusion coefficients of cations, anions and water molecules at T = 353 K increases by factor a of ~ 2 compared to that at T = 303 K. The diffusion coefficient of $Hmim^+$ cations (in this work) is 0.05×10^{-5} cm^2 sec^{-1} (T = 353 K) and it closely resembles the diffusion coefficient of the $Bmim^+$ cations (0.06×10^{-5} cm^2 sec^{-1}, T = 353 K) in hydrated [Bmim][Cl] reported by Niazi et al. [147]. Similarly, the diffusion coefficients of Cl^- anions is 0.07×10^{-5} cm^2 sec^{-1} (λ = 5 or 83 % mole fraction of water, T = 353 K) and is in remarkable agreement with the diffusion coefficient of 0.11×10^{-5} cm^2 sec^{-1} reported by Niazi et al. [147] (80 % mole fraction of water, T = 350 K). The trends in the diffusion coefficients of ions and water molecules in both ILs can be further examined by a characterization of inter-molecular interactions obtained from IP Lifetimes and IE.

4.4 IP lifetimes

The IP lifetimes were calculated using a distance autocorrelation function based on the work of Zhang and Maginn [116]. The cutoff distance was chosen as the first minima of the cation-anion RDFs (see Figure **B4-5** of Appendix B). For both ILs, the effect of water concentration and temperature shows an insignificant change in the first minima of the respective RDFs. The IP lifetimes were calculated between various sites on the $Hmim^+$ cations with the corresponding anions of each IL. The cationic sites are represented by three hydrogen atoms (H1, H2, and H3) on the imidazolium ring. The Cl atom (in the Cl^- anion) and the Nitrogen atom (in the NTf_2^- anion) are the anionic sites in [Hmim][Cl] and [Hmim] [NTf_2] ILs, respectively. The IP lifetimes corresponding to each water concentration for both ILs are shown in Table **4.2**.

4.4.1 IP lifetimes in [Hmim][Cl] and [Hmim][NTf_2] ILs

In [Hmim][Cl] IL, the IP lifetimes (H1-Cl, H2-Cl and H3-Cl) are 30.0 - 50.1 ps when λ = 5 and they decreases to 12.2 - 18.0 ps when λ = 10. Further, an increase in hydration causes the IP lifetimes to show a very marginal decrease from 8.1 - 10.3 ps (λ = 25) to 6.8

Table 4.2: IP life-time (ps) in hydrated [Hmim][Cl] and [Hmim][NTf_2] ILs at T = 303 K.

λ		IP life-time (ps)					
		[Hmim][Cl]			[Hmim][NTf_2]		
		H1...Cl	H2...Cl	H3...Cl	H1...N	H2...N	H3...N
Neat	0	564.4	1115.6	1711.7	18.8	21.6	17.4
Ultra-low	0.25	448.6	922.1	1703.8	18.7	22.8	16.5
	0.5	439.3	780.7	1301.0	18.0	21.5	16.1
	1	316.9	426.9	760.7	17.2	19.5	14.4
	2	195.5	192.5	371.2	16.5	18.1	13.4
Low	5	40.1	30.0	50.1	15.7	21.1	13.6
Intermediate	10	17.2	12.2	18.0	13.9	18.0	12.1
	25	10.3	8.1	10.0	12.4	13.2	10.2
High	50	8.7	7.2	8.5	12.3	12.4	9.5
	100	8.2	6.9	8.0	11.8	12.0	9.1
	150	8.1	7.0	7.9	11.7	11.4	8.6
	200	8.0	6.8	7.8	11.5	11.9	8.6

- 8.0 ps (λ = 200). The trend of IP lifetimes shows the following order: H2-Cl < H1-Cl < H3-Cl which, indicates a lower probability of interaction between the Cl^- anions and the H2 site of the imidazolium ring of the $Hmim^+$ cations. In neat [Hmim][Cl] IL, very long IP lifetimes times are observed. For example, the H1-Cl, H2-Cl and H3-Cl IP lifetimes are 564.4 ps, 1115.6 ps, and 1711.7 ps, respectively, which indicate strong electrostatic interactions between the $Hmim^+$ cations and the hydrophilic Cl^- anions. Even with the addition of few water molecules, the electrostatic interactions are significantly reduced,

as can be seen from the lower IP lifetimes (between λ = 0.25 and λ = 2). Between λ = 0 and λ = 1, the order of IP lifetimes is H1-Cl < H2-Cl < H3-Cl, which indicates a lower probability of interactions between the Cl^- anions and the H1 site of the imidazolium ring of the $Hmim^+$ cations.

In [Hmim][NTf_2] IL, the IP lifetimes (H1-N, H2-N, and H3-N) are 17.4 - 21.6 ps (λ = 0) and they show a gradual decrease to 8.6 - 11.9 ps (λ = 200). This again shows that inclusion of water molecules does not significantly change the correlated motion of the $Hmim^+$ cations and NTf_2^- anions, in contrast to the significant changes in the IP lifetimes seen in [Hmim][Cl] IL. The order of IP lifetimes is: H3-N < H1-N < H2-N, which suggests to the preferential interaction of NTf_2^- anions with the H2 site of the imidazolium ring of the $Hmim^+$ cations. The IP lifetimes in neat [Hmim][NTf_2] IL are 50 - 100 times lower compared to those in neat [Hmim][Cl] IL, due to lower electrostatic interactions between the $Hmim^+$ cations and the NTf_2^- anions. However, at intermediate and high water concentrations, the IP lifetimes in [Hmim][Cl] IL and [Hmim][NTf_2] IL are similar due to a substantial presence of bulk water molecules.

4.4.2 Effect of temperature on IP lifetimes

The qualitative trends in IP lifetimes are similar at T = 353 K (See Table **A4-4** of Appendix A). At low, intermediate and high water concentrations, the magnitude of IP lifetimes in [Hmim][Cl] IL at T = 353 K is 1.2 - 2.5 times lower compared to that at T = 303 K. Similarly, the magnitude of IP lifetimes in [Hmim][NTf_2] IL at T = 353 K is 1.2 - 2.1 times lower compared to that at T = 303 K. At ultra-low water concentrations of [Hmim][Cl] IL, the magnitude of IP lifetimes at T = 353 K is 2.1 - 4.6 times lower compared to that at T = 303 K. At ultra-low water concentrations in [Hmim][NTf_2] IL, the magnitude of IP lifetimes at T = 353 K is 1.6 - 1.8 times lower compared to that at T = 303 K. The difference in IP lifetime between different hydrogen atoms (H1, H2, and H3) of the imidazolium ring of $Hmim^+$ cation with the anions is further studied from the calculation of IE (as discussed in the next section).

4.5 IEs in [Hmim][Cl] and [Hmim][NTf_2] IL

The qualitative features of IP lifetimes are supported by calculation of site-specific cation-anion IE, using the same sites used for calculation of IP lifetimes. The calculated IE is a time and system averaged non-bonded potential energy obtained from the production run simulations. The cation-anion IEs are obtained between various hydrogen atoms of the imidazolium ring of the cation and the anionic sites (Cl in [Hmim][Cl] and N atom in [Hmim] [NTf_2] ILs, respectively). The cation-anion and water-water IE are shown in Table 4.3 and 4.4 where increasing negative value of IE denotes the increasing strength of the interactions. At λ = 5, in [Hmim][Cl] ILs, the cation-anion IE (corresponding to H1-Cl, H2-Cl and H3-Cl interactions) are -21.5 kJ/mol to -27.9 kJ/mol, and water-water IE are -11.2 kJ/mol respectively. However, at λ = 10, cation-anion interactions are significantly reduced as seen from relatively lower cation-anion IE (-12.7 kJ/mol to -17.4 kJ/mol). The lower cation-anion IE is primarily due to the disruption of ionic interactions with increasing water concentration. The difference in cation-anion IE between λ = 100 and λ = 200 is $\sim$ 1 kJ/mol, which confirms the presence of largely dissociated ions or IPs. The water-water IE of $\sim$ -42 kJ/mol resembles bulk water which again indicates complete dissociation of ions and IPs. In neat [Hmim][Cl] IL, the cation-anion IE vary from -40.8 kJ/mol to -45.9 kJ/mol. As expected, the cation-anion IE is reduced at ultra-low water concentrations. For example, the cation-anion IE are -40.3 kJ/mol to -44.9 kJ/mol (λ = 0.25) and reduces to -34.5 kJ/mol to -37.2 kJ/mol (λ = 2). On the contrary, positive water-water IE (between λ = 0.25 and λ = 2) are observed due to contributions of interactions from very geometrically close water...anion...water or anion...water...anion bridge structures (see Figure 4.3 and Table 4.3). The positive value of water-water IE increases between λ = 0.25 and λ = 1, due to the presence of several such bridge structures with a slight decrease in IE at λ = 2. The trends in cation-anion and water-water IE between λ = 1 and λ = 2 are similar to that observed from IP lifetimes. In [Hmim][NTf_2] IL, the cation-anion IE (corresponding to H1-N, H2-N and H3-N) are -21.0 kJ/mol to -15.7 kJ/mol (λ = 0) and gradually decreases to -5.4 kJ/mol to -9.8 kJ/mol (λ = 200), which shows relatively

Table 4.3: Site-specific Non-bonded IE (kJ/mol) in hydrated [Hmim][Cl] IL (deviations in parentheses).

λ	H1-Cl	H2-Cl	H3-Cl	$H_2O..H_2O$ [Hmim][Cl]
0	-41.0 (0.2)	-43.4 (0.4)	-46.0 (0.5)	-
0.25	-40.3 (0.4)	-42.5 (0.5)	-44.9 (0.5)	1.6 (0.4)
0.5	-39.6 (0.4)	-42.0 (0.5)	-44.5 (0.6)	3.2 (0.2)
1	-38.4 (0.4)	-39.5 (0.6)	-42.0 (0.5)	5.0 (0.4)
2	-35.4 (0.5)	-34.5 (0.6)	-37.2 (0.6)	4.0 (0.8)
5	-25.5 (1.1)	-21.5 (1.3)	-27.9 (1.3)	-11.2 (1.0)
10	-15.1 (1.0)	-12.7 (1.0)	-17.4 (1.2)	-23.2 (0.7)
25	-6.4 (0.7)	-5.8 (0.7)	-7.7 (0.9)	-34.3 (0.4)
50	-3.3 (0.6)	-4.1 (0.7)	-12.6 (1.0)	-38.9 (0.2)
100	-1.7 (0.4)	-1.6 (0.4)	-2.2 (0.5)	-41.5 (0.2)
150	-1.2 (0.4)	-1.1 (0.4)	-1.5 (0.4)	-42.4 (0.1)
200	-0.9 (0.3)	-0.9 (0.3)	-1.2 (0.4)	-42.8 (0.1)

less effect of water concentration on $Hmim^+$ cation - NTf_2^- anion interactions. The water-water IE at $\lambda \geq 5$ resembles the IE of bulk water due to reduced interactions between the water molecules and the hydrophobic NTf_2^- anions. At ultra-low water concentration, the water-water IE shows the following features: At $\lambda = 0.25$, the water-water IE is -7.5 kJ/mol and increases to -23.5 kJ/mol ($\lambda = 0.25$ to $\lambda = 2$) indicating the complex distribution of local water clusters.

The calculated values of cation-water IE (see Table **A4-5** of Appendix A) are considerably smaller (< 2 kJ/mol) across all the concentrations of water for both ILs, which suggests negligible interaction between the $Hmim^+$ cations and water molecules. The anion-water IE shows the following trends: large negative values of Cl^--water IE at ultra-low concentration suggests hydrogen bonding interactions (largest negative -142 kJ/mol at $\lambda = 1$) which supports presence of anion...water bridge structures. The values of NTf_2^--water IE are much lower compared to Cl^--water IE which also supports the low probability of anion-water bridge structures at ultra-low water concentration of [Hmim][NTf_2] IL.

Table 4.4: Site-specific Non-bonded IE (kJ/mol) in hydrated [Hmim][NTf_2] IL (deviations in parentheses).

λ	H1-N	H2-N	H3-N	$H_2O..H_2O$ [Hmim][NTf_2]
0	-20.0 (0.4)	-21.0 (0.5)	-15.7 (0.4)	-
0.25	-19.3 (0.4)	-20.5 (0.5)	-15.4 (0.4)	-7.5 (1.8)
0.5	-18.8 (0.4)	-20.0 (0.5)	-15.0 (0.4)	-11.6 (1.1)
1	-17.8 (0.4)	-18.8 (0.5)	-14.3 (0.4)	-17.1 (1.0)
2	-16.8 (0.4)	-17.8 (0.5)	-13.1 (0.4)	-23.5 (0.9)
5	-15.9 (0.7)	-16.9 (0.9)	-11.9 (0.7)	-38.1 (0.9)
10	-15.2 (0.8)	-16.3 (0.9)	-11.0 (0.7)	-40.3 (0.6)
25	-13.5 (1.0)	-14.5 (1.2)	-9.3 (0.8)	-41.0 (0.5)
50	-12.6 (1.0)	-13.5 (1.2)	-7.9 (0.8)	-43.0 (0.3)
100	-11.1 (1.0)	-11.8 (1.1)	-6.9 (0.7)	-43.4 (0.2)
150	-10.2 (0.9)	-10.6 (1.0)	-6.0 (0.6)	-43.4 (0.1)
200	-9.2 (1.0)	-9.8 (1.2)	-5.4 (0.8)	-43.5 (0.1)

4.5.1 Effect of temperature on IEs

All qualitative trends in cation-anion and water-water IE at T = 353 K (See Table **A4-6** of Appendix A) is similar to that seen at T = 303 K. At all water concentrations (for both ILs), the cation-anion IE at T = 353 K is lower by ~ 1 kJ/mol compared to T = 303 K. At low, intermediate and high water concentration (for both ILs), the water-water IE at T = 353 K is lower by ~ 3 kJ/mol compared to T = 303 K. The water-water IE at T = 353 K are similar to T = 303 K at ultra-low water concentration of [Hmim][Cl] and [Hmim][NTf_2][NTf_2] IL. The cation-water and anion-water IE at T = 353 K are tabulated in Table **A4-7** of the Appendix A.

4.6 Rotational auto-correlation functions

The rotational dynamics of a molecule is characterized using a Rotational Auto-Correlation Function (RACF), defined as C(t), which can be written as [181]

$$C(t) = \int_0^\infty P_n \cos \angle(p(\xi), p(\xi + t)) \tag{4.1}$$

where, $\angle(p(\xi), p(\xi + t)$ is the angle formed between a vector normal to the reference vector defining the axis of rotation at time t = ξ and t = (ξ + t). P_n is the nth order Legendre polynomial and is chosen as first order for the calculation of the RACF based on a previous study [182]. The choice of the first order Legendre polynomial is associated with IR absorption and dielectric relaxation measurements [183]. Here, the C-H1 vector of the $Hmim^+$ cation and the vector bisecting the H-O-H angle in water have been chosen as a reference for calculation of RACFs.

4.6.1 Rotational dynamics in low, intermediate and high water concentrations of [Hmim][Cl] and [Hmim][NTf_2] ILs

The RACFs (T = 303 K) corresponding to the rotation of $Hmim^+$ cations and water molecules at low, intermediate and high water concentrations of [Hmim][Cl] and [Hmim][NTf_2] ILs are shown in Figures **B4-6** and **B4-7** of Appendix B, respectively. The RACFs decay rapidly to zero within the timescale of simulation runs. As expected, a faster decay of the RACF of $Hmim^+$ cations and water molecules is also seen with increasing water concentration (T = 303 K and T = 353 K). A quantitative estimate of the rotational dynamics (which can be measured by experiments) was obtained by a calculation of the rotational correlation time (τ_{rot}) from the RACF [184]. Here, the calculated RACF is found to be best fitted using a single exponential function to obtain an analytical value of τ_{rot}. The values of τ_{rot} obtained from the numerical integration of the RACF and the analytical solution of the fitted function are almost identical. The τ_{rot} value of $Hmim^+$ cations and water molecules are shown in Table **4.5**. A high value of τ_{rot} (1143.4 ps) of

$Hmim^+$ cations in [Hmim][Cl] IL at λ = 5 is due to slow rotational motion (diffusion).

Table 4.5: Rotational correlation time (τ_{rot}) in low, intermediate and high water concentrations of [Hmim][Cl] and [Hmim][NTf_2] ILs at T = 303 K.

λ	τ_{rot} (ps)			
	[Hmim][Cl]		[Hmim][NTf_2]	
	Cation	H_2O	Cation	H_2O
5	1143.4	424.4	1163.5	19.1
10	144.4	66.8	774.5	12.5
25	40.0	16.6	269.5	11.2
50	28.5	9.7	244.9	8.1
100	22.6	7.2	165.8	6.5
150	21.2	6.5	148.9	6.1
200	21.3	6.1	153.4	5.9

With an increase in the water concentration, the τ_{rot} value of the $Hmim^+$ cations decreases by $\sim$ 8 times to 144.4 ps (λ = 10) and $\sim$ 3.6 times to 40.0 ps (λ = 25). A Subsequent increase in the water concentration changes the τ_{rot} value of $Hmim^+$ cations to 28.5 ps (λ = 50) and 21.3 ps (λ = 200). The τ_{rot} value of the water molecules is 424.4 ps (λ = 5) and it decreases by $\sim$ 6 times to 66.8 ps (λ = 10) and $\sim$ 4 times to 16.6 ps (λ = 25). The τ_{rot} value of the water molecules is 9.7 ps (λ = 50) and 6.1 ps (λ = 200), which confirms again the significant presence of bulk water at $\lambda \geq 50$.

In [Hmim][NTf_2] IL, the τ_{rot} of $Hmim^+$ cations at λ = 5 is 1163.5 ps, which decreases by $\sim$ 1.5 times to 774.5 ps (λ = 10) and $\sim$ 3 times to 269.5 ps (λ = 25). A Further increase in hydration change the τ_{rot} value to 244.9 ps at λ = 50 and 153.4 ps at λ = 200, respectively. The τ_{rot} value of water in [Hmim][NTf_2] IL does not vary significantly over the entire range of water concentration. This is due to the reduced interaction between the water molecules and the $Hmim^+$ cations/NTf_2^- anions. However, similar trends in τ_{rot} are observed at T = 353 K (See Table **A4-8** of Appendix A), the RACFs decay more rapidly compared to that at T = 303 K, resulting in a lower value of τ_{rot} of the $Hmim^+$ cations and water molecules.

4.6.2 Rotational dynamics in neat [Hmim][Cl] and [Hmim][NTf_2] ILs

The RACF (see Figure 4.5) in neat [Hmim][Cl] and neat [Hmim][NTf_2] ILs were found to be best fitted with a biexponential function:

$$C(t) = ae^{-t/\tau_1} + (1-a)e^{-t/\tau_2} \tag{4.2}$$

where 'a' is the normalization factor, and τ_1 and τ_2 are rotational autocorrelation times.

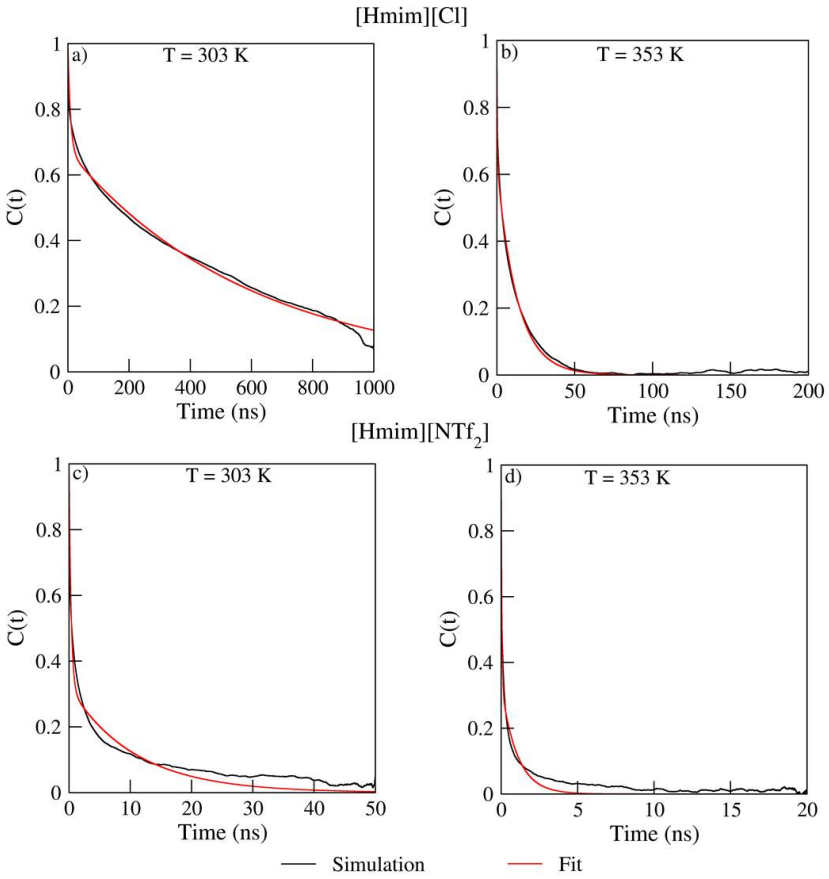

Figure 4.5: RACFs of $Hmim^+$ cations in neat [Hmim][Cl] and neat [Hmim][NTf_2] ILs at T = 303 K and T = 353 K.

The values of the normalization factor 'a' and normalized rotational relaxation times (τ_1 and τ_2) are provided in Table 4.6. The integration of the RACFs produces two relaxation times: a faster primary relaxation time (τ_1) and a slower secondary relaxation time (τ_2). The detection of two relaxation processes for a similar class of ILs have also been reported

Table 4.6: Rotational dynamics in neat [Hmim][Cl] and [Hmim][NTf_2] ILs.

IL	T(K)	Trajectory length (ns)	Normalization factor a	Analytical			Numerical τ_{rot} (ns)
				τ_1 (ns)	τ_2 (ns)	τ_{rot} (ns)	
[Hmim][Cl]	303	1000	0.3256	2.8	403.2	406.0	350.0
[Hmim][Cl]	353	200	0.3697	0.134	8.106	8.240	9.539
[Hmim][NTf_2]	303	50	0.6780	0.226	3.436	3.662	4.374
[Hmim][NTf_2]	353	20	0.6677	0.029	0.342	0.371	0.655

previously by experiments [185]. A total relaxation time (τ_{rot}), where $\tau_{rot} = \tau_1 + \tau_2$ is used for discussion in the following section.

Figure **4.5**a shows the RACF (T = 303 K) of $Hmim^+$ cations in neat [Hmim][Cl]. The RACF shows an extremely slow exponential decay due to a very slow rotational motion of the $Hmim^+$ cations, which arise from strong electrostatic interactions between the $Hmim^+$ cations and Cl^- anions. In addition, the RACF for neat [Hmim][Cl] at T = 303 K does not decay to zero even during long timescale simulations (1 microsecond); the approximate value of τ_{rot} can still serve as a benchmark for any future experimental investigation. The numerical integration of the RACF from the 1 microsecond trajectory shows a τ_{rot} value of ~ 350 ns, whereas an analytical solution to the fitted biexponential function shows a τ_{rot} value of ~ 406 ns. The RACFs of $Hmim^+$ cations at T = 353 K (from a trajectory of 200 ns, see Figure **4.5**b) shows a faster exponential decay compared to that at T = 303 K, with a numerical and analytical value of τ_{rot} of ~ 9.5 ns and ~ 8.2 ns, respectively. Figure **4.5**c shows the RACF (T = 303 K) of the $Hmim^+$ cations in neat [Hmim][NTf_2] IL from a trajectory of 50 ns. The RACF shows a steep exponential decay due to fewer electrostatic interactions between the $Hmim^+$ cations and the NTf_2^- anions with a numerical and analytic value of τ_{rot} of ~ 4.4 ns and ~ 3.7 ns respectively. Similarly, the RACF of $Hmim^+$ cations in neat [Hmim][NTf_2] IL at T = 353 K (from a trajectory of 20 ns, Figure **4.5**d) shows a very fast decay compared to that at T = 303 K

with a numerical and an analytic value of τ_{rot} of ~ 0.7 ns and ~ 0.4 ns, respectively. The difference in the numerical and analytic values of τ_{rot} arises primarily from the sluggish decay of the RACFs.

4.6.3 Rotational dynamics in ultra-low water concentrations of [Hmim][Cl] and [Hmim][NTf_2] ILs

The RACFs of the $Hmim^+$ cations and water molecules at ultra-low water concentrations of [Hmim][Cl] and [Hmim][NTf_2] IL are shown in Figure **B4-8** and **B4-9** of Appendix B, respectively. Similar to the RACFs in the neat ILs, the biexponential function shown in eqn (4.2) was found to be the best fit to the RACFs in ultra-low water concentration environments. The decay of the RACF of the $Hmim^+$ cations at T = 303 K is much slower in [Hmim][Cl] IL compared to [Hmim][NTf_2] IL at all ultra-low water concentrations. The expected correlation time for the $Hmim^+$ cations with the Cl^- anions at these ultra-low concentrations is of the order of hundreds of nanoseconds. The analysis of local water clusters explains the slower rotational motion of the $Hmim^+$ cations in [Hmim][Cl] IL. The RACF of the water molecules also decays slowly, which is consistent with the local water cluster distribution and the existence of anion...water bridges in [Hmim][Cl] IL. The relatively faster decay of the RACF of water molecules at ultra-low concentrations of [Hmim][NTf_2] IL is supported by the examination of the local water cluster distribution and a minimal presence of anion...water bridges. At T = 353 K, the qualitative features of the RACF of the $Hmim^+$ cations and water molecules are similar to those at T = 303 K, though all the RACFs decay much faster due to thermal effects.

Chapter 5

Summary

5.1 Conclusions

The salient features of this thesis are as follows:

- **Chapter 1** of the thesis provides a background of ILs with literature on physical, structural, and dynamical properties of imidazolium ILs. The properties calculated from MD simulations are also presented.

- **Chapter 2** of the thesis describes the effect of anion on structure and dynamics of neat ILs containing the 1-hexyl-3-methylimidazolium cation. The simulations show that the size of anions is an important factor that qualitatively and quantitatively influences various interionic interactions. The RDFs show that interactions remain invariant to changes in temperature from 300 K to 453 K. [Hmim][Cl] and [Hmim][Br] ILs have higher cation-anion interactions and hence result in lower diffusion and conductivity. The SDFs show that large anionic distributions along the CR-H bond vector of the imidazolium ring. In [Hmim][PF_6], [Hmim][OTf] and [Hmim][NTf_2] ILs, the anionic distribution are seen more above and below the plane of the imidazolium ring of the cation, compared to anionic densities along the CR-H bond vector. In all ILs, there are additional anionic densities in the neighborhood of the nonacidic hydrogen atoms of the imidazolium ring of the cation. A comparison of ILs containing a common cation shows that the diffusion and con-

ductivity of the ILs depend only on the choice of anions (at each temperature). ILs containing Cl^- and Br^- show lower diffusion (conductivity), and IL with large size anions like OTf^- and NTf_2^- show higher diffusion coefficients (conductivity). Consistent with previous investigations, while the magnitude of diffusion coefficients is primarily dependent on anionic size and shape, IP lifetimes will decisively provide a direct qualitative trend with diffusion coefficients (conductivity) of ILs.

- **Chapter 3** of the thesis describes the structural properties of hydrated [Hmim][NTf_2] ILs. The cation-anion, cation-cation, and anion-anion interactions decrease with increase in water concentration. At low water concentration, water molecules are trapped by cations and anions. At intermediate water concentrations, phase separation between the IL and water is observed. At higher water concentration, aggregates of cations and anions are solvated by water channels. At all water concentrations, no hydrogen bonding interactions exist between water molecules and anions due to hydrophobicity. The cationic tail aggregation leads to micelle formation at high water concentration. The IE show that IL-IL and IL-water IE decreases and water-water IE increases with water concentration.

- **Chapter 4** of the thesis describes translational and rotational dynamics in hydrated [Hmim][Cl] and [Hmim][NTf_2] ILs. The effect of water causes the diffusion coefficients of the $Hmim^+$ cations to be higher in [Hmim][Cl] IL compared to [Hmim][NTf_2] IL, and the Cl^- anions diffuse faster compared to the NTf_2^- anions with an opposite behavior of the diffusion coefficients compared to those seen in the neat ILs. The effect of water leads to reduced inter-ionic interactions in [Hmim][Cl] IL, which facilitates faster diffusion of Cl^- anions. The diffusion coefficients of the $Hmim^+$ cations and NTf_2^- anions are similar in hydrated [Hmim][NTf_2] IL due to their similarity in size and symmetry. The diffusion coefficient of water molecules in [Hmim][Cl] IL is lower compared to [Hmim][NTf_2] IL due to interactions between hydrophilic Cl^- anions and water molecules, unlike the hydrophobic NTf_2^- anions, which do not interact with water molecules. At a low water concentration, the IP

lifetimes in [Hmim][Cl] IL are much higher compared to [Hmim][NTf_2] IL due to strong electrostatic interactions and supported by corresponding IE. However, comparable lifetimes are observed at intermediate and high water concentration. At ultra-low water concentrations of [Hmim][Cl] IL, multi-bridged structures formed between Cl^- anions and water molecules are observed and is supported by the positive water-water IE. However, at ultra-low water concentration of [Hmim][NTf_2] IL, multi-bridged structures are rarely seen and is supported by the negative values of water-water IE. The simulations predict that very long simulation time scales are required to observe converged RACFs in neat ILs (especially at T = 303 K), whereas a 20 ns simulation run was sufficient for accurate characterization of the dynamical properties under hydrated conditions. The calculated τ_{rot} suggests that the rotational diffusion of $Hmim^+$ cations is faster (lower τ_{rot}) in hydrated [Hmim][Cl] compared to [Hmim][NTf_2] IL and is strongly associated with the translational diffusion coefficients. However, the τ_{rot} value of water is lower (higher τ_{rot}) in hydrated [Hmim][Cl] compared to [Hmim][NTf_2] IL, especially at low and intermediate water concentrations.

5.2 Future directions

5.2.1 Modeling of Benzene Extraction from Benzene-Hexane Mixture by Imidazolium IL

Aromatic hydrocarbons (e.g., benzene, pyridine) and alkanes (e.g., hexane, heptane) and cyclohexane hydrocarbon mixtures have very similar boiling points which makes their separation very difficult [186]. The commonly employed processes are liquid extraction (20-65 wt% of aromatic compound), extractive distillation (65-90 wt% of aromatic compound), and azeotropic distillation (>90 wt% of aromatic compound) [187]. Among these methods, the liquid extraction is found to be the most effective and also have low energy demands compared to azeotropic and extractive distillation techniques [187].

Polar organic solvents like sulfolane [188, 189], dimethylsulfoxide [190], ethylene

glycols [191], N-methylpyrrolidone [192] etc. have been widely used for liquid extraction. However, these solvents do not satisfy the requirements of high thermal and chemical stability, low toxicity, low dynamic viscosity, high solvent extraction selectivity, and non-corrosivity [193]. ILs offer an excellent alternative to the traditional polar organic solvents [194, 195]. The vapor pressure of ILs are negligible compared to the extracted hydrocarbons, and hence can be recovered easily after extraction. Further, ILs do not degrade even with repeated cycles of extraction and hence can be regenerated from the extractant.

Arce et al. [196] examined benzene separation from a benzene-hexane mixture us-

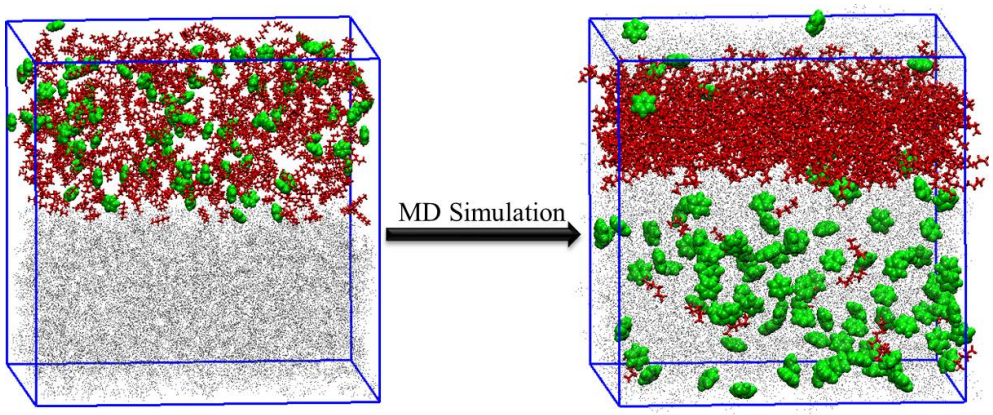

Figure 5.1: Model of liquid separation by MD simulation. Colour scheme: grey dots represents IL, green vdW represents benzene and red licorice represents hexane.

ing the [Emim][NTf_2] IL. The authors observed that selectivity and solute distribution ratio in ILs was higher compared to conventional solvents like sulfolane. In a subsequent study [197], the authors studied the effect of alkyl chain length in [$C_n$mim][NTf_2] IL on benzene separation from the benzene-hexane mixture. The authors observed that ILs with a shorter alkyl chain on the imidazolium cation have higher selectivity towards benzene separation. In another study, [198] the authors investigated the effect of cation ([A][NTf_2], A = 1-ethylpyridinium, (2-hydroxyethyl)trimethylammonium, and [$N_{111}(C_2OH)]^+$) on benzene separation from benzene-hexane mixture. The authors observed that ILs containing the [$N_{111}(C_2OH)]^+$ cation showed higher benzene extraction selectivity compared to ILs containing the NTf_2^- anion and aromatic cations.

MD simulations can offer detail mechanistic pathways and energies of benzene separation in benzene-hexane mixtures. A molecular model of benzene separation is presented in Figure **5.1**. MD simulations can provide a quantitative measure of benzene extraction at various composition of benzene-hexane mixtures and this can be one of the focus of future activities. MD simulations can also provide physical insights into solvent separation in various mixtures by a family of imidazolium ILs (by specifically tuning the alkyl chain length of the imidazolium cation and different anions), which can serve as an excellent benchmark for several experimental studies in this research area.

Appendix A

Table A2-1: First minima from Cation-Cation and Cation-Anion RDFs.

IL	Cation-Cation (Å)	Cation-Anion (Å)
[Hmim][Cl]	9.7	4.3
[Hmim][Br]	10.3	4.6
[Hmim][BF_4]	10.8	4.1
[Hmim][PF_6]	11.1	4.2
[Hmim][OTf]	11.5	4.4
[Hmim][NTf_2]	12.3	4.4

Table A2-2: Distance criteria (Derived from Cation-Anion RDFs) for calculation of IP life times.

IL	Distance (pm)
[Hmim][Cl]	310-660
[Hmim][Br]	330-700
[Hmim][BF_4]	320-730
[Hmim][PF_6]	360-760
[Hmim][OTf]	360-790
[Hmim][NTf_2]	360-870

Table A3-1: Non-bonded potential energies and IE (kJ/mol).

λ	IL-IL non-bonded potential energy (IE)	IL-Water non-bonded potential energy (IE)	Water-Water non-bonded potential energy (IE)
5	-121470.07 (-97.15)	-6842.05 (-9.12)	-23786.67 (-38.07)
10	-11062.96 (-88.49)	-8962.80 (-6.53)	-50317.08 (-40.25)
25	-6812.60 (-54.52)	-18744.70 (-5.77)	-128069.31 (-40.96)
50	-5131.13 (-41.04)	-22071.48 (-3.47)	-264418.21 (-42.30)
100	-2982.94(-23.85)	-26530.00 (-2.34)	-538386.28 (-43.05)
150	-1486.03 (-11.88)	-29677.36 (-1.55)	-813598.51 (-43.39)
200	-565.80 (-4.52)	-33631.03 (-1.34)	-1087471.81 (-43.51)

Table A4-1: System size, density of neat and hydrated [Hmim][Cl] IL.

λ	Number of IPs	Number of water molecules	[Hmim][Cl]			
			Total number of atoms	H_2O(wt %)	ρ (g cm^{-3}) (303 K)	ρ (g cm^{-3}) (353 K)
Neat	500	-	16000	-	1.010	0.983
0.25	500	125	16375	2.17	1.015	0.990
0.5	500	250	16750	4.25	1.023	0.995
1	500	500	17500	8.15	1.032	1.006
2	500	1000	19000	15.08	1.046	1.015
5	125	625	5875	30.74	1.056	1.018
10	125	1250	7750	47.02	1.049	1.009
25	125	3125	13375	68.94	1.033	0.992
50	125	6250	22750	81.61	1.017	0.978
100	125	12500	41500	89.87	1.005	0.968
150	125	18750	60250	93.01	1.001	0.964
200	125	25000	79000	94.67	0.998	0.962

Table A4-2: System size, density of neat and hydrated [Hmim][NTf_2] IL.

λ	Number of IPs	Number of water molecules	[Hmim][NTf_2]			
			Total number of atoms	H_2O(wt %)	ρ (g cm^{-3}) (303 K)	ρ (g cm^{-3}) (353 K)
Neat	500	-	23000	-	1.428	1.377
0.25	500	125	23375	1.00	1.421	1.371
0.5	500	250	23750	1.97	1.416	1.365
1	500	500	24500	3.87	1.405	1.354
2	500	1000	26000	7.45	1.387	1.333
5	125	625	7625	16.74	1.302	1.256
10	125	1250	9500	28.69	1.245	1.199
25	125	3125	15125	50.14	1.156	1.114
50	125	6250	24500	66.79	1.095	1.055
100	125	12500	43250	80.01	1.051	1.012
150	125	18750	62000	85.78	1.037	0.999
200	125	25000	80750	88.94	0.989	0.979

Table A4-3: Fraction of bridging water molecules at ultra-low water concentrations of [Hmim][Cl] and [Hmim][NTf_2] ILs at T = 353 K.

λ	[Hmim][Cl]	[Hmim][NTf_2]
0.25	0.495	0.054
0.50	0.500	0.051
1.0	0.470	0.047
2.0	0.200	0.039

Table A4-4: IP life-time (ps) in hydrated [Hmim][Cl] and [Hmim][NTf_2] ILs at T = 353 K.

λ		IP life-time (ps)					
		[Hmim][Cl]			[Hmim][NTf_2]		
		H1...Cl	H2...Cl	H3...Cl	H1...N	H2...N	H3...N
Neat	0	181.1	394.2	639.0	11.6	12.4	10.0
Ultra-low	0.25	171.4	306.5	481.7	11.7	12.5	9.9
	0.5	154.4	254.8	380.7	11.4	12.1	9.5
	1	158.2	206.0	297.5	11.0	11.4	9.1
	2	66.1	55.8	80.5	10.4	10.6	8.5
Low	5	20.1	14.6	19.9	10.1	10.2	9.4
Intermediate	10	10.4	8.0	9.9	9.8	9.9	9.1
	25	7.4	6.3	7.1	8.4	8.4	7.4
High	50	6.8	5.9	6.6	8.7	8.2	7.2
	100	6.5	5.8	6.4	8.6	8.1	7.2
	150	6.4	5.7	6.3	8.6	8.2	7.2
	200	6.4	5.8	6.2	8.2	7.6	6.7

Table A4-5: Site-specific Non-bonded IE (kJ/mol) of cation-water and anion-water in hydrated [Hmim][Cl] and [Hmim][NTf_2] ILs at T = 303 K. Deviations in parentheses.

	[Hmim][Cl]				[Hmim][NTf_2]			
λ	H1-water	H2-water	H3-water	Cl-water	H1-water	H2-water	H3-water	N-water
0.25	2.2 (0.2)	0.6 (0.2)	0.6 (0.2)	-52.6 (1.0)	-1.1 (0.3)	-1.3 (0.3)	-0.8 (0.3)	-8.3 (0.6)
0.5	2.8 (0.3)	0.7 (0.3)	0.8 (0.4)	-75.0 (1.1)	-1.3 (0.3)	-1.6 (0.3)	-1.0 (0.3)	-10.9 (0.6)
1	3.5 (0.2)	0.8 (0.3)	0.8 (0.3)	-145.0 (1.1)	-1.5 (0.2)	-1.9 (0.3)	-1.1 (0.2)	-13.7 (0.6)
2	3.1 (0.3)	0.3 (0.3)	0.3 (0.3)	-138.4 (1.5)	-1.5 (0.2)	-1.8 (0.3)	-1.3 (0.2)	-15.9 (0.6)
5	1.0 (0.4)	-1.4 (0.5)	0.1 (0.5)	-131.5 (2.5)	-0.6 (0.2)	-0.7 (0.3)	-0.7 (0.2)	-7.7 (0.7)
10	-1.1 (0.3)	-1.9 (0.3)	-1.0 (0.4)	-119.8 (1.0)	-0.5 (0.2)	-0.6 (0.2)	-0.6 (0.2)	-7.0 (0.5)
25	-1.8 (0.2)	-1.7 (0.2)	-1.5 (0.2)	-84.8 (1.2)	-0.7 (0.2)	-0.7 (0.2)	-0.7 (0.2)	-9.1 (0.8)
50	-1.6 (0.1)	-1.4 (0.1)	-1.4 (0.1)	-62.4 (0.8)	-0.6 (0.1)	-0.6 (0.1)	-0.7 (0.1)	-7.6 (0.7)
100	-1.2 (0.1)	-1.1 (0.1)	-1.1 (0.1)	-45.1 (0.5)	-0.6 (0.1)	-0.6 (0.1)	-0.6 (0.1)	-6.3 (0.4)
150	-1.0 (0.1)	-0.9 (0.1)	-1.0 (0.1)	-37.2 (0.4)	-0.6 (0.1)	-0.5 (0.1)	-0.5 (0.1)	-5.8 (0.3)
200	-0.9 (0.1)	-0.8 (0.1)	-0.8 (0.1)	-32.3 (0.3)	-0.6 (0.1)	-0.6 (0.1)	-0.5 (0.1)	-5.4 (0.4)

Table A4-6: Site-specific Non-bonded IE (kJ/mol) of cation-water and anion-water in hydrated [Hmim][Cl] and [Hmim][NTf_2] ILs at T = 353 K. Deviations in parentheses.

	[Hmim][Cl]				[Hmim][NTf_2]			
λ	H1-water	H2-water	H3-water	Cl-water	H1-water	H2-water	H3-water	N-water
0.25	2.3 (0.3)	0.5 (0.3)	0.5 (0.3)	-51.4 (1.2)	-1.0 (0.3)	-1.3 (0.4)	-0.8 (0.3)	-8.3 (0.7)
0.5	3.0 (0.3)	0.6 (0.3)	0.5 (0.3)	-72.48 (1.2)	-1.3 (0.3)	-1.6 (0.4)	-1.0 (0.3)	-10.7 (0.6)
1	3.4 (0.3)	0.7 (0.3)	0.7 (0.4)	-102.3 (1.3)	-1.6 (0.3)	-1.9 (0.3)	-1.3 (0.3)	-13.6 (0.6)
2	3.1 (0.3)	0.3 (0.3)	0.3 (0.3)	-131.4 (1.5)	-1.9 (0.2)	-2.1 (0.3)	-1.4 (0.2)	-16.1 (0.6)
5	0.6 (0.4)	-1.4 (0.5)	-0.3 (0.6)	-133.6 (2.5)	-0.8 (0.2)	-0.9 (0.3)	-0.7 (0.2)	-7.8 (0.7)
10	-1.2 (0.3)	-1.9 (0.3)	-1.2 (0.4)	-114.6 (2.1)	-0.7 (0.2)	-0.7 (0.2)	-0.7 (0.2)	-6.8 (0.5)
25	-1.8 (0.2)	-1.7 (0.2)	-1.6 (0.2)	-82.0 (1.2)	-1.0 (0.2)	-1.1 (0.2)	-0.9 (0.2)	-10.0 (0.8)
50	-1.6 (0.1)	-1.4 (0.1)	-1.4 (0.1)	-60.5 (0.8)	-0.9 (0.1)	-0.9 (0.2)	-0.8 (0.1)	-8.11 (0.6)
100	-1.2 (0.1)	-1.1 (0.1)	-1.1 (0.1)	-43.8 (0.5)	-0.8 (0.1)	-0.8 (0.1)	-0.6 (0.1)	-6.5 (0.5)
150	-1.0 (0.1)	-0.9 (0.1)	-0.9 (0.1)	-36.0 (0.4)	-0.7 (0.1)	-0.7 (0.1)	-0.5 (0.1)	-5.8 (0.4)
200	-0.9 (0.1)	-0.8 (0.1)	-0.8 (0.1)	-31.4 (0.3)	-0.8 (0.1)	-0.7 (0.1)	-0.5 (0.1)	-5.9 (0.4)

Table A4-7: Site-specific Non-bonded IE (kJ/mol) of cation-anion and water-water in hydrated [Hmim][Cl] and [Hmim][NTf_2] ILs at T = 353 K. Deviations in parentheses.

λ	H1-Cl	H2-Cl	H3-Cl	H1-N	H2-N	H3-N	$H_2O..H_2O$ [Hmim][Cl]	$H_2O..H_2O$ [Hmim][NTf_2]
0	-40.0 (0.5)	-42.6 (0.5)	-45.2 (0.5)	-19.0 (0.4)	-20.3 (0.5)	-15.0 (0.4)	-	-
0.25	-39.4 (0.5)	-41.8 (0.5)	-44.0 (0.6)	-18.3 (0.5)	-19.4 (0.5)	-14.5 (0.4)	1.0 (0.3)	-5.0 (1.7)
0.5	-39.2 (0.5)	-41.1 (0.5)	-43.3 (0.6)	-17.8 (0.4)	-18.9 (0.5)	-14.1 (0.4)	2.6 (0.4)	-9.0 (0.7)
1	-37.6 (0.5)	-39.0 (0.6)	-41.3 (0.6)	-16.9 (0.4)	-17.9 (0.5)	-13.4 (0.4)	4.5 (0.4)	-13.8 (1.0)
2	-34.3 (0.5)	-33.8 (0.7)	-36.4 (0.6)	-15.5 (0.4)	-16.4 (0.5)	-12.2 (0.4)	4.0 (0.6)	-19.2 (0.8)
5	-24.3 (1.1)	-21.1 (1.3)	-26.4 (1.3)	-14.6 (0.8)	-15.6 (0.9)	-11.2 (0.7)	-9.9 (1.0)	-34.1 (1.0)
10	-14.5 (1.0)	-12.3 (1.0)	-16.3 (1.2)	-14.2 (0.8)	-15.0 (0.7)	-10.5 (0.9)	-21.2 (0.7)	-36.9 (1.2)
25	-6.1 (0.7)	-5.6 (0.7)	-7.3 (0.9)	-13.4 (0.9)	-14.0 (1.0)	-9.6 (0.8)	-31.7 (0.4)	-39.2 (0.8)
50	-3.2 (0.6)	-3.0 (0.5)	-3.9 (0.7)	-10.8 (1.0)	-11.3 (1.0)	-7.2 (0.7)	-36.1 (0.3)	-39.9 (0.3)
100	-1.7 (0.4)	-1.6 (0.4)	-2.1 (0.5)	-9.6 (1.1)	-10.1 (1.1)	-6.3 (0.8)	-38.6 (0.2)	-40.0 (0.2)
150	-1.2 (0.4)	-1.2 (0.4)	-1.5 (0.4)	-8.7 (0.9)	-9.2 (1.0)	-5.8 (0.7)	-39.5 (0.1)	-40.3 (0.2)
200	-0.9 (0.3)	-0.9 (0.3)	-1.2 (0.4)	-6.8 (1.0)	-7.2 (1.1)	-4.4 (0.8)	-39.9 (0.1)	-40.4 (0.1)

Table A4-8: Rotational correlation time (τ_{rot}) in low, intermediate and high water concentrations of [Hmim][Cl] and [Hmim][NTf_2] ILs at T = 353 K.

λ	τ_{rot} (ps)			
	[Hmim][Cl]		[Hmim][NTf_2]	
	Cation	H_2O	Cation	H_2O
5	177.5	67.4	225.8	5.7
10	28.2	14.4	171.3	4.1
25	11.8	5.5	55.9	4.1
50	8.3	4.0	51.5	3.5
100	6.9	3.5	44.7	3.2
150	6.7	3.3	46.6	3.2
200	7.5	3.2	28.3	3.2

Appendix B

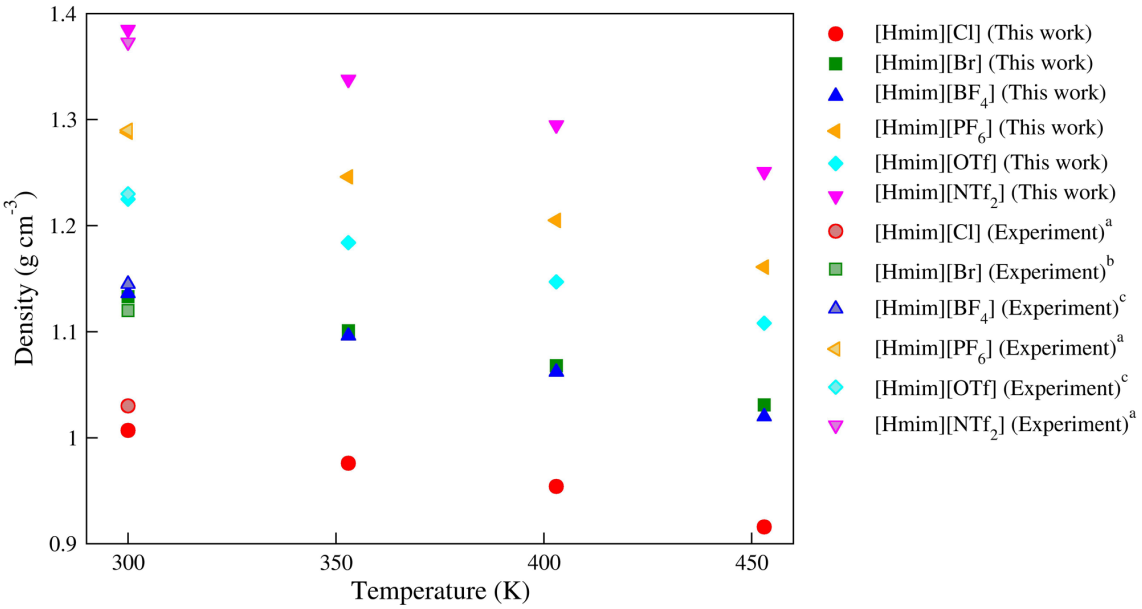

Figure B2-1: Simulated density vs. Experiment.

[a] S. Zhang, N. Sun, X. He, X. Lu, X. Zhang, *J. Chem. Ref. Data*, **35**, 1475 (2006).

[b] J.-G. Li, Y.-F. Hu, S.-F. Sun, Y.-S. Liu, Z.-C. Liu, *J. Chem. Thermodynamics*, **42**, 904 (2010).

[c] J. Klomfar; M. Součková ; J. Pátek, *J. Chem. Eng. Data*, **55**, 4054 (2010).

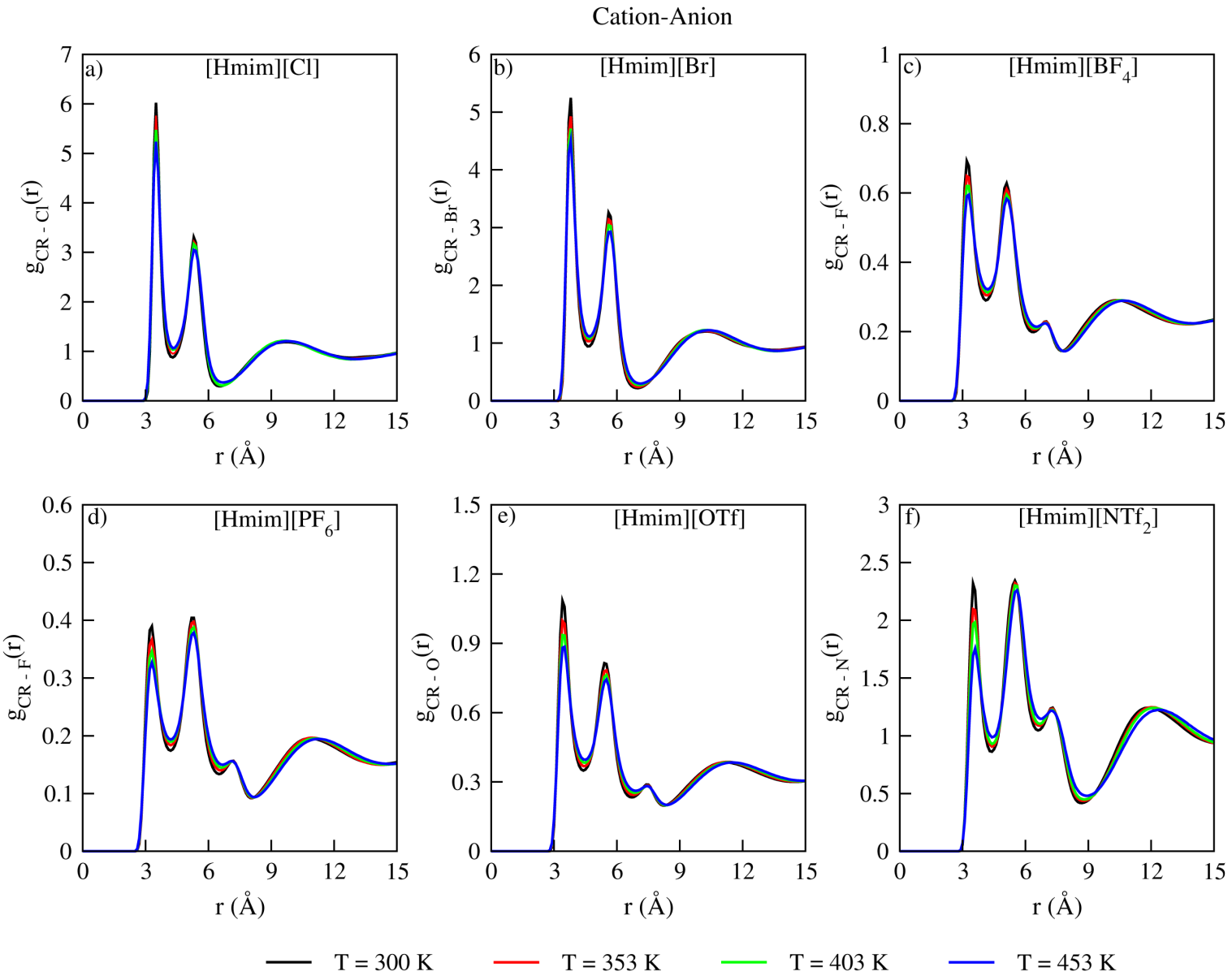

Figure B2-2: Effect of temperature on Cation-Cation interactions.

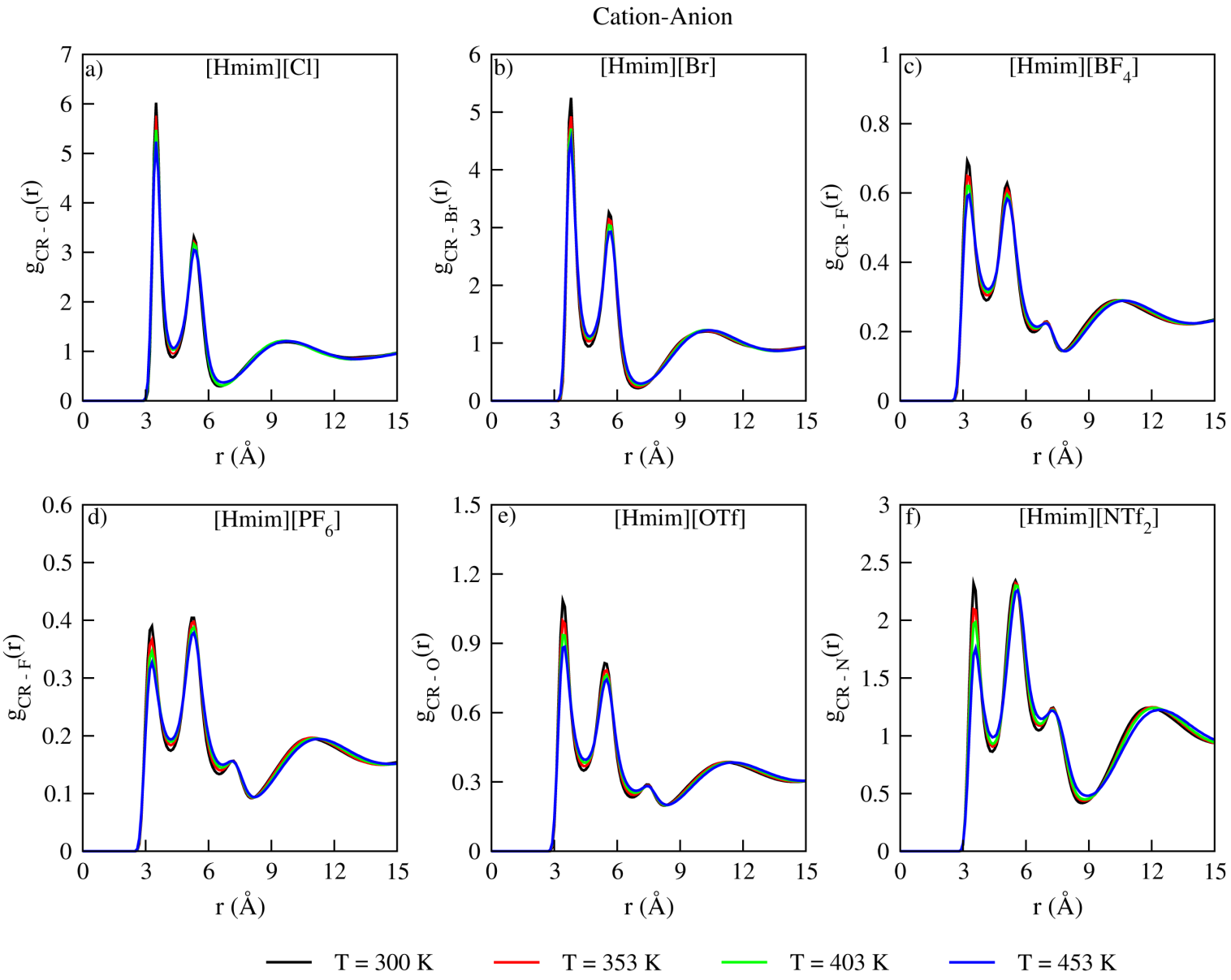

Figure B2-3: Effect of temperature on Cation-Anion interactions.

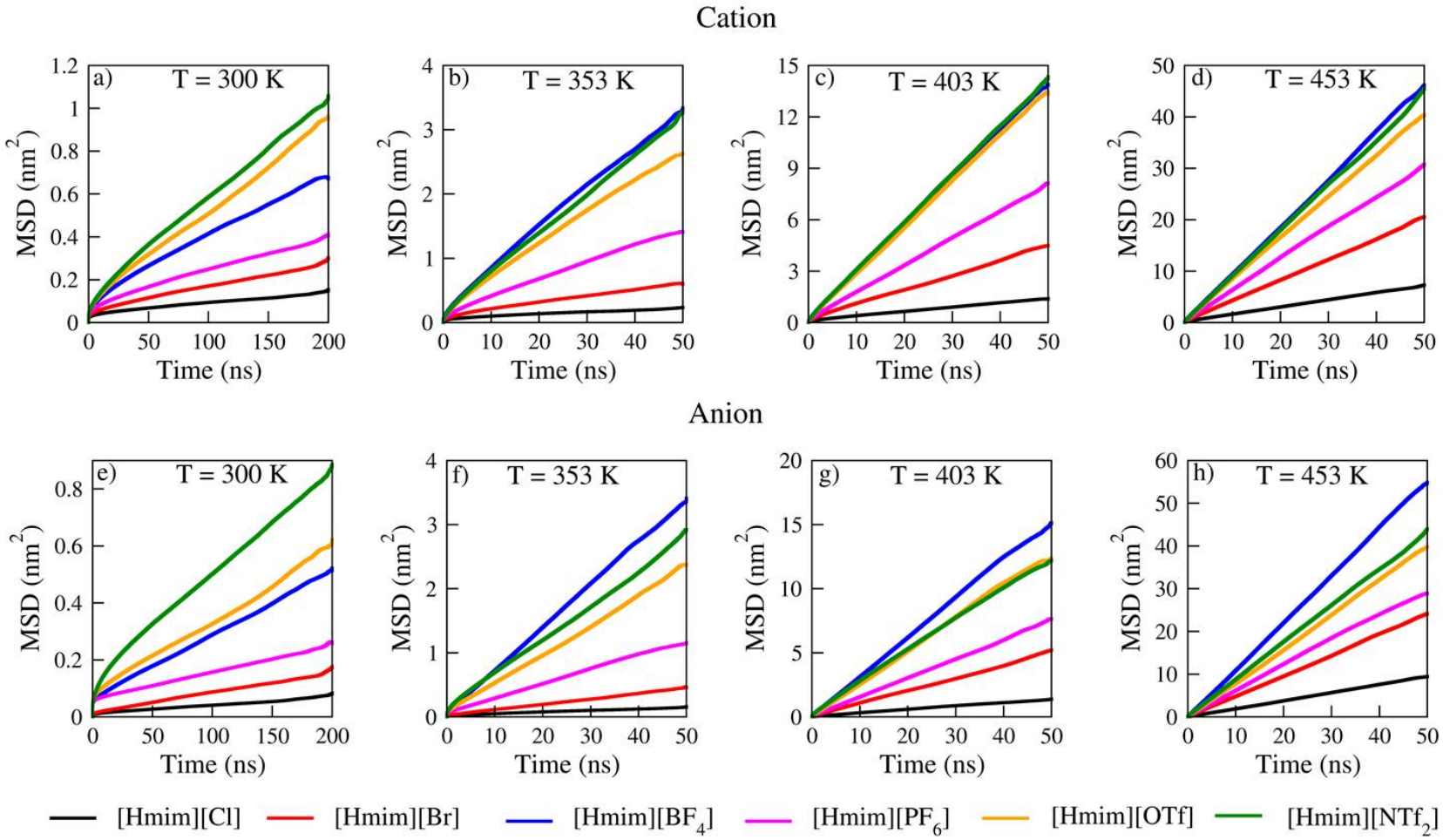

Figure B2-4: Mean Square Displacement of Cations and Anions.

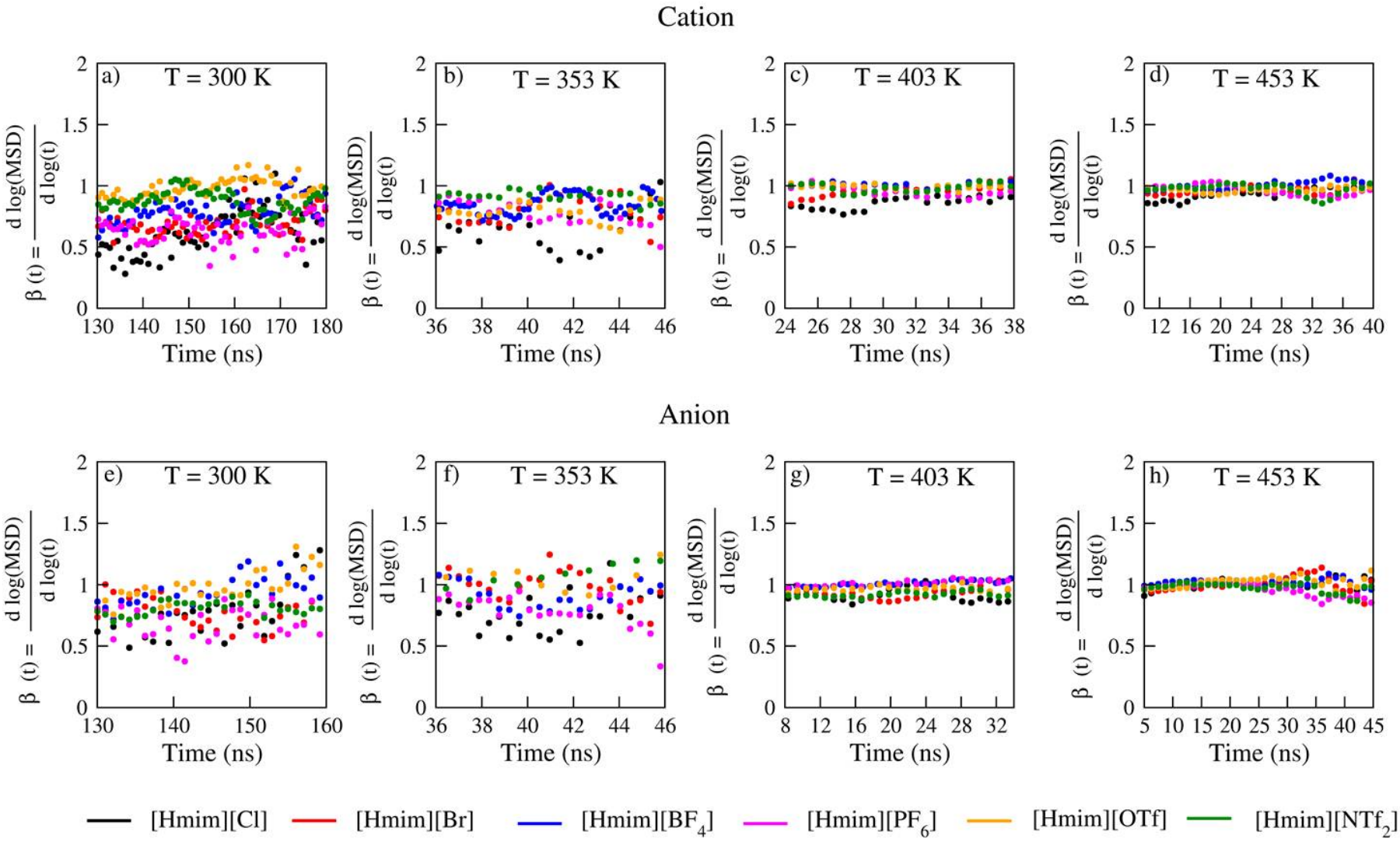

Figure B2-5: First derivative of MSD vs. time.

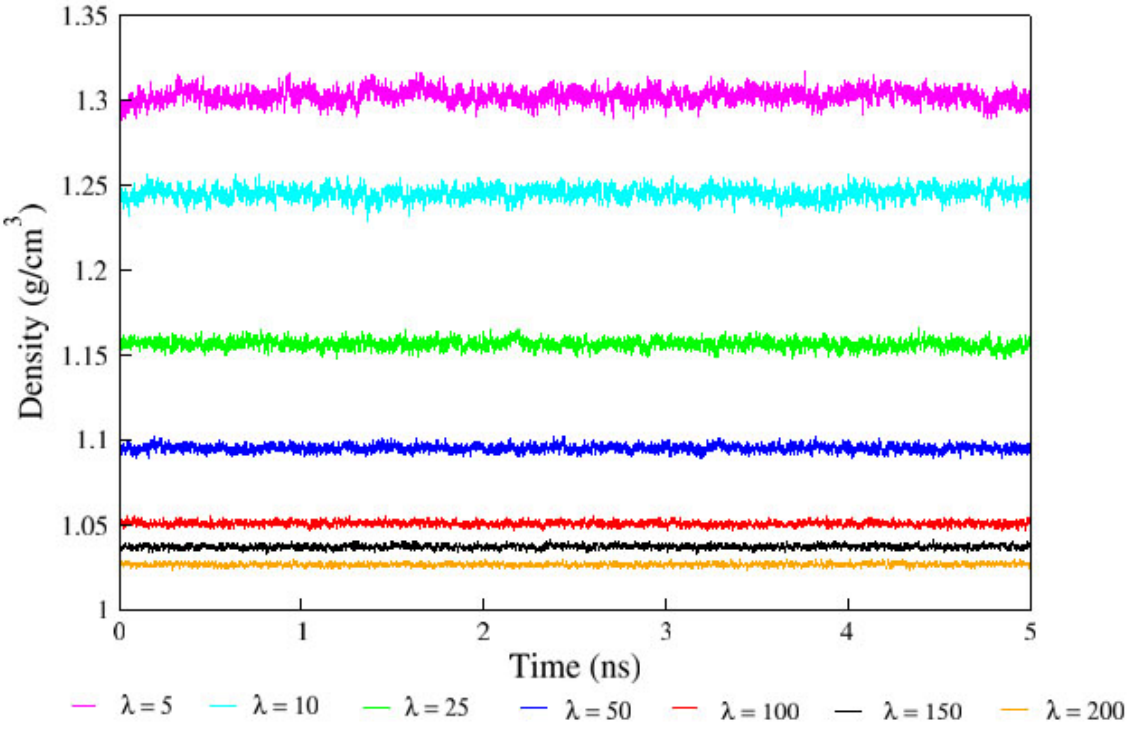

Figure B3-1: Instantaneous Density vs. Time scale of equilibration run at 303 K.

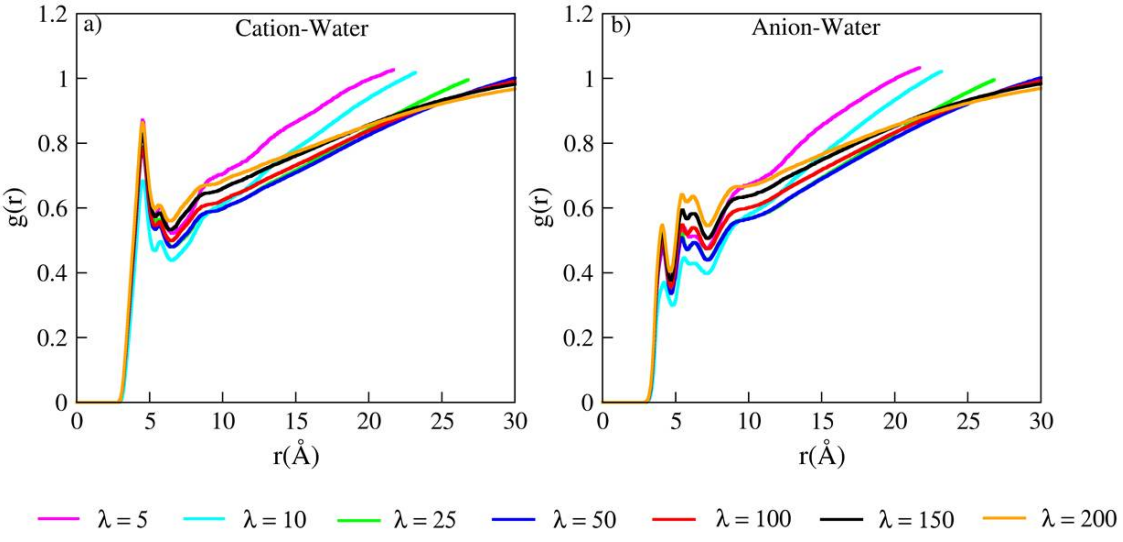

Figure B3-2: RDFs of a) Cation-Water and b) Anion-Water interactions.

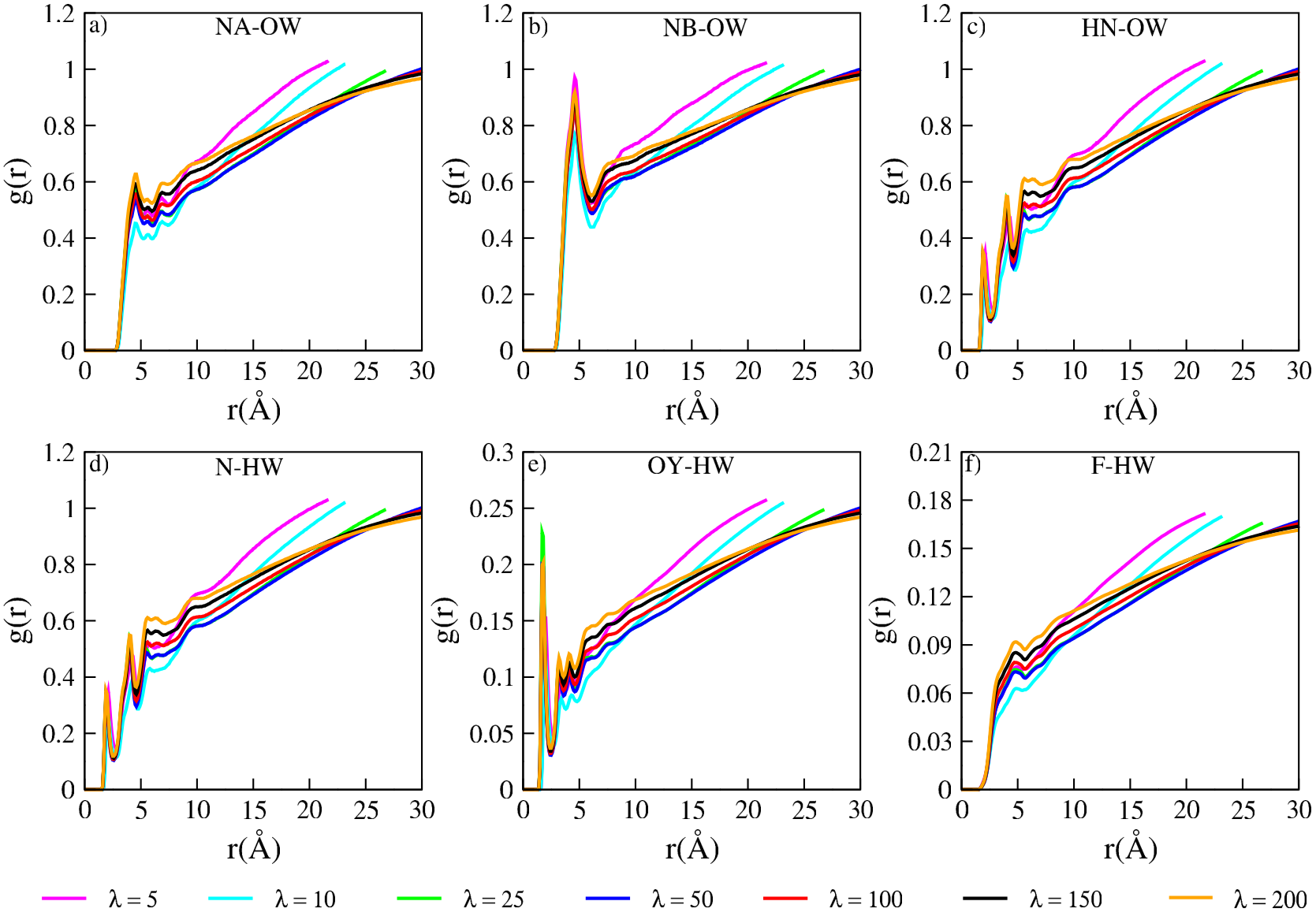

Figure B3-3: Site-Site (a-c) cation-water and (d-f) anion-water interactions.

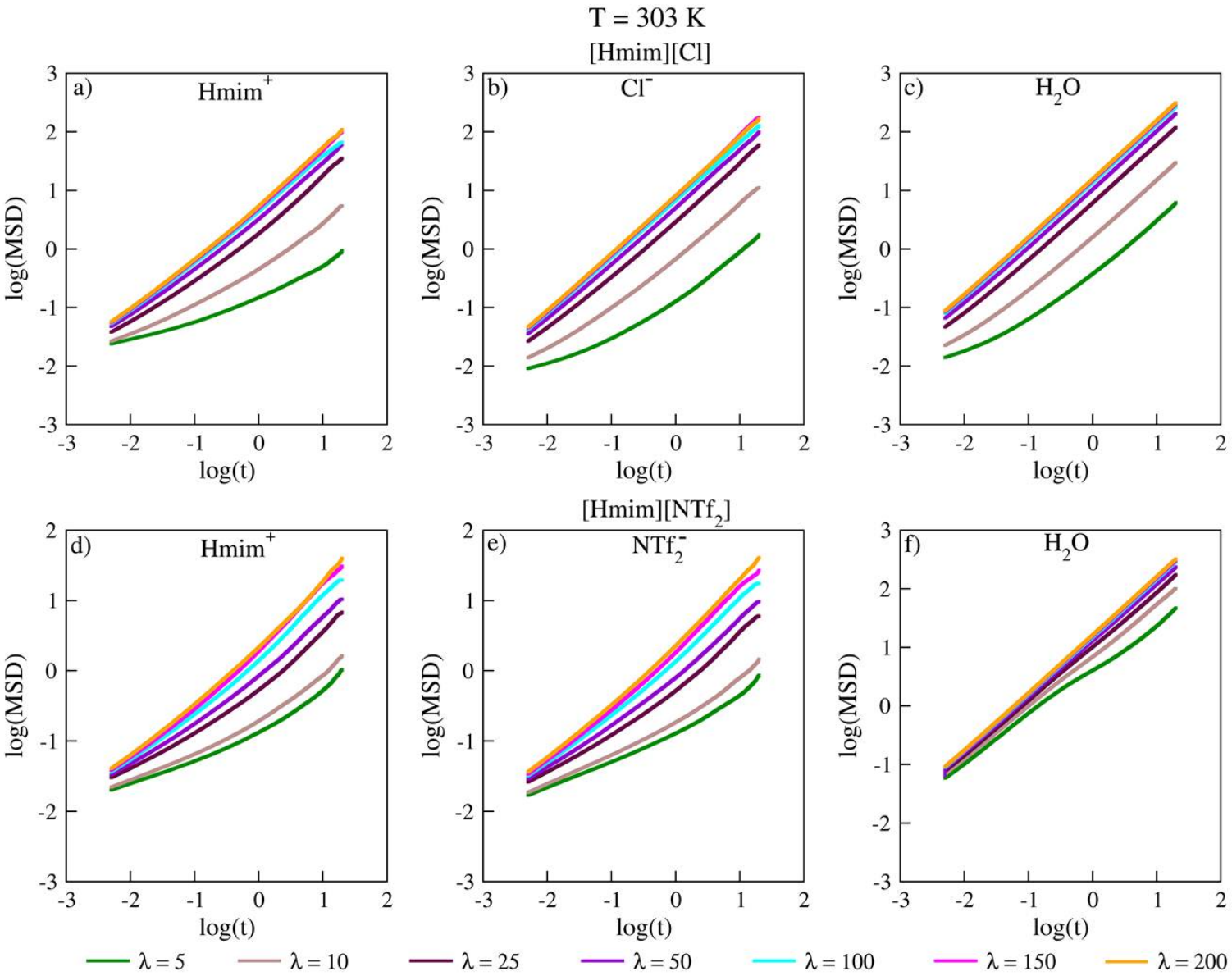

Figure B4-1: log(MSD) vs. log(t) plot for cations, anions and water molecules in low, intermediate and high water concentration of [Hmim][Cl] (a,b,c) and [Hmim] [NTf_2] IL (d, e, f) at T = 303 K.

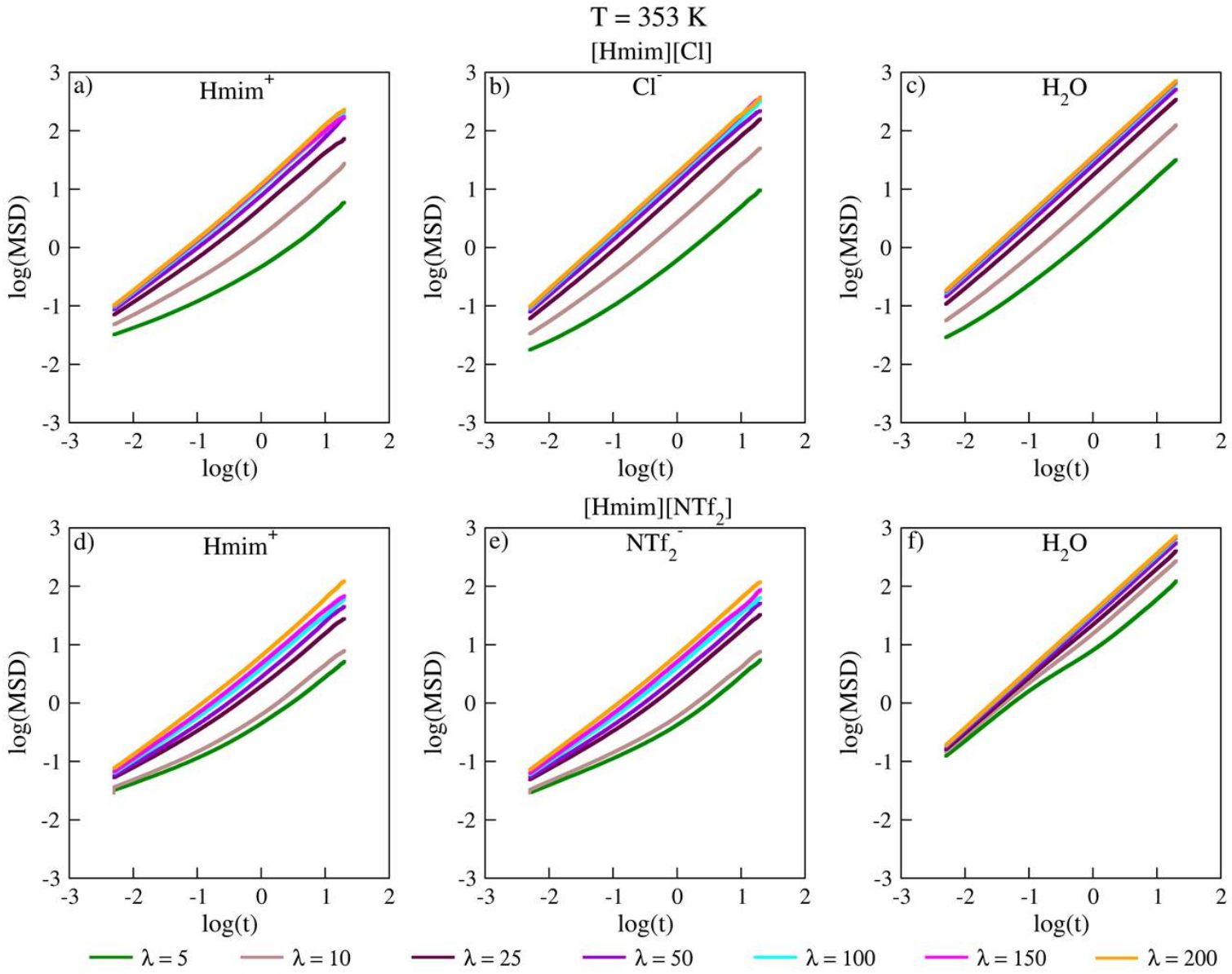

Figure B4-2: log(MSD) vs. log(t) plot for cations, anions and water molecules in low, intermediate and high water concentration of [Hmim][Cl] (a,b,c) and [Hmim] [NTf_2] IL (d, e, f) at T = 353 K.

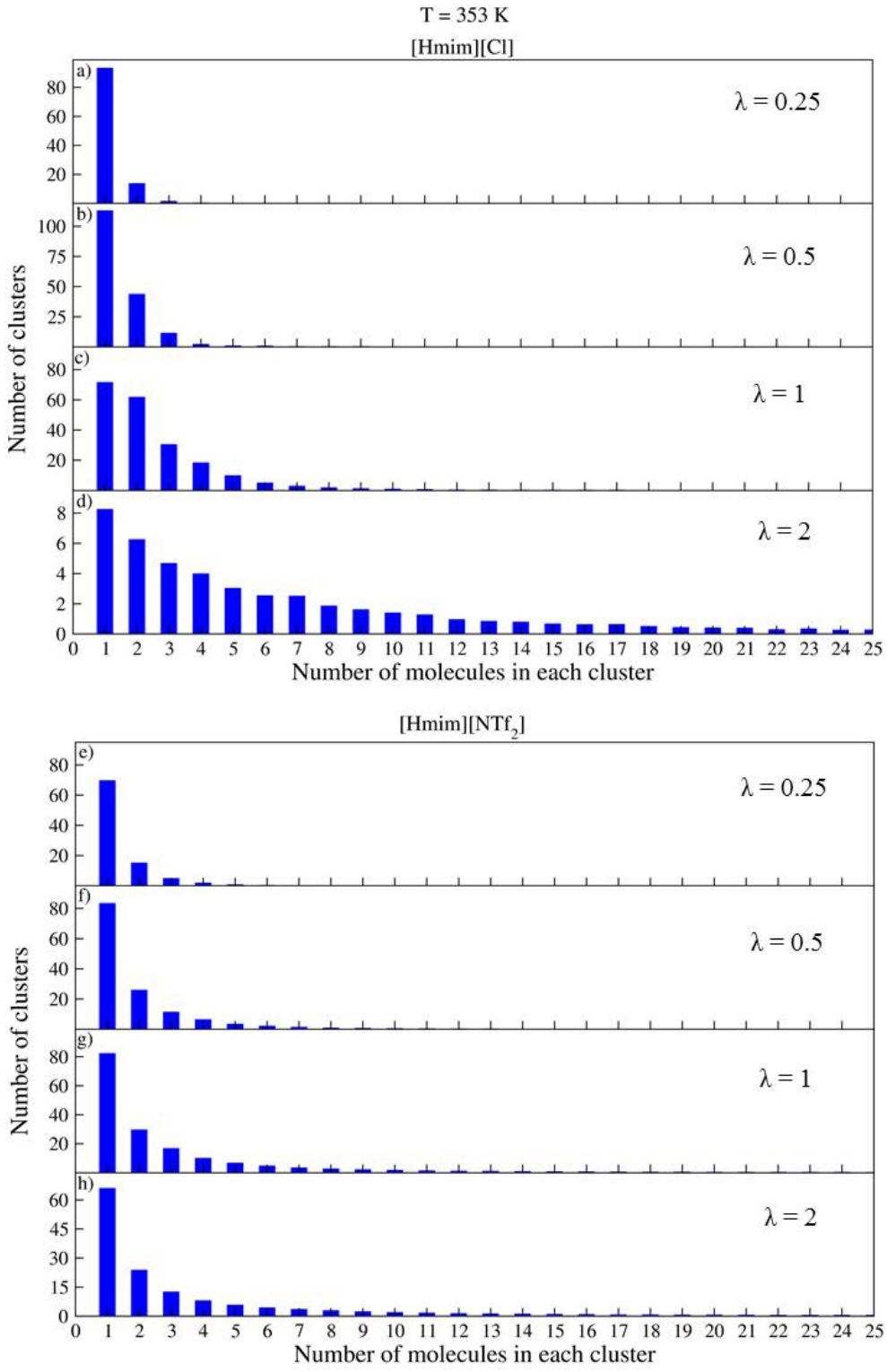

Figure B4-3: Water cluster distribution at ultra-low water concentration in [Hmim][Cl] IL and [Hmim][NTf_2] IL at T = 353 K.

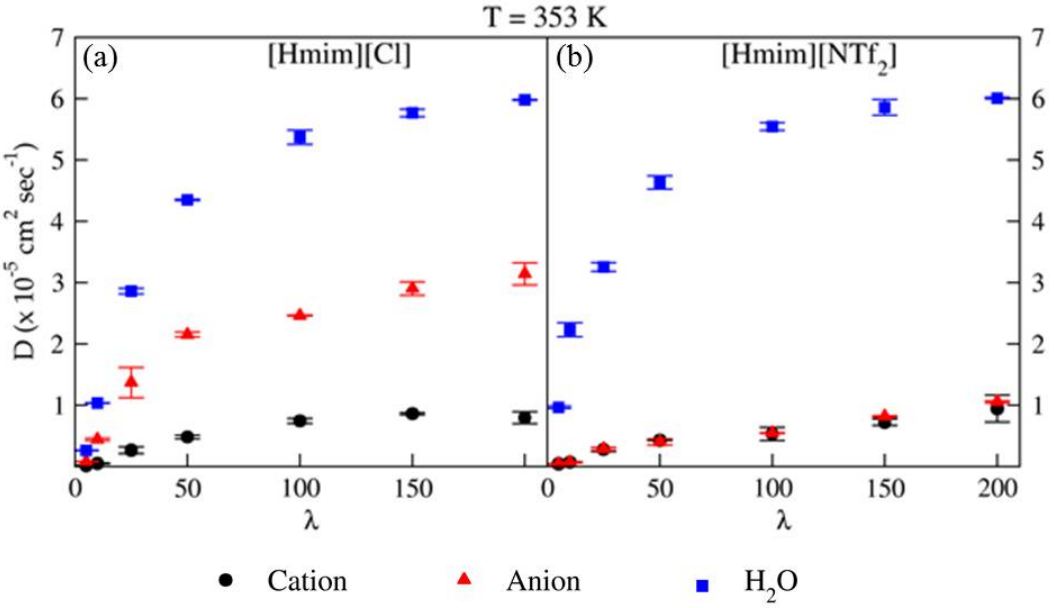

Figure B4-4: Diffusion coefficients of $Hmim^+$ cations, anions and water molecules in hydrated [Hmim][Cl] and [Hmim][NTf_2] ILs at T = 353 K.

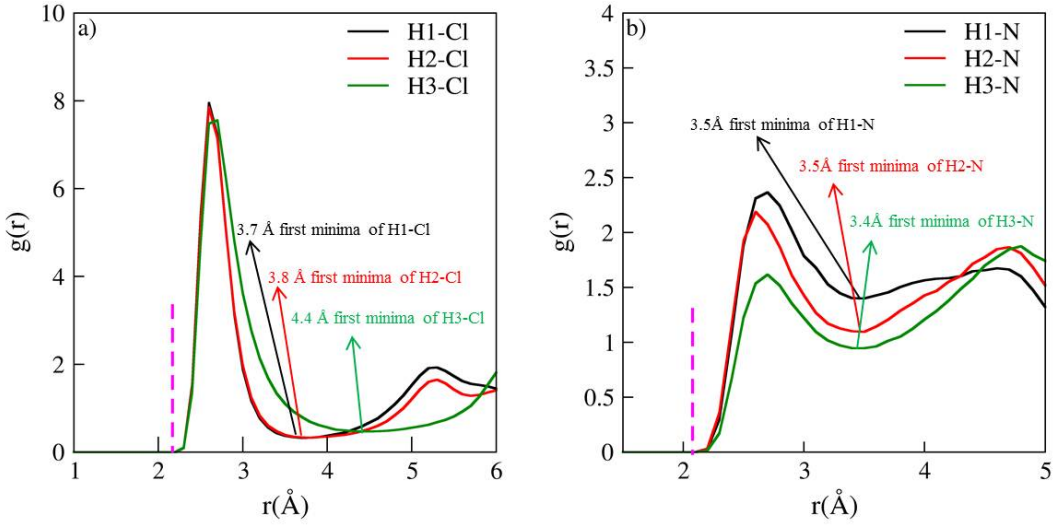

Figure B4-5: RDF (T = 303 K) on site interaction between the hydrogen atoms of $Hmim^+$ cation and anion (Cl^- and N of NTf_2^- anion) in neat IL used for calculation of IP lifetime. Dotted line (Magenta) is the initial distance criterion for calculation of IP lifetime. The final point is chosen as the first minima for the respective interactions.

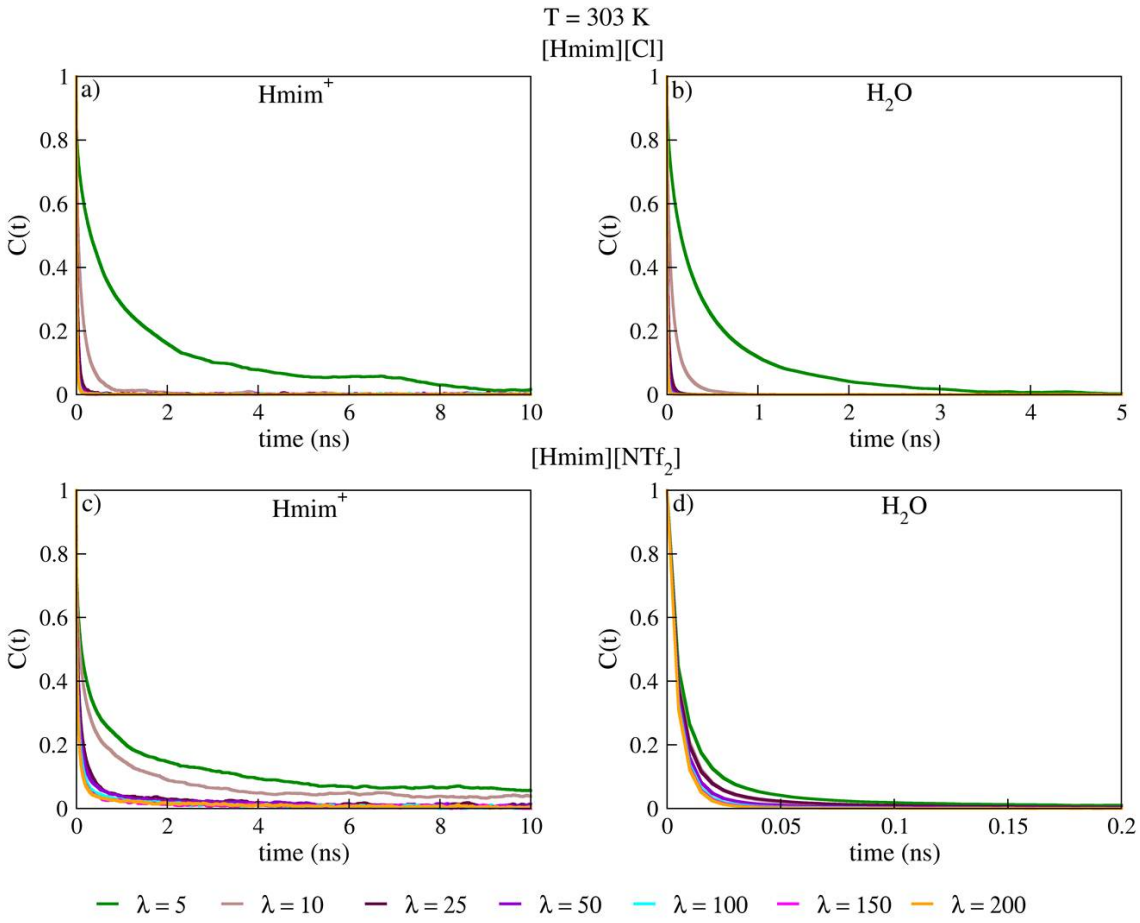

Figure B4-6: RACF (simulation) of $Hmim^+$ cations and water molecules in low, intermediate and high water concentration of [Hmim][Cl] and [Hmim][NTf_2] IL at T = 303 K.

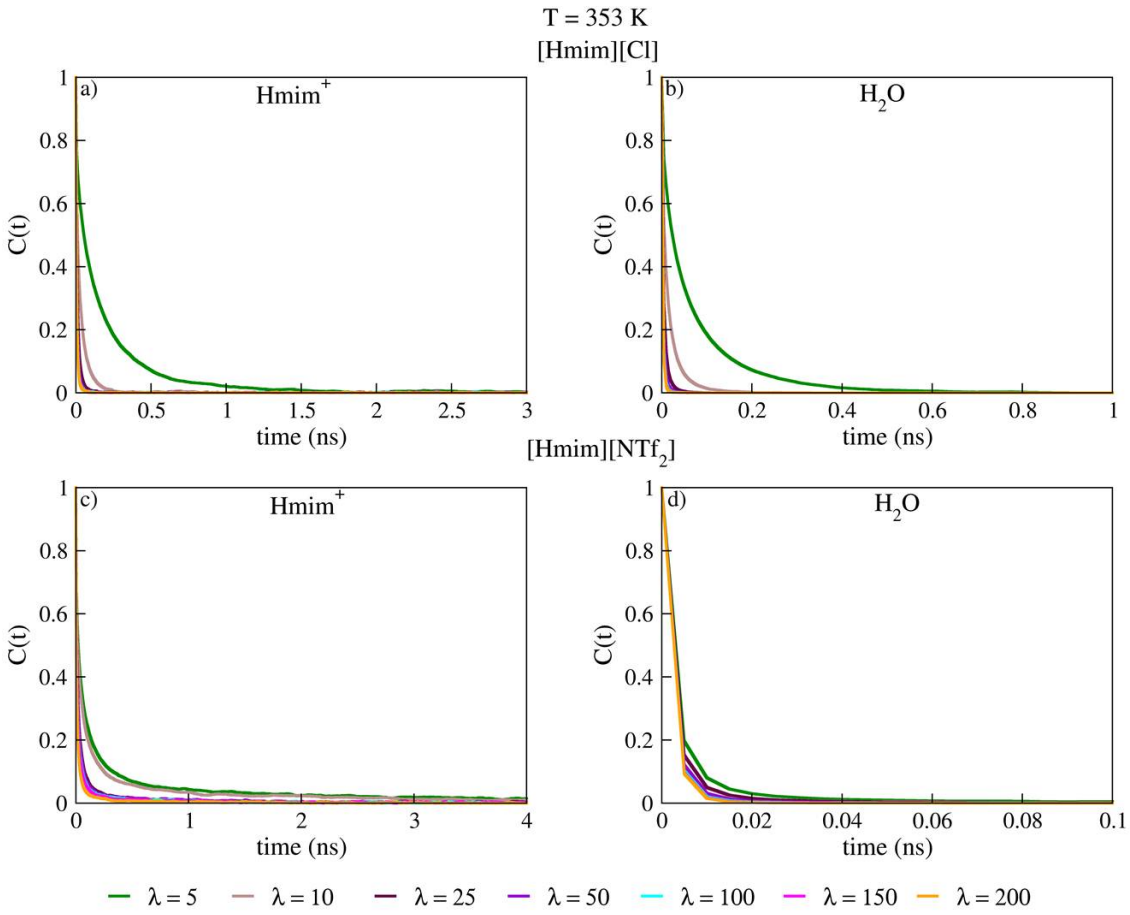

Figure B4-7: RACF (simulation) of $Hmim^+$ cations and water molecules in low, intermediate and high water concentration of [Hmim][Cl] and [Hmim][NTf_2] IL at T = 353 K.

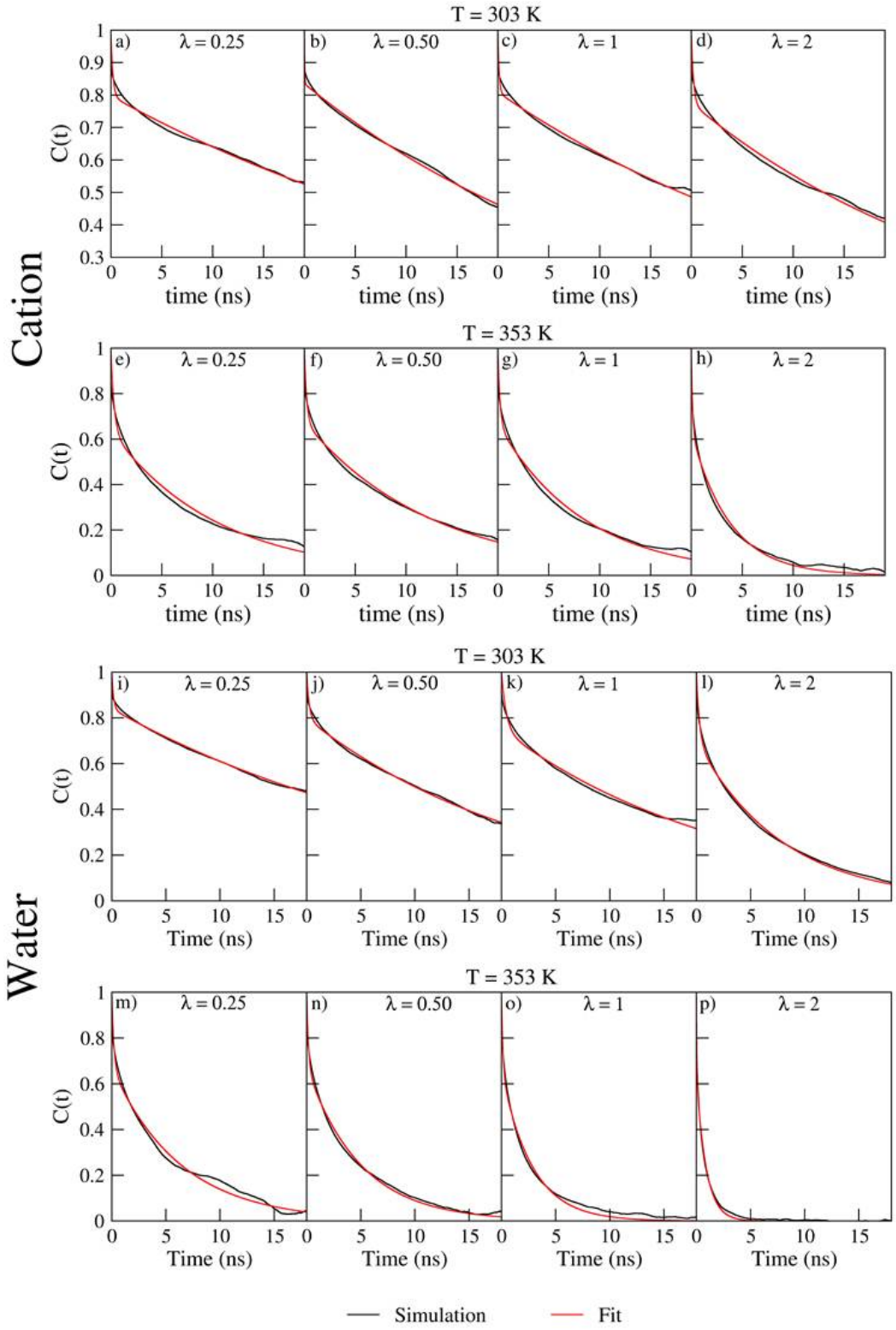

Figure B4-8: RACF of $Hmim^+$ cation and water molecules in ultra-low water concentration of [Hmim][Cl] IL at T = 303 K and T = 353 K.

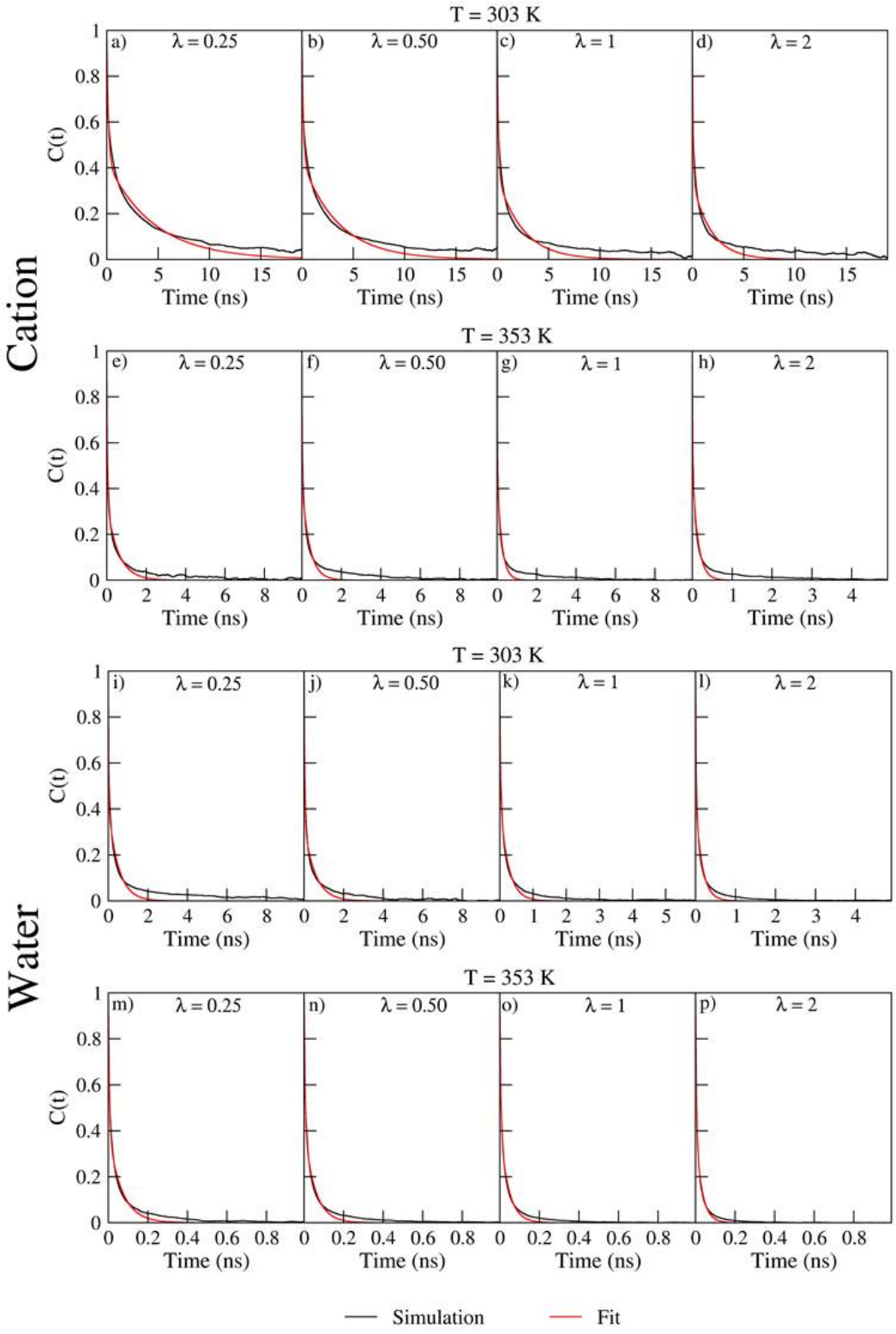

Figure B4-9: RACF of $Hmim^+$ cation and water molecules in ultra-low water concentration of [Hmim][NTf_2] IL at T = 303 K and T = 353 K.

Bibliography

[1] J. S. Wilkes, *Green Chem.*, **4**, 73 (2002).

[2] I. Krossing, J. M. Slattery, C. Daguenet, P. J. Dyson, A. Oleinikova, H. Weingärtner *J. Am. Chem. Soc.*, **128**, 13427 (2006).

[3] M. D. Joshi, J. L. Anderson, *RSC Advances*, **2**, 5470 (2012).

[4] P. Stepnowski, J. Nichthauser, W. Mrozik, B. Buszewski, *Anal. Bioanal. Chem.*, **385**, 1483 (2006).

[5] H. Weingärtner, *Angew. Chem. Int. Ed.*, **47**, 654 (2008).

[6] P. A. Hunt, C. R. Ashworth, R. P. Matthews, *Chem. Soc. Rev.*, **44**, 1257 (2015).

[7] R. D. Rogers, K. R. Seddon, *Science*, **32**, 792 (2003).

[8] N. V. Plechkova, K. R. Seddon, *Chem. Soc. Rev*, **37**, 123 (2008).

[9] S. Zhang, X. Lu, Q. Zhou, X. Li, X. Zhang, S. Li, *Ionic Liquids Physiochemical Properties, Radarweg 29, First edn*, (2009).

[10] T. Welton *Biophys. Rev.*, **10**, 691 (2018).

[11] K. N. Marsh, J. A. Boxall, R. Lichtenthaler, *Fluid Phase Equilibria*, **219**, 93 (2004).

[12] J. D. Holbrey, W. M. Reichert, R. P. Swatloski, G. A. Broker, W. R. Pitner, K. R. Seddon, R. D. Rogers, *Green Chem.*, **4**, 407 (2002).

[13] M. Y. Machado, R. Dorta, *Synthesis*, **15**, 2473 (2005).

[14] J. Langat, S. Bellayer, P. Hudrlik, A. Hudrlik, P.H. Maupin, J. W. Gilman Sr., D. Raghavan, *Polymer*, **47**, 6698 (2006).

[15] T. Köddermann, D. Paschek, R. Ludwig, *Chem. Phys. Chem.*, **8**, 2464 (2007).

[16] G. Yu, S. Zhang, G. Zhou, X. Liu, X. Chen, *Am. Inst. Chem. Eng.*, **53**, 3210 (2007).

[17] O. N. V. Buu, A. Aupoix, G. Vo-Thanh, *Tetrahedron*, **65**, 2260 (2009).

[18] E. Bodo, L. Gontrani, R. Caminiti, N. V. Plechkova, K. R. Seddon, A. Triolo, *J. Phys. Chem. B*, **114**, 16398 (2010).

[19] R. Hayes, G. G. Warr, R. Atkin, *Chem. Rev.*, **115**, 6357 (2015).

[20] J. Yang, C. Fan, D. Kong, G. Tang, W. Zhang, H. Dong, Y. Liang, D. Wang, Y. Cao, *Anal. Bioanal. Chem.*, **410**, 1647 (2018).

[21] J. S. Wilkes. J. A. Levisky, R. A. Wilson, C. L. Hussey, *Inorg. Chem.*, **21**, 1263 (1982).

[22] Y. Chauvin, L. Mussmann, H. Olivier, *Angew. Chem. Int. Ed. Engl.*, **34**, 2698, (1995).

[23] T. Fischer, A. Sethi, T. Welton, J. Woolf. *Tetrahedron Lett.*, **40**, 793 (1999).

[24] S. T. Handy, X. Zhang, *Org. Lett.*, **3**, 233 (2001).

[25] X. Yang, Z. Fei, D. Zhao, W. H. Ang, Y. Li, P. J. Dyson, *Inorg. Chem.*, **47**, 3292 (2008).

[26] W. S. Oh, *Synthesis and applications of imidazolium-based ionic liquids and their polymer derivatives, Doctoral Dissertations* (2012).

[27] S.-gi Lee, *Chem. Commun.*, 1049 (2006).

[28] Y. Wang, H. Yang, *Chem. Eng. J.*, **147**, 71 (2009).

[29] C.-M. Lee, H.-J. Jeong, S. T. Lim, M.-H. Sohn, D. W. Kim, *Appl. Mat. Inter.*, **2**, 756 (2010).

[30] M. Yang, H. Wu, Y. Lian, X. Li, Y. Ren, F. Lai, G. Zhao, *Micro. Cell Fact.*, **13**, 143 (2014).

[31] Y. Tao, R. Dong, I. V. Pavlidis, B. Chen, T. Tan, *Green Chem.*, **18**, 1240 (2016).

[32] M. Gonzalez-Miquel, J. Bedia, C. Abrusci, J. Palomar, F. Rodriguez, *J. Phys. Chem. B*, **117**, 3398 (2013).

[33] X. Wang, M. Sternberg, F. T. U. Kohler, B. U. Melcher, P. Wasserscheid, K. Meyer, *RSC Adv.*, **4**, 12476 (2014).

[34] A. Xu, L. Cao, B. Wang, J. Ma, *Adv. Mat. Sci. Eng.*, **2015**, 1 (2015).

[35] J. G. Huddleston, A. E. Visser, W. M. Reichert, H. D. Willauer, G. A. Broker, R. D.Rogers, *Green Chem.*, **3**, 156 (2001).

[36] A. Triolo, O. Russina, H.-J. Bleif, E. D. Cola, *J. Phys. Chem. B*, **111**, 4641 (2007).

[37] O. Russina, A. Triolo, L. Gontrani, R. Caminiti. D. Xiao, L. G. Hines Jr., R. A. Bartsch, E. L. Quitevis, N. Plechkova, K. R. Seddon *J. Phys.: Condens. Matter*, **21**, 424121 (2009).

[38] D. Xiao, L. G. Hines, S. Li, R. A. Bartsch, E. Quitevis, O. Russina, A. Triolo, *J. Phys. Chem. B*, **113**, 6426 (2009).

[39] C. Hardacre, J. D. Holbrey, S. E. J. McMath, M. Nieuwenhuyzen, *ACS Symposium Series,Washington, DC*, 400 (2002).

[40] J. W. Goodby, M. A. Waugh, S. M. Stein, E. Chin, R. Pindak, J. S. Patel, *Nature*, **337**, 449 (1989).

[41] D. Xiao, J. R. Rajian, A. Cady, S. Li, R. A. Bartsch, E. L. Quitevis, *J. Phys. Chem. B*, **111**, 4669 (2007).

[42] J. N. A. C. Lopes, A. A. H. Pádua, *J. Phys. Chem. B*, **110**, 3330 (2006).

[43] Y. Ji, R. Shi, Y. Wang, G. Saielli, *J. Phys. Chem. B*, **117**, 1104 (2013).

[44] U. Kapoor, J. K. Shah, *J. Phys. Chem. B*, **122**, 213 (2018).

[45] G. Raabe, J. Köhler, *J. Chem. Phys.*, **128**, 154509 (2008).

[46] M. Blesic, M. H. Marques, N. V. Plechkova, K. R. Seddon, L. P. N. Rebelo, A. Lopes, *Green Chem.*, **9**, 481 (2007).

[47] H. Wang, L. Zhang, J. Wang, Z. Li, S. Zhang, *Chem. Commun.*, **49**, 5222 (2013).

[48] J. Gao, N. J. Wagner, *Langmuir*, **32**, 5078 (2016).

[49] C. D. Tran, S. H. D. P. Lacerda, D. Oliveira, *Appl. Spectro.*, **57**, 152 (2003).

[50] S. Palchowdhury, B. L. Bhargava, *J. Phys. Chem. B*, **118**, 6241 (2014).

[51] J. M. Vicent-Luna, J. M. Romero-Enrique, S. Calero, J. A. Anta, *J. Phys. Chem. B*, **121**, 8348 (2017).

[52] S. D. Nickerson, E. M. Nofen, H. Chen, M. Ngan, B. Shindel, H. Yu, L. L. Dai, *J. Phys. Chem. B*, **119**, 8764 (2015).

[53] A. Xu, Y. Zhang, Z. Li, J. Wang, *J. Chem. Eng. Data*, **57**, 3102 (2012).

[54] P. Sippel, P. Lunkenheimer, S. Krohns, E. Thoms, A. Loidl, *Sci. Rep.*, **5**, 13922 (2015).

[55] J. Vila, L. M. Varela, O. Cabeza, *Electrochim. Act.*, **52**, 7413 (2007).

[56] M. H. Kowsari, M. Fakhraee, *J. Chem. Eng. Data 2015*, **60**, 551 (2015).

[57] C. Rey-Castro, L. F. Vega, *J. Phys. Chem. B*, **110**, 14426 (2006).

[58] A. Mondal, S. Balasubramanian, *J. Chem. Eng. Data*, **59**, 3061 (2014).

[59] Z. Pouramini, A. Mohebbi, M. H. Kowsari, *J. Mol. Liq.*, **246**, 39 (2017).

[60] K. Kaneko, K. Saihara, Y. Masuda, Y. Yoshimura, A. Shimizu, *J. Mol. Liq.*, **264**, 337 (2018).

[61] A. Menjoge, J. Dixon, J. F. Brennecke, E. J. Maginn, S. Vasenkov, *J. Phys. Chem. B*, **113**, 6353 (2009).

[62] G. A. Hegde, V. S. Bharadwaj, C. L. Kinsinger, T. C. Schutt, N. R. Pisierra, C. M. Maupin, *J. Chem. Phys.*, **145**, 064504 (2016).

[63] T. Méndez-Morales, J. Carrete, Ó. Cabeza, L. J. Gallego, L. M. Varela, *J. Phys. Chem. B*, **115**, 6995 (2011).

[64] X. Zhong, Z. Fan, Z. Liu, D. Cao, *J. Phys. Chem. B*, **116**, 3249 (2012).

[65] A. R. Leach. *Molecular Modelling: Principles and Applications; Prentice Hall: Harlow, England* (2001).

[66] B. R. Brooks, R. E. Bruccoleri, B. D. Olafson, D. J. States; S. Swaminathan, M. Karplus, *J. Comp. Chem.*, **4**, 187 (1983).

[67] W. D. Cornell, P. Cieplak, C. I. Bayly, I. R. Gould, K. M. M. Jr., D. M. Ferguson, D. C. Spellmeyer, T. Fox, J. W. Caldwell, P. A. Kollman, *J. Am. Chem. Soc.*, **117**, 5179 (1995).

[68] W. L. Jorgensen, D. S. Maxwell, J. Tirado-Rives, *J. Am. Chem. Soc. 1996*, **118**, 11225 (1996).

[69] H. Sun, *J. Phys. Chem. B*, **102**, 7338 (1998).

[70] W. R. P. Scott, P. H. Hünenberger, I. G. Tironi, A. E. Mark, S. R. Billeter, J. Fennen, A. E. Torda, T. Huber, P. Krüger, W. F. van Gunsteren, *J. Phys. Chem. A*, **103**, 3596 (1999).

[71] J. N. C. Lopes, J. Deschamps, A. A. H. Pádua, *J. Phys. Chem. B*, **108**, 2038 (2004).

[72] Z. Liu, S. Huang, W. Wang, *J. Phys. Chem. B*, **108**, 12978 (2004).

[73] J. N. C. Lopes, A. A. H. Pádua, *J. Phys. Chem. B*, **110**, 19586 (2006).

[74] J. N. C. Lopes, A. A. H. Pádua, K. Shimizu, *J. Phys. Chem. B*, **112**, 5039 (2008).

[75] S. V. Sambasivarao, O. Acevedo, *J. Chem. Theory Comput.*, **5**, 1038 (2009).

[76] S. Tsuzuki, W. Shinoda, H. Saito, M. Mikami, H. Tokuda, M. Watanabe, *J. Phys. Chem. B*, **113**, 10641 (2009).

[77] B. Doherty, X. Zhong, S. Gathiaka, B. Li, O. Acevedo, *J. Chem. Theory Comput.*, **13**, 6131 (2017).

[78] M. P. Allen, D. J. Tildesley, *Computer Simulations of Liquids; Oxford Science Publications: New York,* (1987).

[79] B. Weyershausen, K. Lehmann, *Green Chem.*, **7**, 15 (2005).

[80] M. Armand, F. Endres, D. R. MacFarlane, H. Ohno, B. Scrosati, *Nat. Mater.*, **8**, 621 (2009).

[81] T. Payagala, J. Huang, Z. S. Breitbach, P. S. Sharma, D. W. Armstrong, *Chem. Mater.*, **19**, 5848 (2007).

[82] R. D. Noble, D. L. Gin, *J. Membr. Sci.*, **369**, 1 (2011).

[83] C. Wang, H. Luo, H. Li, X. Zhu, B. Yu, S. Dai, *Chem. Eur. J.*, **18**, 2153 (2012).

[84] P. Bonhôte, A.-P. Dias, N. Papageorgiou, K. Kalyanasundaram, M. Grätzel, *Inorg. Chem.*, **35**, 1168 (1996).

[85] H. L. Ngo, K. LeCompte, L. Hargens, A. B. McEwen, *Thermochim. Act.*, 2000, **97**, 357 (2000).

[86] C. P. Fredlake, J. M. Crosthwaite, D. G. Hert, S. N. V. K. Aki, J. F. Brennecke, *J. Chem. Eng. Data*, **49**, 954 (2004).

[87] A. Muhammad, M. I. Abdul Mutalib, C. D. Wilfred, T. Murugesan, A. Shafeeq, *Chem. Thermodyn.*, **40**, 1433 (2008).

[88] S. A. Katsyuba, M. V. Vener, E. E. Zvereva, Z. Fei, R. Scopelliti, G. Laurenczy, N. Yan, E. Paunescu, P. J. Dyson, *J. Phys. Chem. B*, **117**, 9094 (2013).

[89] S. M. Urahata, M. C. C. Ribeiro, *J. Chem. Phys.*, **122**, 024511 (2005).

[90] S. U. Lee, J. Jung, Y.-K. Han, *Chem. Phys. Lett.*, **406**, 332 (2005).

[91] M. Deetlefs, C. Hardacre, M. Nieuwenhuyzen, A. A. H. Padua, O. Sheppard, A. K. Soper, *J. Phys. Chem. B*, **110**, 12055 (2006).

[92] M. H. Kowsari, S. Alavi, M. Ashrafizaadeh, B. Najafi, *J. Chem. Phys.*, **129**, 224508 (2008).

[93] R. P. Swatloski, S. K. Spear, J. D. Holbrey, R. D. Rogers, *J. Am. Chem. Soc.*, **124**, 4974 (2002).

[94] R. Kumar, Saima, A. Shard, N. H. Andhare, Richa, A. K. Sinha, *Angew. Chem., Int. Ed.*, **54**, 828 (2015).

[95] T. M. Letcher, B. Soko, P. Reddy, *J. Chem. Eng. Data*, **48**, 1587 (2003).

[96] S. Corderí, E. J. González, N. Calvar, Á Domínguez, *J. Chem. Thermodyn.*, **53**, 60 (2012).

[97] M. Costantini, V. A. Toussaint, A. Shariati, C. J. Peters, I. Kikic, *J. Chem. Eng. Data*, **50**, 52 (2005).

[98] W. Shi, D. R. Luebke, *Langmuir*, **29**, 5563 (2013).

[99] B. Hess, C. Kutzner, D. van der Spoel, E. Lindahl, *J. Chem. Theor. Comput.*, **4**, 435 (2008).

[100] T. Darden, D. York, L. Pedersen, *J. Chem. Phys.*, **98**, 10089 (1993).

[101] U. Essmann, L. Perera, M. L. Berkowitz, T. Darden, H. Lee, L. G. Pedersen, *J. Chem. Phys.*, **103**, 8577 (1995).

[102] M. C. Payne, M. P. Teter, D. C. Allan, T. A. Arias, J. D. Joannopoulos, *Rev. Mod. Phys.*, **64**, 1045 (1992).

[103] G. Bussi, D. Donadio, M. Parrinello, *J. Chem. Phys.*, **126**, 014101 (2007).

[104] H. J. C. Berendsen, J. P. M. Postma, A. DiNola, J. R. Haak, *J. Chem. Phys.*, **81**, 3684 (1984).

[105] S. Nosé *Mol. Phys.*, **52**, 255 (1984).

[106] W. G. Hoover *Phys. Rev. A*, **31**, 1695 (1985).

[107] S. Zhang, N. Sun, X. He, X. Lu, X. Zhang, *J. Phys. Chem. Ref. Data*, **35**, 1475 (2006).

[108] M. Brehm, B. Kirchner, *J. Chem. Inf. Model.*, **51**, 2007 (2011).

[109] B. L. Bhargava, S. Balasubramanian, *J. Chem. Phys.*, **123**, 144505 (2005).

[110] V. V. Chaban, I. V. Voroshylova, O. N. Kalugin, *Phys. Chem. Chem. Phys.*, **13**, 7910 (2011)

[111] S. Gabl, C. Schröder, O. Steinhauser, *J. Chem. Phys.*, **137**, 094501 (2012).

[112] H. Tokuda, K. Hayamizu, K. Ishii, M. A. B. H. Susan, M. Watanabe, *J. Phys. Chem. B*, **108**, 16593 (2004).

[113] H. Tokuda, S. Tsuzuki, M. A. B. H. Susan, K. Hayamizu, M. Watanabe, *J. Phys. Chem. B*, **110**, 19593 (2006).

[114] U. L. Bernard, E. I. Izgorodina, D. R. MacFarlane, *J. Phys. Chem. C*, **114**, 20472 (2010).

[115] R. P. Matthews, C. Ashworth, T. Welton, P. A. Hunt, *J. Phys.: Condens. Matter*, **26**, 284112 (2014).

[116] Y. Zhang, E. Maginn, *J. Phys. Chem. Lett.*, **6**, 700 (2015).

[117] A. M. O'Mahony, D. S. Silvester, L. Aldous, C. Hardacre, R. G. Compton, *J. Chem. Eng. Data*, **53**, 2884 (2008).

[118] J. Dupont, R. F. de Souza, P. A. Z. Suarez, *Chem. Rev.*, **102**, 3667 (2002).

[119] B. F. Goodrich, J. C. de la Fuente, B. E. Gurkan, Z. K. Lopez, E. A. Price, Y. Huang, J. F. Brennecke, *J. Phys. Chem. B*, **115**, 9140 (2011).

[120] A. Z. Hezave, S. Dorostkar, S. Ayatollahi, M. Nabipour, B. Hemmateenejad, *Colloids Surf. A*, **421**, 63 (2013).

[121] T. C. Schutt, G. A. Hegde, V. S. Bharadwaj, A. J. Johns, C. M. Maupin, *J. Phys. Chem. B*, **121**, 843 (2017).

[122] J. Jacquemin, P. Husson, A. A. H. Padua, V. Majer, *Green Chem.*, **8**, 172 (2006).

[123] H. Rodríguez, J. F. Brennecke, *J. Chem. Eng. Data*, **51**, 2145 (2006).

[124] E. Gómez, B. González, N. Calvar, E. Tojo, Á. Domínguez, *J. Chem. Eng. Data*, **51**, 2096 (2006).

[125] M. S. Kelkar, E. J. Maginn, *J. Phys. Chem. B*, **111**, 4867 (2007).

[126] M. G. Freire, P. J. Carvalho, A. M. Fernandes, I. M. Marrucho, A. J. Queimada, J. A. P. Coutinho, *J. Colloid Interface Sci.*, **314**, 621 (2007).

[127] S. Zhang, X. Li, H. Chen, J. Wang, J. Zhang, M. Zhang, *J. Chem. Eng. Data*, **49**, 760 (2004)

[128] U. Schröder, J. D. Wadhawan, R. G. Compton, F. Marken, P. A. Z. Suarez, C. S. Consorti, R. F. de Souza, J. Dupont, *New J. Chem.*, **24**, 1009 (2000).

[129] M. Kanakubo, T. Umecky, T. Aizawa, Y. Kurata, *Chem. Lett.*, **34**, 324 (2005).

[130] Y. Kohno, H. Ohno, *Chem. Commun.*, **48**, 7119 (2012).

[131] M. A. P. Martins, C. P. Frizzo, D. N. Moreira, N. Zanatta, H. G. Bonacorso, *Chem. Rev.*, **108**, 2015 (2008).

[132] A. E. Visser, M. P. Jensen, I. Laszak, K. L. Nash, G. R. Choppin, R. D. Rogers, *Inorg. Chem.*, **42**, 2197 (2003).

[133] V. A. Cocalia, M. P. Jensen, J. D. Holbrey, S. K. Spear, D. C. Stepinski, R. D. Rogers, *Dalton Trans.*, 1966 (2005).

[134] A. E. Visser, R. P. Swatloski, W. M. Reichert, S. T. Griffin, R. D. Rogers, *Ind. Eng. Chem. Res.*, **39**, 3596 (2000).

[135] L. Cammarata, S. G. Kazarian, P. A. Salter, T. Welton, *Phys. Chem. Chem. Phys.*, **3**, 5192 (2001).

[136] S. Rivera-Rubero, S. Baldelli, *J. Am. Chem. Soc.*, **126**, 11788 (2004).

[137] T. Takamuku, Y. Kyoshoin, T. Shimomura, S. Kittaka, T. Yamaguchi, *J. Phys. Chem. B*, **113**, 10817 (2009).

[138] S. Saha, H. Hamaguchi, *J. Phys. Chem. B*, **110**, 2777 (2006).

[139] M. G. Freire, P. J. Carvalho, R. L. Gardas, I. M. Marrucho, L. M. N. B. F. Santos, J. A. P. Coutinho, *J. Phys. Chem. B*, **112**, 1604 (2008).

[140] B. Fazio, A. Triolo, G. D. Marco, *J. Raman Spectrosc.*, **39**, 233 (2008).

[141] L. Zhang, Z. Xu, Y. Wang, H. Li, *J. Phys. Chem. B*, **112**, 6411 (2008).

[142] C. G. Hanke, R. M. Lynden-Bell, *J. Phys. Chem. B*, **107**, 10873 (2003).

[143] N. Sieffert, G. Wipff, *J. Phys. Chem. B*, **110**, 13076 (2006).

[144] C. E. S. Bernardes, M. E. M. da Piedade, J. N. C. Lopes, *J. Phys. Chem. B*, **115**, 2067 (2011).

[145] W. Jiang, Y. Wang, G. A. Voth, *J. Phys. Chem. B*, **111**, 4812 (2007).

[146] S. Feng, G. A. Voth, *Fluid Phase Equilibria*, **294**, 148 (2010).

[147] A. A. Niazi, B. D. Rabideau, A. E. Ismail, *J. Phys. Chem. B*, **117**, 1378 (2013).

[148] S. S. Sarangi, B. L. Bhargava, S. Balasubramanian, *Phys. Chem. Chem. Phys.*, **11**, 8745 (2009).

[149] S. G. Raju, S. Balasubramanian, *J. Phys. Chem. B*, **113**, 4799 (2009).

[150] B. L. Bhargava, M. L. Klein, *J. Phys. Chem. B*, **113**, 9499 (2009).

[151] B. L. Bhargava, M. L. Klein, *Soft Matter*, **5**, 3475 (2009).

[152] B. L. Bhargava, M. L. Klein, *J. Phys. Chem. A*, **113**, 1898 (2009).

[153] B. L. Bhargava, Y. Yasaka, M. L. Klein, *Chem. Commun.*, **47**, 6228 (2011).

[154] P. Yee, J. K. Shah, E. J. Maginn, *J. Phys. Chem. B*, **117**, 12556 (2013).

[155] W. Shi, E. J. Maginn, *J. Phys. Chem. B*, **112**, 2045 (2008).

[156] H. J. C. Berendsen, J. R. Grigera, T. P. Straatsma, *J. Phys. Chem.*, **91**, 6269 (1987).

[157] M. Haberler, C. Schröder, O. Steinhauser, *J. Chem. Theor. Comput.*, **8**, 3911 (2012).

[158] C.-L. Wong, A. N. Soriano, M.-H. Li, *Fluid Phase Equilibria*, **271**, 43 (2008).

[159] P. Atkins, J. De Paula, *Physical Chemistry Oxford UP, Oxford, 8th edn*, (2006).

[160] A. R. Porter, S. Y. Liem, P. L. A. Popelier, *Phys. Chem. Chem. Phys.*, **10**, 4240 (2008).

[161] H. V. Spohr, G. N. Patey, *J. Chem. Phys.*, **132**, 234510 (2010).

[162] A. Heintz, R. Ludwig, E. Schmidt, *Phys. Chem. Chem. Phys.*, **13**, 3268 (2011).

[163] G. Taylor, *Proc. R. Soc. London, Ser. A*, **219**, 186 (1953).

[164] H. K. Kashyap, H. V. R. Annapureddy, F. O. Raineri, C. J. Margulis, *J. Phys. Chem. B*, **115**, 13212 (2011).

[165] P. D'Angelo, A. Zitolo, G. Aquilanti, V. Migliorati, *J. Phys. Chem. B*, **117**, 12516 (2013).

[166] V. Migliorati, A. Zitolo, P. D'Angelo, *J. Phys. Chem. B*, **117**, 12505 (2013).

[167] U. Salma, M. Usula, R. Caminiti, L. Gontrani, N. V. Plechkova, K. R. Seddon, *Phys. Chem. Chem. Phys.*, **19**, 1975 (2017).

[168] A. Sharma, P. K. Ghorai, *J. Chem. Phys.*, **144**, 114505 (2016).

[169] H. Higashi, M. Kumita, T. Seto, Y. Otani, *Mol. Simul.*, **7022**, 1 (2017).

[170] F. Khabaz, Y. Zhang, L. Xue, E. L. Quitevis, E. J. Maginn, R. Khare, *J. Phys. Chem. B*, **122**, 2414 (2018).

[171] T. Köddermann, C. Wertz, A. Heintz, R. Ludwig, *Chem. Phys. Chem.*, **7**, 1944 (2006).

[172] K. Fumino, A. Wulf, R. Ludwig, *Angew. Chem. Int. Ed.*, **47**, 8731 (2008).

[173] S. Tsuzuki, T. Umecky, H. Matsumoto, W. Shinoda, M. Mikami, *J. Phys. Chem. B*, **114**, 11390 (2010).

[174] T. Pal, R. Biswas, *Theor. Chem. Acc.*, **132**, 1 (2013).

[175] K. R. Ramya, P. Kumar, A. Kumar, A. Venkatnathan, *J. Phys. Chem. B*, **118**, 8839 (2014).

[176] K. R. Ramya, P. Kumar, A. Venkatnathan, *J. Phys. Chem. B*, **119**, 14800 (2015).

[177] J. N. C. Lopes, J. Deschamps, A. A. H. Padua, *J. Phys. Chem. B*, **108**, 2038 (2004).

[178] E. Gómez, B. González, Á. Domínguez, E. Tojo, J. Tojo, *J. Chem. Eng. Data*, **51**, 696 (2006).

[179] P. Mark, L. Nilsson, *J. Phys. Chem. A*, **105**, 9954 (2001).

[180] D. Ghoshdastidar, S. Senapati, *Soft Matter*, **12**, 3032 (2016).

[181] D. van Der Spoel, E. Lindahl, B. Hess, A. R. van Buuren, E. Apol, P. J. Meulenhoff, D. P. Tieleman, A. L. T. M. Sijbers, K. A. Feenstra, R. van Drunen, H. J. Berendsen, *Gromacs User Manual Version 4.5.4*, (2010).

[182] N.-T. Van-Oanh, C. Houriez, B. Rousseau, *Phys. Chem. Chem. Phys.*, **12**, 930 (2010).

[183] Y. Shim, H. J. Kim, *J. Phys. Chem. B*, **112**, 11028 (2008).

[184] B. J. Berne, G. D. Harp, *Adv. Chem. Phys.*, **17**, 63 (1970).

[185] C. A. Rumble, A. Kaintz, S. K. Yadav, B. Conway, J. C. Araque, G. A. Baker, C. Margulis, M. Maroncelli, *J. Phys. Chem. B*, **120**, 9450 (2016).

[186] A. B. Pereiro, J. M. M. Araújo, J. M. S. S. Esperança, I. M. Marrucho, L. P. N. Rebelo, *J. Chem. Thermodyn.*, **46**, 2 (2012).

[187] K. Weissermel, H.-J. Arpe, *Industrial Organic Chemistry, 4th Completely Revised edition, Wiley-VCH, Weinheim*, 313 (2003).

[188] M. S. Hassan, M. A. Fahim, C. J. Mumford, *J. Chem. Eng. Data*, **33**, 162 (1988).

[189] S. A. Ahmad, R. S. Tanwar, R. K. Gupta, A. Khanna, *Fluid Phase Equilibria*, **220**, 189 (2004).

[190] G. W. Cassell, M. M. Hassan, A. L. Hines *J. Chem. Eng. Data*, **34**, 328 (1989).

[191] G. M. Radwan, S. A. A1-Muhtaseb, M. A. Fahim, *Fluid Phase Equilibria*, **129**, 175 (1997).

[192] T. M. Letcher, P. K. Naicker, *J. Chem. Eng. Data*, **43**, 1034 (1998).

[193] J. Gmehling, A. Schedemann, *Ind. Eng. Chem. Res.*, **53**, 17794 (2014).

[194] G. W. Meindersma, A. (J. G.) Podt, M. G. Meseguer, A. B. de Haan, *Chapter 5, Ionic Liquids IIIB: Fundamentals, Progress, Challenges, and Opportunities ACS Symposium Series; American Chemical Society: Washington, DC*, 57 (2005).

[195] G. W. Meindersma, A. B. de Haan, *Chem. Eng. Res. and Des.*, **86**, 745 (2008).

[196] A. Arce, M. J. Earle, H. Rodríguez, K. R. Seddon. *Green Chem.*, **9**, 70 (2007).

[197] A. Arce, M. J. Earle, H. Rodríguez, K. R. Seddon, *J. Phys. Chem. B*, **111**, 4732 (2007).

[198] A. Arce, M. J. Earle, H. Rodríguez, K. R. Seddon, A. Soto, *Green Chem.*, **11**, 365 (2009).